LIBRARY
Michigan State
University

This is to certify that the

thesis entitled

THE DESIGN AND CHARACTERIZATION OF A MINIATURE, NANOSECOND SPARK DISCHARGE FOR ANALYTICAL EMISSION SPECTROSCOPY

presented by

Gary Thomas Seng

has been accepted towards fulfillment
of the requirements for

Ph.D. degree in Chemistry

Stanley R. Crouch

Major professor

Date September 29, 1978

O-7639

OVERDUE FINES:
25¢ per day per item

RETURNING LIBRARY MATERIALS:
Place in book return to remove charge from circulation records

THE DESIGN AND CHARACTERIZATION OF A MINIATURE, NANOSECOND SPARK DISCHARGE FOR ANALYTICAL EMISSION SPECTROSCOPY

By

Gary Thomas Seng

A DISSERTATION

Submitted to

Michigan State University

in partial fulfillment of the requirements

for the degree of

DOCTOR OF PHILOSOPHY

Department of Chemistry

1978

ABSTRACT

THE DESIGN AND CHARACTERIZATION OF A MINIATURE, NANOSECOND SPARK DISCHARGE FOR ANALYTICAL EMISSION SPECTROSCOPY

By

Gary T. Seng

The design, construction, and characterization of a miniature, nanosecond spark is described. The present spark design features a coaxial, double-gap system powered by a direct current power supply. Pure argon continuously flushes the secondary gap. The analyte solution is nebulized via an ultrasonic nebulizer and desolvated in a heated chamber. The dry aerosol is swept into the analytical gap in a laminar stream of argon or helium directed either parallel to, or perpendicular to the inter-electrode axis. A quartz lens collimates the discharge radiation onto the slit of a programmable monochromator. A gated photomultiplier tube transduces the emitted radiation into an electric current. Integration of the photocurrent is performed under the control of digital time-resolution electronics with time windows adjustable in 0.1 μs increments. Timing is initiated by a fast photodiode-Darlington system

which monitors radiation from the secondary gap.

Time-resolved studies of the excitation temperature, ionization temperature, electron density, and background emission are presented and discussed.

For analytical determinations, the analyte emission line is selected under minicomputer control. Additionally, the minicomputer directs the time-resolution circuitry, acquires emission data, and performs statistical calculations.

The miniature spark has been found to be an excellent source for the determination of a number of elements including Ca, Al, B, C, Si, P, Mo, Cu and others.

To My Entire Family,

My Parents,

and Leslie

ACKNOWLEDGMENTS

First and foremost, I wish to thank my wife, Leslie, my Parents, my Brothers, my Grandparents, my Relatives, and my Friends for their love, encouragement, and guidance through the years. I only hope that I can repay even a fraction of their past sacrifice and support in the future.

During my stay at Michigan State, a number of people aided me in reaching my goals and many of them have become extremely close personal friends. To this group, I offer my deepest and sincerest thanks, best wishes, and hopes for frequent contact in the years to come. A special note of gratitude is due to my coworker, Sandra, Gene (Hero), Dan (Rock), Roy (Evil), Marty, Dave, Ed, Mike, Jim, Kathy, Rytis and the entire Crouch Group, past and present. This they richly deserve for their advice, both personal and professional, their support, and many, many indescribably good times.

My thanks are sincerely extended to Dr. Stanley R. Crouch, my preceptor, and Dr. Andrew Timnick, my conscientious Second Reader, for their guidance and friendship. Furthermore, I owe thanks to Dr. Fred Horne and the Department of Chemistry for my teaching experience (and salary), my teaching awards, and an introduction to the world of management. The Department is also due recognition for the excellent research facilities and technical services

provided. More specifically, I thank Ron Haas, Len Eisele, and Jerry DeGroot of the electronics, machine, and glass shops, respectively.

A final note of thanks is expressed to Michigan State University for being the great institution that it is, to Dow Chemical for the loan of needed research equipment, and to Peri-Anne Warstler for converting my scrawlings to something presentable.

TABLE OF CONTENTS

Chapter Page

Chapter Page

LIST OF TABLES

LIST OF FIGURES

I. INTRODUCTION

A spectrochemical Source is a device which converts an analytical sample (gas, solution or solid) into an atomic vapor and provides the energy necessary to excite a certain fraction of the analyte atoms to electronic levels above the ground state. The spectrochemical source thus serves as a sample atomizer, as well as an excitation source. It can be viewed as a transducer whose output is $(N_A)_j^*$, the number of density of excited analyte atoms in the jth electronic energy state. The input to the source is C_A, the concentration of analyte-containing molecules in the original sample. The ratio of $(N_A)_j^*/C_A$ is the transfer function of the source is generally an extremely small value. An inspection of such fundamental principles permit one to envision an "ideal" spectrochemical source.

The "ideal" spectrochemical source might be characterized in a number of ways. However, some of the more general and desirable characteristics are:

1. good sensitivity to all analytes;
2. no background emission;
3. controllable excitation energy;
4. ability to examine samples in any form;
5. no chemical, spectral or physical interferences;
6. accurate and precise results;

7. rapid and low-cost analyses;
8. simple construction and simplicity in use;
9. compactness and portability; and
10. safety for the operator.

Through the years spectroscopists have repeatedly attempted to create such a source with varying degrees of success. Unfortunately, although a variety of ingeneous and useful spectrochemical techniques have been developed, no source available today can claim to approach the "ideal" source. This is substantiated through the literature where one finds a continuing effort to develop and evaluate analytically useful sources.

Modern atomic emission techniques include flames, arcs, plasma jets, sparks, and the high frequency plasmas. Each source exhibits unique good and poor qualities when compared to the "ideal" case. The task of the emission spectroscopist is to select the optimum source for the particular analysis to be performed from the resources available. Intelligent selections are made by recognizing the strengths and weaknesses of each technique.

The primary advantages of conventional flames are simplicity, low cost, and good reproducibility; especially for solution analyses of easily excited atoms (alkali metals, alkaline earths, etc.). These qualities account for their extreme popularity as spectrochemical tools. On the other hand, flames suffer from several types of

severe interferences which limit their utility in a number of applications. Furthermore, the flame provides a rather low excitation energy, and is limited in the extent of energy variation. To reduce both problems, a multitude of burners, fuels and oxidants have been employed. However, routine users often avoid the inconvenience and danger associated with many of the varieties on the market and simply resort to other techniques when faced with problem analytes.

The family of electrical discharge devices classified as arcs reduces or eliminates many of the interferences normally observed in the flame. Due to the continuous, high-temperature, high excitation-energy conditions which exist within the arc, the technique is extremely sensitive to a wide variety of elements. Furthermore, the analyst generally has some control over the excitation energy. Disadvantages include poor precision, bulky, expensive electronics, and problems associated with sample preparation. Solid samples or solution residues provide the most favorable results and are almost exclusively used.

The DC plasma jet is an attempt to meld the high temperature characteristics of the arc and the reproducibility of the flame. Although the precision is much better than that of the arc, the detection limits do not reach those attainable by flame emission; nor do flame interferences disappear to the extent predicted.

To realize the full potential of the technique, a large concentration of an easily ionizable element must be combined with the analyte solution. As a result, the DC plasma jet has not enjoyed widespread use.

The classical high-voltage spark discharge preserves the high temperature and controllable excitation energy of the arc, while affording greater precision in the final results. Large continuum backgrounds, ionization interferences, and radio frequency (RF) noise generation are the major problems associated with the spark. As in the case of the arc, bulky electronics are necessary and most early work involved solid samples or residues. However, more recently, solutions have been analyzed as well.

The high frequency plasmas have received a great deal of prominence in recent times. This is especially true for the RF and microwave-induced plasmas. The major reasons stem from two characteristics which are the high temperature and a flame-like nature; i.e., those sought for the plasma jet. The high-frequency plasmas exhibit substantial freedom from matrix effects, respectable precision, and good detection limits for a number of elements. The most serious drawbacks are the expense, bulk, and problems incurred when attempting to introduce solutions into the torch. To avoid extinguishing the plasma regularly, rather complex electronics are necessary.

The performance of the introduction system is also extremely critical. These requirements have limited the use of such techniques for routine analyses.

The miniature, nanosecond spark was developed at Michigan State University (1-3) as a viable addition to the sources previously described. The instrument consists of a small coaxial spark source, a Veillon and Margoshes (4) introduction system, a monochromator and photomultiplier modular combination, a data acquisition system, and a minicomputer. The introduction system produces a dry aerosol which is swept into the spark gap using an argon carrier gas. Emission results as the spark discharges between two thoriated tungsten electrodes. The radiation emitted is collected by the monochromator and passed to a photomultiplier tube for conversion to the current domain. The current produced is transferred to a series of transducers which ultimately yield numerical data. Good precision and ease of sample introduction are provided by the discontinuous nature of the plasma. The spark source has been coaxially designed for maximum power, a spark of nanosecond duration, and freedom from significant RF noise. These properties permit the use of compact low-power, electronic supplies to produce the discharge, and virtually unshielded digital circuitry in the vicinity of the spark source. It is therefore possible to employ boxcar integration of the emission

photocurrent which drastically improves the analytical results. The spark, in essence, appears arc-like through a delayed examination of the discharge. In a comparison of overall expense and simplicity, the miniature, nanosecond spark fares well against arcs, conventional sparks and the high-frequency plasmas. Furthermore, it has been found to be an excellent source for the determination of a variety of elements including those which form refractory oxides. However, continued research on the system by several workers suggested that a number of modifications might be beneficial.

It is readily apparent when examining today's numerous, complex spectrochemical instruments that the loss of analytical information through the separate components is quite large. Although it is the heart of the system, an "ideal" source is only one of the "ideal" units which are necessary to construct the "ideal" instrument. It seems appropriate to apply the cliché, "a chain is only as strong as its weakest link", to spectrochemical instrumentation.

The approach taken in this research follows the "weakest link" philosophy. Each successive unit of the miniature spark was examined and modified in an attempt to produce a more "ideal" instrument. Improvements have been made on the nebulizer, the gas flow system, the spark design, the electronic triggering device, the optical system, the boxcar integrator, and the entire data

acquisition system. The software and hardware developed permit the user to control the boxcar integrator, as well as collect, manipulate, store, and print the data from a console.

In the chapters of this dissertation which follow, a brief survey of the recent literature relevant to the present work is first presented. In Chapter III, the instrumentation which was developed to improve the miniature spark is described in detail, while in Chapter IV, the minicomputer software necessary to control the instrumentation and to acquire and analyze the data is described briefly. Chapter V deals with the characterization of the improved spark source, both in terms of its physical properties, and its analytical capabilities. The final section of this dissertation is a commentary which examines the present status of the miniature spark and offers the author's views on its future.

II. HISTORICAL

A. Introduction

To understand the use of the relevant literature in the redesign of the original miniature spark, one must first examine the key papers concerned with its conception. After presentation of the major design considerations and the results obtained from analyses, it is then possible to discuss system modifications on the previously developed miniature spark instrumentation intelligently. The section entitled the "Modified Miniature Spark Design" deals with the bases for the instrumental changes made excluding the introduction systems and the time resolution electronics. The introduction systems are described in a separate section of this Historical, while the electronics are presented in a later chapter.

B. Original Miniature Spark Design

1. Miniature, Nanosecond Spark Source Design

The miniature, nanosecond spark (MNS), reported by Zynger and Crouch (1,2), was originally designed to be a short duration pulsed light source for fluorescence lifetime measurements. Such sources have been previously

reported with flash durations of 20 to 350 ns (5,6), These sources produce a short, high-power, capacitative discharge between two tungsten electrodes. Various atmospheres are employed to produce the radiation required. Zynger developed the MNS to achieve lower pulse widths (7 to 15 ns) and high electrical power dissipation (on the order of 10^7 w) by building a coaxial capacitor directly into the source. Due to the fact that the MNS provides rather large amounts of energy over very short periods of time and retains the classical spark characteristic of good precision, it was felt that the source should also function well as a spectrochemical tool for the analysis of samples externally introduced.

2. Spark Solution Techniques

For a variety of reasons, solutions are extremely popular spectrochemical samples (1). Although arcs and sparks are generally associated with solid samples, solution methods have also been under development for some time. The earliest methods involved spark-to-bulk techniques whereby the spark passes between one solid electrode and the surface of a liquid (7,8). These systems suffer from solution spattering problems. As a result, later researchers developed the spark-to-thin-film techniques which include the rotating disk and porous-cup designs (9,10). Although these methods show some

improvement over spark-to-bulk techniques, some spattering is still observed, as well as solution uptake problems. Spark-in-spary techniques offer somewhat of a reduction in spattering by introducing the solution as a fine mist which is passed through the spark gap (11,12). However, great care must be taken to avoid contamination of the sparking region. Furthermore, the spark-in-spray method does not show any real improvement in sensitivity due to the inefficiency of particle desolvation by the discharge.

To improve the sensitivity of a number of spectrochemical techniques, various researchers have developed desolvation systems to remove the solvent from the analyte prior to introduction into the excitation cell (3,13,14). Desolvation of the aerosol alleviates many of the problems incurred in the spark-in-spray method, and appears to be an attractive feature for spark solution analyses. The MNS employs such a system to produce a desolvated aerosol which is then introduced directly into the discharge (1,3).

3. Time-Resolution Spectroscopy

Since 1900 it has been known that the continuous background and atmospheric lines present in a spark discharge disappear before the analyte lines become prominent (15). Given this fact, it seems apparent that

the observation of the total emission of a spark results in a large amount of analytically useless information. In a process known as time slicing, the observation of the emission is delayed for some preset time interval relative to the beginning of the discharge. Thus, early, large background-to-analyte emission ratios and the associated optical noise problems are avoided. As a result, the use of this method increases the sensitivity of the spark to virtually all analytes. Modern spark researchers have taken the timing process one step further by limiting the observation time of the discharge in addition to providing the initial delay period. This method, known as time resolution, increases the sensitivity of the spark even further due to the fact that spectral information is collected only during the period of time yielding the maximum analyte signal-to-noise ratio. A great deal of spark research has been aimed at the construction of time-resolution and time-slicing instrumentation for both photographic and electronic detectors. Optical shutters, rotating mirror and rotating disk assemblies, and photomultiplier gating circuits have been studied as time-resolution devices (16-19).

Recently, the photoelectric detector-electronic gating methods have become popular due to their good precision and to advances in electronic component technology. Walters (20) and Piepen and Schroeder (21)

described a modern integrated circuit version of the vacuum tube gated integrator constructed by Steinhaus, et al. (19,20). Zynger (1,3) used a circuit similar to those presented previously to time resolve the MNS. The electronics, which were employed, involved a dual gating system whereby both the photomultiplier tube and the solid state integrator become active after some preset delay period. The use of this monostable timing system permitted one to sample the spark emission over time intervals of approximately 2 to 100 μs with delay intervals over the same range.

4. MNS Characterization and Applications

After constructing the MNS and using it as a light source, Zynger (1,3) evaluated the system as a spectrochemical instrument. Studies indicated that the excitation temperature varies between 4300 °K and 3800 °K as time (following spark initiation) increases from 2 to 20 μs. On the other hand, the ionization temperature ranges from 6600 °K to 5200 °K from 2 to 30 μs. The difference in the excitation and ionization temperatures indicates that thermodynamic equilibrium is not achieved during the period of observation. As is expected from the temporal difference between the background and analyte emission, each particular element exhibits a maximum signal-to-noise ratio at a different time relative to spark

initiation. Zynger studied the signal-to-noise versus time profiles for a number of elements and determined the MNS detection limits for these same elements. The MNS was found to have better detection limits than either the flame or the inductively coupled plasma for silicon and phosphorus. The values for boron and carbon were found to be superior to those of flames, while calcium and molybdenum results proved to be better than those obtained using the inductively coupled plasma. Matrix effect studies were also performed and the results indicated that the effects of cesium and aluminum on the emission of calcium (neutral and ion) can be reduced or eliminated by properly choosing the observation time. However, since the effects of the matrix are smallest early in time, the signal-to-noise ratio is decreased and the calcium detection limit increases.

In our laboratory, Glass (22,23,71) performed a sizable amount of unpublished work which further characterized the MNS. The research included physical design changes to vary the spark capacitance and inductance, carrier gas studies, interelement and anion effects, and real sample analyses. His findings indicated that the MNS is a viable instrument for real sample analysis, although sample introduction problems, memory effects and an increase in background emission somewhat limited its usefulness.

Lantz (24,25) reported the use of the MNS as a gas and liquid chromatographic detector. The system was found to be a successful, element-specific addition to the family of detectors now available. In addition to the ease of selectivity, the MNS provides sufficient information for the user to determine the empirical formula of the analyte.

C. Modified Miniature, Nanosecond Spark

In spite of the well-documented evidence for the fine performance of the MNS as a spectrochemical tool, the work performed by former researchers, as well as early work of the author and co-worker Sandra Koeplin, pointed out several general areas where the method might be improved. The suggested improvements are directly aimed at increases in the precision and overall sensitivity of the technique.

1. General System Modifications

A number of factors contributed to the overall noise observed in the final analog signal obtained from the MNS and, thus, to imprecision in the data. Optical noise appeared to be the primary source of noise. This noise is generated as a result of spark "wander", i.e., the movement of the discharge channel away from the axis

joining the electrodes. Some of the factors that influence the spatial stability of the spark include the stability and direction of the gas flow, the electronic circuitry, the geometry and condition of the electrodes, and the composition of the discharge region (1,26). The MNS employs needle-point electrodes to reduce "wander" due to electrode geometry. However, the gas flow is directed perpendicular to the inter-electrode axis and this, combined with variations in the flow rate due to the introduction system was thought to be largely responsible for the observed spatial instability. Several workers have found that increased stability is obtained if a thin stream of gas is directed through a hole in one of the electrodes (21,26,27).

Walters and Goldstein (28) published a classic article which discusses designing and sampling spatially-stabilized spark sources. They indicated that the best flow system consists of a thin laminar jet of gas directed from a small cone surrounding the anode towards the cathode. This would more readily lend itself to use with the MNS introduction system than would gas flow through the electrode. However, it must be pointed out that none of the authors were faced with the additional problem of using the stabilizing gas to nebulize solutions and carry particulate matter into the discharge. Walters and Goldstein also advocated the use of a high-frequency,

unidirectional source to stabilize the discharge further. The original MNS, being a critically-damped discharge, is unidirectional, but is definitely not high frequency.

A reduction in optical noise is also possible through partial isolation of the charging circuitry from the analyte gap. This can be accomplished by adding a secondary gap which is generally purged by a well-stabilized, uncontaminated gas flow (29-31). The double gap circuit permits one to increase the excitation energy, while ensuring a constant breakdown potential at each particular secondary gap length without disturbing the analytical gap. Rather than use a classical spark gap for control, several researchers have turned to encapsulated systems such as the hydrogen thyratron (30,32). The advantages of these tubes include the ability to initiate the spark reliably from a remote, accurate pulse source and the fact that sensitive adjustments of the gap length are unnecessary. Since imprecision in timing is another major source of noise, the hydrogen thyratron might first appear to be an attractive choice as a secondary gap for the MNS. However, the tubes are somewhat expensive and limited in their electronic capabilities. It should be more advantageous to "free-run" the spark with a direct current power supply and use inexpensive photodetectors to determine the beginning of the discharge combined with precise digital timers to perform time resolution. Electronic noise can be minimized through proper, hard-

wired circuitry layout, proper shielding, and expeditious conversion of the signal to the digital domain (33).

In this work, spatial stability and the stability of the breakdown potential were improved in the MNS through an axial, laminar flow of the carrier gas and a double-gap system powered by a direct current power supply. The correct choice of a direct current supply has permitted the user to increase the spark discharge rate for faster data acquisition. To retain the high power of the discharge, and to promote spatial stability, the discharge is somewhat over-damped. The data acquisition electronics included a fast photodetector, an accurate, precise digital timing network, a fast integrator, an analog-to-digital converter, and the electronics necessary to interface the system to a minicomputer or a microcomputer. Finally, improvements in multielement capabilities and the nebulizer are desirable and are discussed in the following sections.

2. Multielement Spectroscopic Measurement Techniques

Multielement analysis techniques have become increasingly important and popular as the number and complexity of analytical samples has increased. With the present demand for such techniques, the development of instrumentation has increased dramatically. Winefordner, et al. (34) divided the multielement detection systems into

temporal, spatial, and multiplex devices.

Temporal devices are the most common and include the rotating filter systems, the scanning or programmed monochromators, and the image dissector photomultiplier. Each of these methods requires some type of sequential wavelength selection, either through the wavelength isolation device, as in the case of the monochromators and the rotating filter system or the detector itself, as in the case of the image dissector (35). The rotating filter assemblies eliminate the need for the expense of a monochromator, and in addition, offer a larger spectral throughput. However, high background problems and poor resolution have generally limited their usage to atomic fluorescence. Both monochromator methods reduce background and spectral overlap problems, but they require some form of wavelength control. The scanning technique is limited by the response time of the detector and the measurement time allotted to each individual analysis line (36). The sequentially programmed technique is generally more complex, but is superior in that the spectral areas containing no relevant information are quickly passed by slewing through these regions. The image dissector involves an electronic scanning system which passes an electron image of the analyte line to an aperature. The image is electronically swept into the aperature and is then amplified using the classical dynode chain.

This has been found to be an excellent detector for atomic absorption and atomic emission (37,38). The major drawback is the cost of the apparatus.

The spatial devices, which perform true simultaneous multielement determinations, include polychromators combined with photomultiplier tubes and slits (direct readers), or with silicon vidicon detectors, or with photodiode arrays. The direct reader is the oldest and most sensitive of the three, but is expensive and limited to a number of specific lines by space considerations. The photodiode arrays provide the means by which one may examine a complete portion of the spectrum (39). The major drawback is the low sensitivity. Codding (40) used a linear diode array as a detector for the MNS and found that the detection limits increased by a factor of at least 200 over those observed with a photomultiplier tube. Although the conventional silicon vidicon tube possesses approximately the same sensitivity as the photodiode array, recent developments in vidicon technology incorporate image intensifiers into the detector which greatly enhance the signal power and make the device much more attractive (35).

Multiplex techniques, such as Hadamond transform spectroscopy and Fourier transform spectroscopy, use a single channel detector, yet simultaneously record several spectral components by encoding the information in the

frequency domain (34). Both methods require computer facilities capable of handling the sophisticated software. In general, for ultraviolet and visible work, the techniques are at a disadvantage when compared to spatial and temporal techniques.

Busch and Morrison (35) concluded that at the present state of technology, the programmable monochromator and the intensified vidicon tubes show the most promise as multielement tools. Winefordner, et al. (41) agree to a certain extent, but feel that the choice should be based on fundamental considerations, such as signal-to-noise characteristics and the complexity of the sample. In another earlier work, Winefordner and co-workers (42) concluded that at the present "state-of-the-art", the vidicons and diode arrays would find only limited use for atomic emission.

Since the previous MNS equipment was easily interfaced to a programmable monochromator system, and since the single channel photomultiplier detector is less expensive and more sensitive than other detectors, it was felt that this method of multielement analysis would prove to be the most advantageous. The design of such a system necessitates the use of a dependable means of wavelength determination (35). Dawson and co-workers (43) have constructed an instrument which employs an electrooptical device to determine the wavelength accurately. More recently, Malmstadt and Cordos (44,45)

described a multielement system which employs an encoder to track the monochromator. The encoder is a compact device which fits easily inside a commercial monochromator and produces electronic pulses as the drive chain is moved. Due to the fact that the monochromator described in the Malmstadt paper is the same make and model as that now in use in the MNS, an updated version of the Malmstadt design was found to be a viable method for MNS multielement work.

D. Methods of Sample Injection (Introduction)

Although sample injection is known to be extremely important in achieving good analytical results, it has not received the amount of attention that sources or techniques have received. Obviously, poor injection will result in low sensitivity and may provide a large source of unwanted noise. With recent advances in sources, wavelength isolation techniques, background correction techniques, and data acquisition systems, atomic spectroscopy may rapidly be approaching the point at which the sensitivity of a determination is limited by the process of sample injection. Therefore, it is important to examine the methods of sample introduction for possible incorporation into the MNS system.

Zynger (1,3) initially used a Beckman total-consumption burner to create a liquid aerosol which was directed

into a Veillon and Morgoshes (4) desolvation chamber. This nebulizer was relatively inefficient and was replaced with a modified design. In spite of the improvement observed in the emission, pneumatic nebulizers of this type are inefficient, require large operating gas flow rates and pressures, and in the case of the MNS, partially cause optical noise problems (23,46). For the MNS, other introduction systems may prove more advantageous.

Electrothermal atomizers, such as the various furnaces, carbon rods, and loops or strips, have been extensively employed in atomic absorption and atomic fluorescence spectroscopy (48). They offer the advantages of requiring small sample volumes and performing pre-analysis ashing and desolvation (47). In the case of the MNS, the atomization step would reduce problems associated with particle loss through the introduction system and remove one energy requirement of the discharge. However, due to the transitory nature of the atomized gas and the spark discharge itself, as well as the large dilution effects of the carrier gas, the inherent sensitivity of these techniques would be low. A crude electrothermal graphite braid atomizer has been studied as an introduction system on the MNS with the predicted results (23).

Sample boats, sampling rods and microprobes are generally associated with flame analyses (48). As is the

case with the electrothermal atomizers, small volumes of both solid and liquid samples can be analyzed by placement of the sample container directly into the flame. Unfortunately, the use of these injection systems with the MNS would introduce the imprecision due to sample placement and flame fluctuations, in addition to the problems encountered with the electrothermal atomizers.

Chemical vaporization methods have been reported by a number of authors (48-51). The process is based on volatile compound formation by elements in groups IVA, VA and VIA, as they are exposed to suitable reducing agents. The gases generated are swept into the source by a carrier gas. In the case of the MNS, the technique may suffer from problems similar to those of the electrothermal atomizers, and furthermore is limited to a few elements. On the other hand, it provides an interesting way to determine a group of elements which are generally difficult to determine.

To reduce the time-consuming work involved in solution preparation of certain difficult samples (geological, metal, etc.), several researchers have developed rather unique methods for solid sample introduction. Gilbert (52) and Willis (53) suspended finely ground samples in solvent mixtures for aspiration into flames. With finely-ground samples, other workers utilized vibrations from pulsating pistons or ultrasonic generators to create a

cloud of material which is carried into the source (48). Jones, et al. (54) and Fassel, et al. (55) reported a rapidly moving arc sampler for use with solid metal samples. With the exception of the arc sampler, the solid samplers would be difficult to interface to the MNS.

A large portion of everyday solution analysis is performed with nebulizers which generate an aerosol from the sample. In addition to that previously explained as a part of the original MNS, two other nebulizers have recently gained prominence. The crossed-flow nebulizer described by Davies, et al. (56) consists of two adjustable channels placed perpendicular to one another. As gas is fed through the venturi and over the perpendicular capillary, liquid is drawn into the gas stream and is converted to a fine mist. The design permits easy interchange of various sizes of capillaries and venturis. Valente and Schrenk (57) modified the design by using stainless steel hypodermic syringes for gas and liquid flow. Fassel and co-workers (58) simplified the crossed-flow system and introduced glass capillaries in place of the hypodermic syringes. They found that the flow rate of gas necessary to operate the nebulizer efficiently was as low as 0.8 ℓ/min with a pressure of 25 psi. Recently, Donahue and Carter (59) have further simplified the use of the nebulizer by constructing the Fassel design so that the capillaries are easily adjustable.

In contrast to the pneumatic nebulizer which is based on gas pressure, ultrasonic nebulizers generate liquid aerosols through ultrasonics. Modern ultrasonic systems employ radiofrequency generators in the range of 20 KHz to 6 MHz to supply a piezoelectric transducer with sufficient energy to create an aerosol from liquids placed on the surface (48). Although ultrasonic nebulizers are much more complex than are pneumatic nebulizers, they enjoy such advantages as producing smaller, more uniform droplets of controllable size, and independence of aerosol generation from the pressure and flow rate of the carrier gas (64). A number of ultrasonic nebulizer designs have been reported in the literature (60-66). In addition, several researchers have studied the performance of such systems (67-70). Comparisons of ultrasonic and pneumatic nebulizers have shown the former to be superior in all cases. Recently, Fassel, et al. (46) developed a well-designed ultrasonic system for use with an inductively-coupled plasma. This system is now available commercially as a product of Plasma-Therm, Inc.

Due to their excellent performance and the ease of interfacing the crossed-flow and ultrasonic nebulizers to the MNS, these nebulizers have been examined as possible alternatives to the original MNS nebulizer.

III. SPARK INSTRUMENTATION

A. Introduction

The general, overall configuration of the present MNS system is outlined in Figure 1, while Figure 2 is a photograph of the instrument. The analyte solution is drawn up to one of three possible nebulizers either through pressure differentials within the nebulizer or by an external peristaltic pump. The nebulizer produces a fine mist which is directed into a heated chamber similar to that of Veillon and Margoshes (4). There desolvation occurs and the resulting mixture is passed through a modified Friedrichs condenser to remove the solvent vapor. The dry salt particles are swept through the analyte cone in the MNS housing and along the inter-electrode axis in a laminar flow of argon or helium. The secondary gap is continuously flushed with tank argon. A high voltage power supply charges the coaxial capacitor located at the top of the spark housing to the breakdown potential of the system. Spark discharge radiation is monitored by a photodiode-Darlington trigger in the secondary gap and a spectrometer in the analyte gap. The trigger pulse signifies the beginning of the discharge to the gated integrator (or sample-and-hold) circuitry which is employed to time resolve the emission from the MNS. In the analytical gap, the spark atomizes the

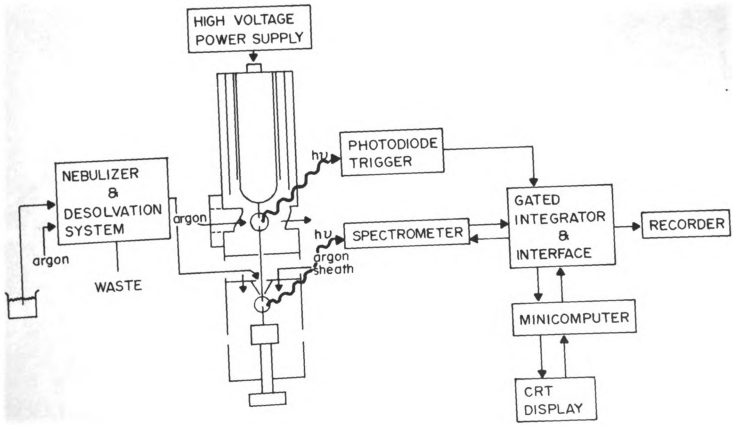

Figure 1. A diagram of the MMF system.

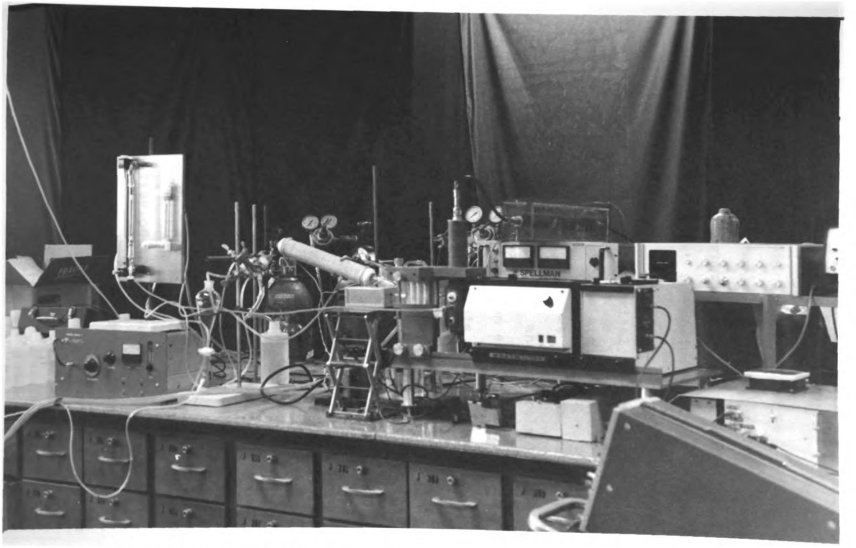

Figure 2. Photograph of the MNS system.

salt particles and excites the atomic cloud produced. Emission from the discharge is collimated to fill the entrance slit of a programmable monochromator and passed to a gated photomultiplier tube. The signal obtained by integrating or sampling the photocurrent is available for direct output use by a recorder and oscilloscope, or as an input to an analog-to-digital converter. In the latter case, the digitized data are accessible to a minicomputer. The minicomputer stores the data, performs simple statistical calculations, and controls the monochromator and the time-resolution electronics. Manual control of the timing circuitry is also provided. A detailed description of the MNS design is presented in the following sections. Separate discussions are apportioned to the introduction system, the spark housing and electronics, the data acquisition circuitry, and the minicomputer. Optimum operating conditions and physical MNS determinations are primarily left to Chapter V.

B. MNS Description

The present MNS source design was developed to increase the spatial stability of the discharge, and to reduce background emission fluctuations by decreasing the influence of the analytical gap on the breakdown potential (28,31). An explanation of the MNS source can most

conveniently be treated by dividing the system into two sections. The physical description of the housing is first discussed followed by the power supply and the spark circuitry.

1. MNS Housing

Preliminary work on the design of a simple prototype was performed by co-worker, S. Koeplin and myself. The present design, shown in Figure 3, was independently developed by S. Koeplin (72). The housing can easily be separated into four main sections. They are from top to bottom, the capacitor housing, the secondary gap housing, and the analytical gap housing, which consists of two pieces. The capacitor housing is similar to that developed by Zynger (1). It is constructed from two concentric copper tubes connected by a brass plate on one end. The inner tube runs the length of the housing and provides the ground connection to the bottom electrode of the analytical gap. A solid aluminum cylinder covered by a 0.02 in polyethylene sheath (Cadillac Plastics) fits inside the inner copper tube to form the coaxial capacitor. A high-voltage connector screws into the top of the aluminum cylinder to provide the electronic connection to the power supply. The most recent design is 3-3/4 in. longer than that shown in the diagram and features a removable capacitor for simplified maintenance and for quick

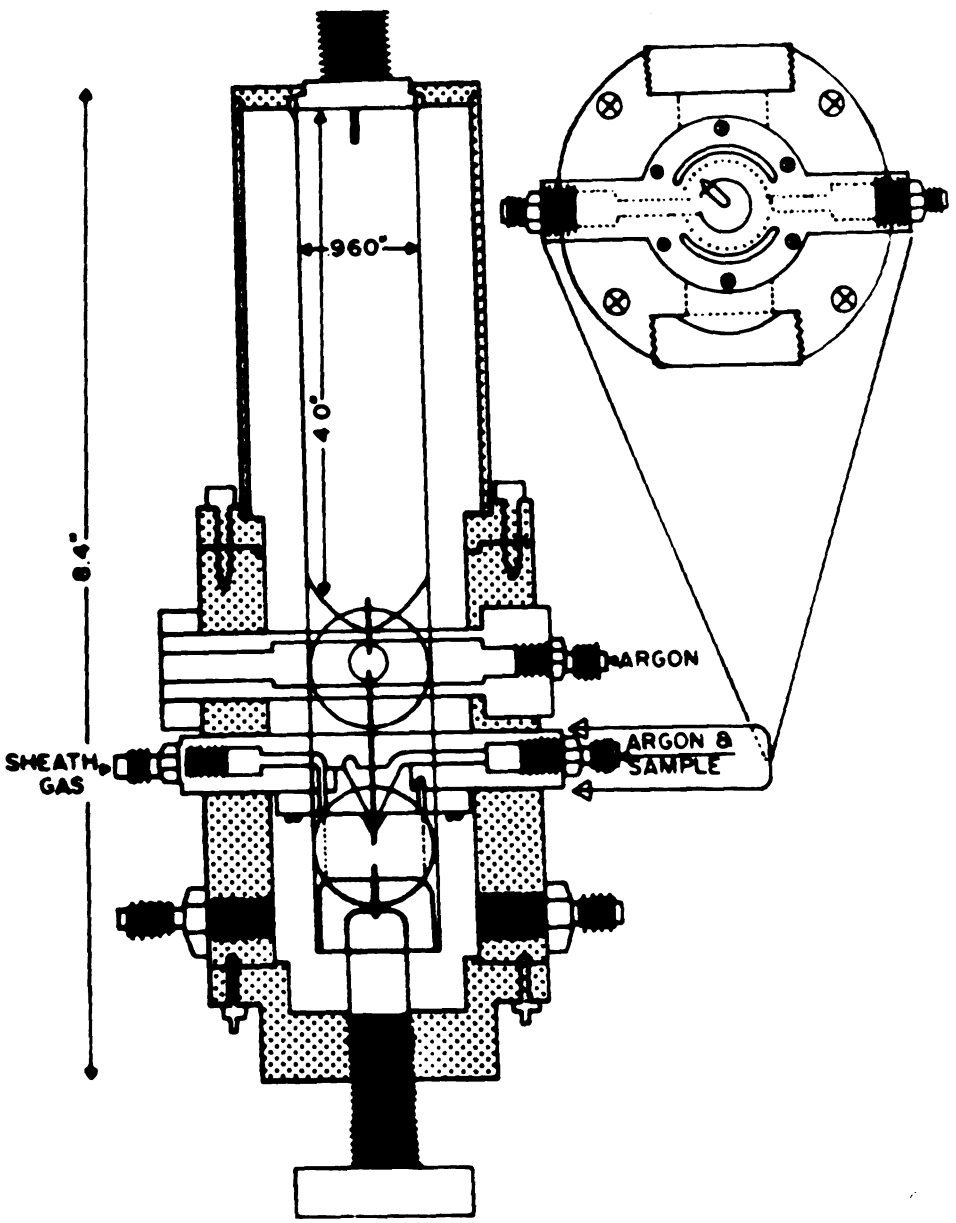

Figure 3. The MNS housing.

interchange of power supplies.

The brass secondary gap housing supports a teflon chamber with quartz windows and is similar in design to that reported by Lantz (24). Argon, monitored by a Gilmont flow meter, continuously passes through the secondary gap region. The discharge is formed between two 2% thoriated tungsten electrodes (Union Carbide, Linde Div.). A light pipe (Edmund Scientific), used to conduct emission from the secondary gap to an optical trigger system, passes through a teflon support in the brass housing, and butts up against one of the quartz windows.

The brass analytical gap housing supports a rather complex teflon gas flow system. The analyte stream from the heated chamber passes into this system via one of the male Swagelock fittings on the side of the unit. The analyte stream is guided into the cone surrounding the upper electrode and along the inter-electrode axis (note bottom view of flow system). A port on the opposite side of the unit is available for a sheath gas. If employed, the sheath gas flow parallels the inter-electrode axis. The length of the analytical gap is easily adjusted over a 1.5 cm range by twisting the threaded brass rod which extends from the bottom of the housing. A quartz lens of 1.0 in focal length is set 1.0 in from the center of the discharge to collimate the radiation produced. The vertical height of the lens is adjustable and it is

aligned with the gap following gap length changes. The lengths of both gaps are accurately determined using a reticle (Edmund Scientific) and an optical coupler developed by S. Koeplin (72).

2. Power Supplies and MNS Circuitry

To reduce the overvolting problems found in the original MNS, a direct current (DC) power supply (Spellman, UHR10P100, 10 mA at 10 kV) is employed in the present system. To current limit the supply during the discharge, a 1.0 MΩ, 100 W carbon film resistor (American Component Co.) has been introduced into the charging circuit. For safety and RF noise reduction, the resistor is totally enclosed in a plastic container, which in turn is surrounded by a Faraday cage. Current is delivered to the resistor and ultimately to the MNS coaxial capacitor via coaxial cable (Beldon, RG 8/u) and Amphenol connectors (82-843, 82-320). The DC supply has been found to produce sparks at repetition rate more than an order of magnitude higher than that found to be possible using the original MNS pulsed supply. It is also possible to use the original pulsed supply (Xenon Corp., 473A Nanopulser) by simply changing the coaxial capacitor system to that compatible with the supply. The pulsed supply needs no current limiting resistor and uses RG 58 c/u (Beldon) coaxial cable with appropriate Amphenol connectors (29100, 27025).

A simplified schematic diagram of the MNS is presented in Figure 4. To obtain the power necessary for high atomization efficiency and excitation energy, and yet use a small-sized power supply, as well as to simplify the time resolution process, the spark discharge should be nearly critically damped. Equation 1 indicates the relationship between the equivalent circuit resistance, inductance, and capacitance for such a discharge (76).

$$R = 2\sqrt{L/C} \qquad (1)$$

For a more complete understanding of the present MNS discharge, a semiquantitative solution to this equation is useful. The calculation of MNS values for R and L are presented in Appendix A. They are 210 Ω and 0.3 μH, respectively for a typical gap combination (secondary = 3.0 mm, analytical - 3.0 mm) in an argon atmosphere. The capacitance of the system has been found to be 350 pF (Chapter V, Section B1.).

Using the previously calculated quantities, the right-hand side of Equation 1 becomes 60 Ω. Since R was determined to be 210 Ω, the present MNS discharge appears to be somewhat overdamped. However, these semiquantitative calculations assume that the gap atmosphere is pure argon, while in reality, the analytical gap contains water vapor and some type of analyte(s) or analyte(s) and matrix

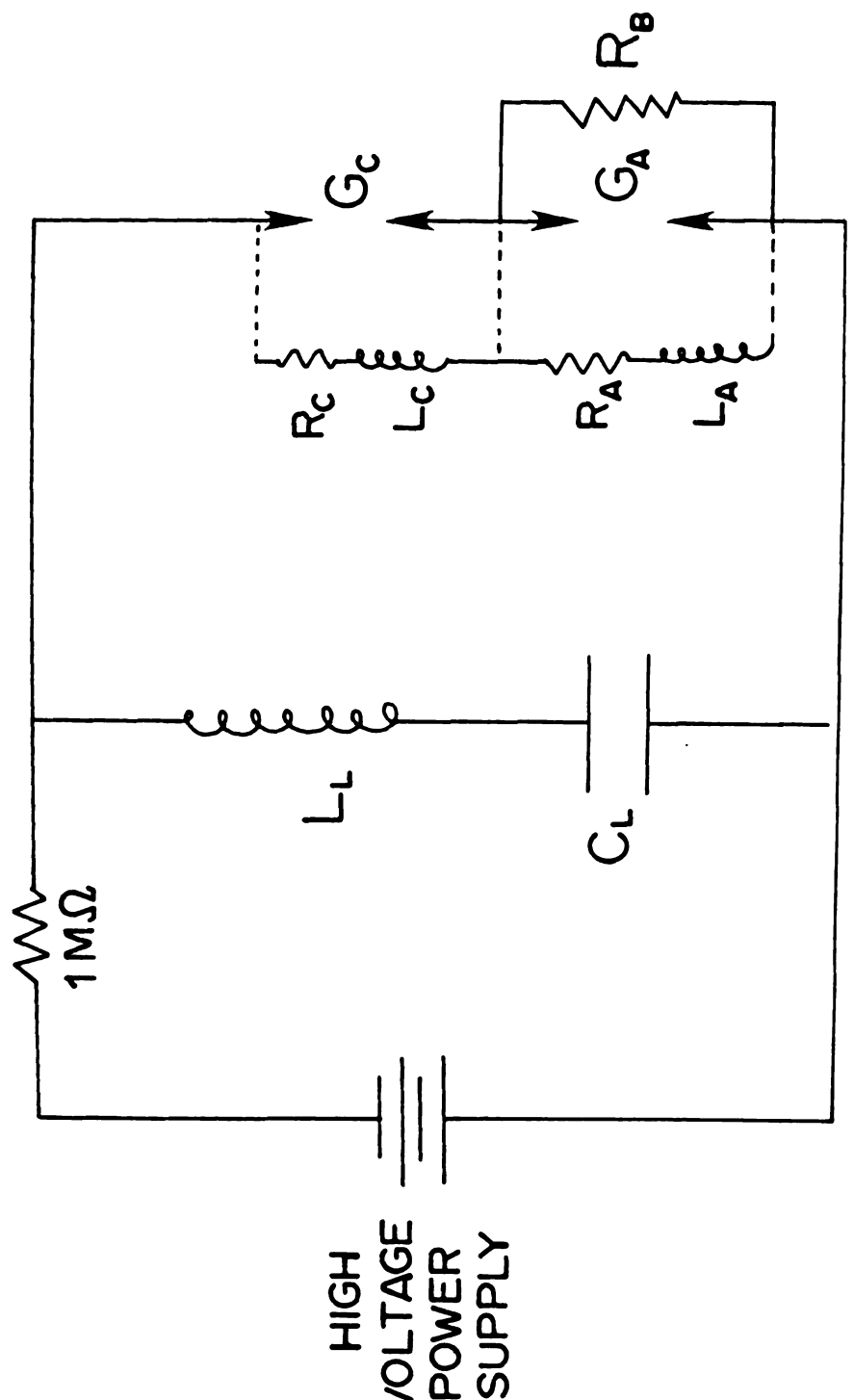

Figure 4. MNS high-voltage circuit.

which definitely change, and probably lower R and L (78,79). Therefore, from the calculations presented, it is difficult to exactly determine the extent of overdamping quantitatively. The true character of the discharge lies somewhere between the overdamped discharge described, and a critically damped discharge. Obviously, the use of other gases in the gap will greatly affect the discharge character by changing R and L.

The bridging resistor, R_B (10 MΩ or greater), is often employed in the MNS circuit. It decreases the influence of the analytical gap on the breakdown potential of the system (31). With this resistor connected, the bottom electrode of the secondary gap becomes a true ground. Gap breakdown occurs when the voltage on the capacitor reaches that amount necessary to initiate the discharge in this gap alone. Upon discharge formation, current passing through the resistor increases the voltage across the analytical gap quickly and, finally, this gap begins to conduct. During the period of time that the analytical gap is conducting, R_B presents a resistance which is too large to affect the discharge appreciably. Bridging resistors of this type are generally employed in classical double-gap sparks to stabilize the breakdown potential and, thus, the total spark energy.

C. Injection (Introduction) Systems

The modified Veillon and Margoshes (4) pneumatic nebulizer performed well in use with the original MNS system. On the other hand, coaxial-flow nebulizers are, as is the case with most pneumatic nebulizers, somewhat inefficient (46). Furthermore, the large operating pressure and flow rate become problems when interfacing this nebulizer to the present MNS flow system. Walters (73) stated that for flow systems similar to that employed in the present MNS, stability decreased for flow rates above 0.6 ℓ/min (a rather low flow rate to realize with any nebulizer). However, the crossed-flow and ultrasonic nebulizers described in this section perform efficiently at flow rates much nearer those required for good stability.

A desolvation system developed by Veillon and Margoshes (4) is employed with all three nebulizers to desolvate the sample. The apparatus, shown in Figure 5, is constructed from a cylindrical, glass, heated chamber and a modified Friedrichs condenser. The heat is supplied by heating tape (Biskeat, 768W, Brisco Mfg. Co.) which encompasses the chamber. At a Powerstat (Superior Electric Co.) setting of 55 V, under nebulizing conditions, the inside temperature of the chamber reaches approximately 160 °C. In the water-cooled condenser, 98% of the solvent (water) is removed (1). The dry aerosol is carried to

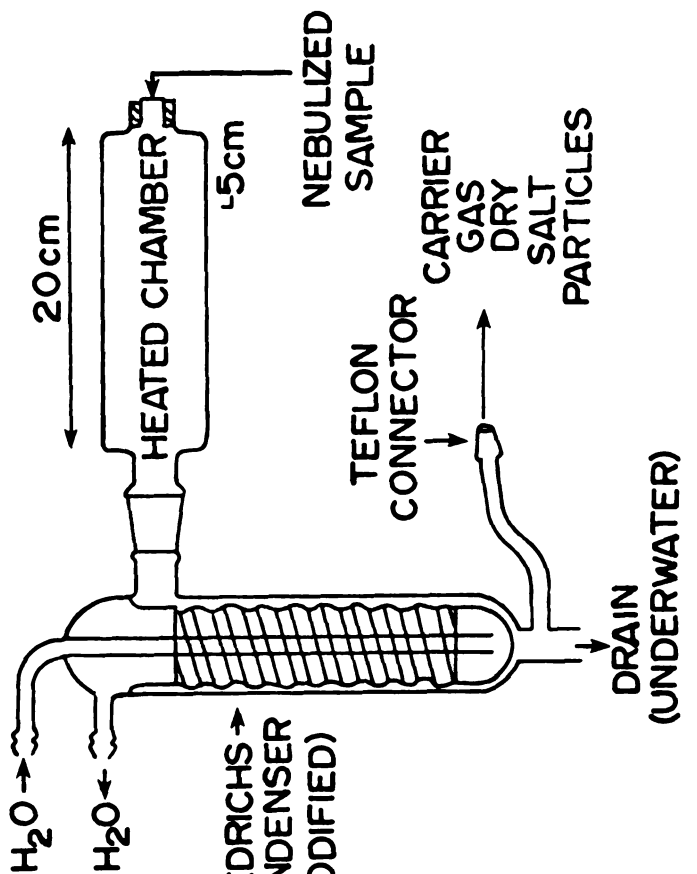

Figure 5. The desolvation system.

the spark housing through large bore tygon tubing. A tapped teflon connector couples the tubing to the male Swagelock fitting on the MNS housing.

1. Modified Veillon and Margoshes Nebulizer

For all MNS studies, Zynger (1) employed the modified Veillon and Margoshes (4) nebulizer as diagrammed in Figure 6. A teflon-coated stainless steel ball-joint fits over the nebulizer and serves to seal it to the heated chamber. Solution is directly aspirated into the heated chamber. For original MNS use, normal operating conditions were a tank pressure of 50 psi (3.5 kg/cm^2), an argon flow rate of 3.8 ℓ/min, and a solution uptake rate of 2.5 mℓ/min.

2. Crossed-Flow Nebulizer

Recently a crossed-flow pneumatic nebulizer has been reported by Fassel, et al. (58). A modified version of that nebulizer, which was used in this work, is shown in Figure 7a. Argon is directed through the horizontal capillary (0.23 mm tip orifice) at flow rates of 0.8 ℓ/min or greater (Ca. 25 psi). Solution is drawn through the vertical capillary (5 μℓ pipet, 0.28 mm i.d.) and nebulized into the aerosol chamber diagrammed in part b of Figure 7. Although, the solution capillary used is

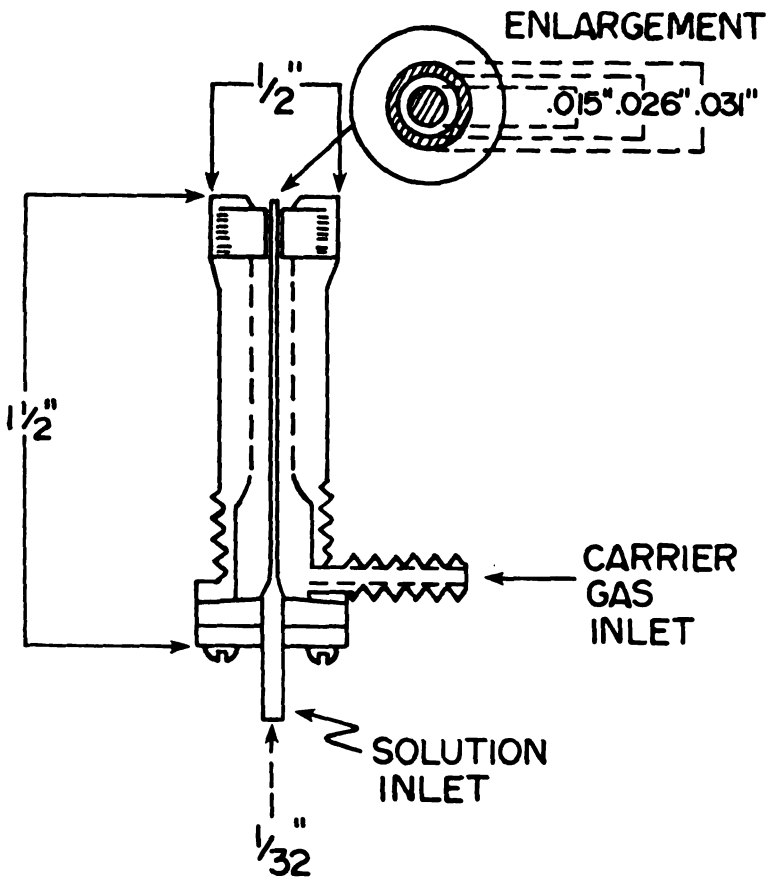

Figure 6. Modified Veillon and Margoshes nebulizer.

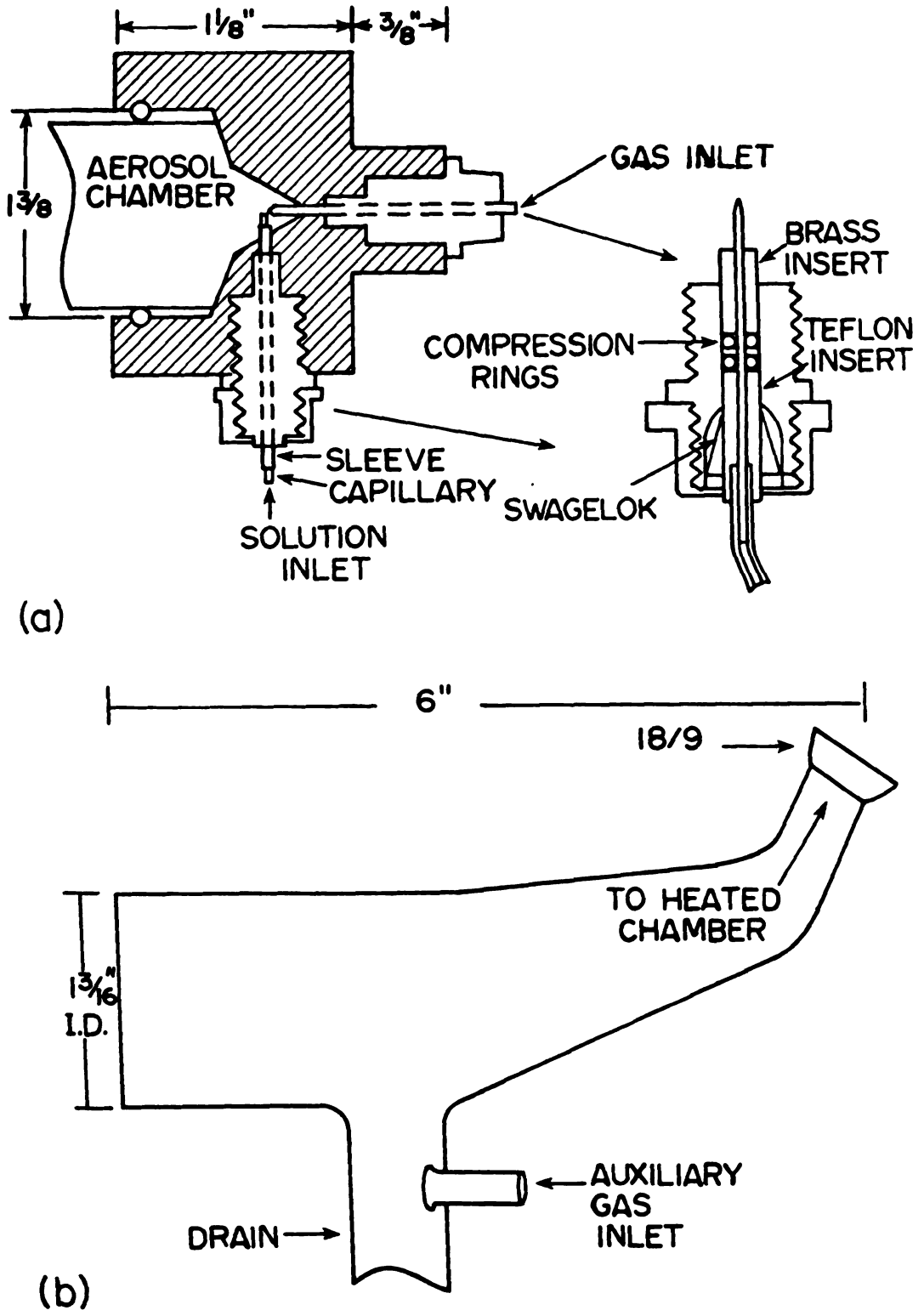

Figure 7. Crossed-flow nebulizer and aerosol chamber.

convenient and simple to adjust, the solution uptake rate is low (the original design employed a 0.25 mm orifice diameter). To obtain good results in the present design, it is better to pump the solution through the capillary. A peristaltic pump (Ismatec) operating at 2.3 mℓ/min is used to deliver the solution to the nebulizer.

The capillaries are secured by compressing two O-rings which are seated between a brass insert and a teflon insert-Swagelock combination. Pressure is exerted on the teflon insert by tightening the external female Swagelock fitting. Optimum nebulization is observed to occur when the capillary to capillary distance is approximately 0.1 to 0.15 mm.

The aerosol chamber (Figure 7b) design has been described by Fassel and co-workers (46) for use with an ultrasonic nebulization system they developed. The design minimizes the number of large droplets which reach the heated chamber. The vaporization of such droplets cause gas flow pulsations which can lead to source instability. The aerosol chamber is easily interfaced to the heated chamber via an 18/9 male-to-male elbow.

3. Ultrasonic Nebulizer

A Plasma-Therm ultrasonic nebulizer (Model UNS1) has also been examined as a nebulizer for the present MNS. The design, presented in Figure 8, is extremely similar

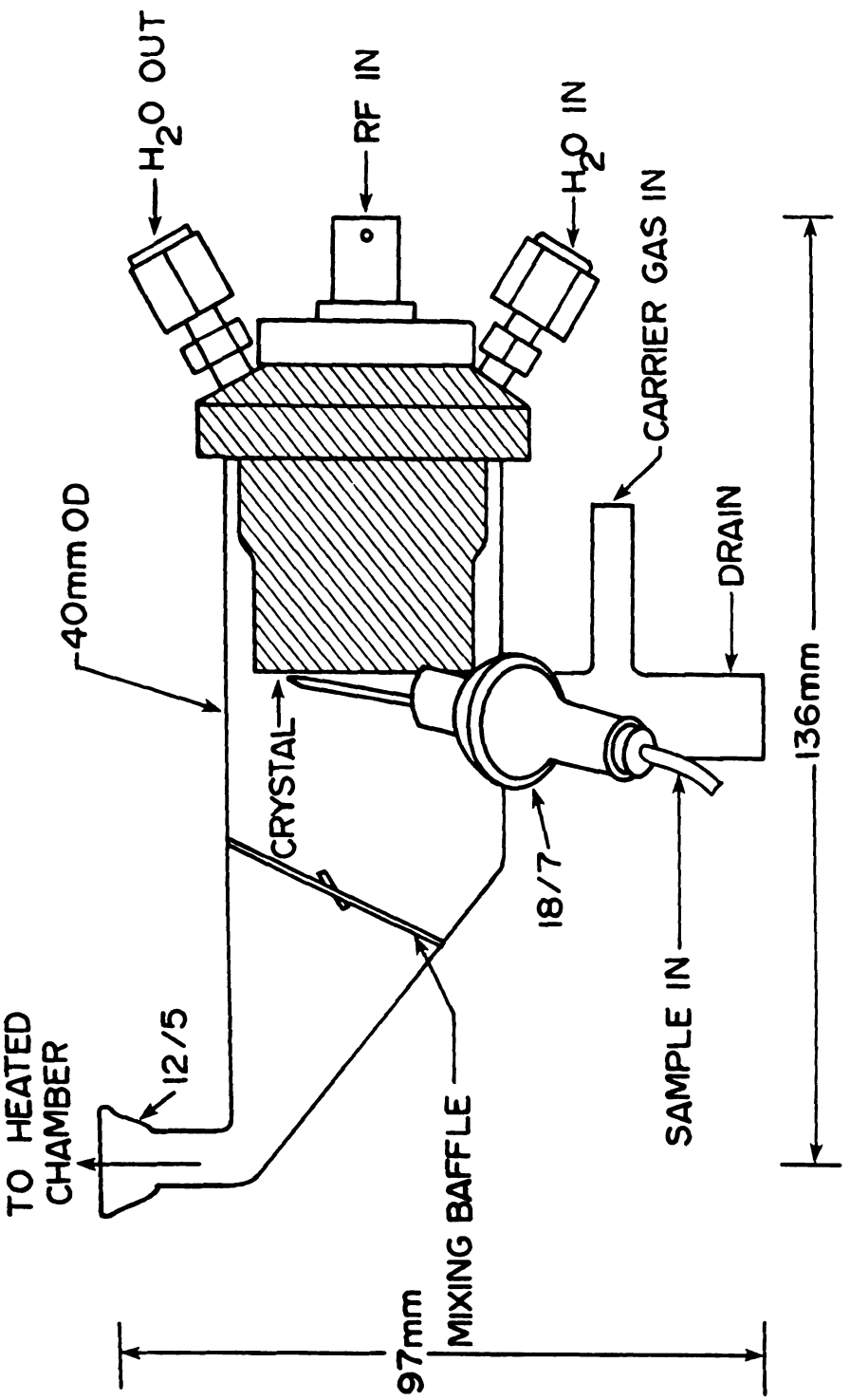

Figure 8. Plasma-therm ultrasonic nebulizer-crystal housing and aerosol chamber.

to that described by Fassel, et al. (46). The piezoelectric crystal is seated in a cylindrical teflon housing which permits a constant flow of cooling water to play over the back face. Electrical connections to the crystal are made through this chamber. Power is supplied by a 50W radiofrequency generator of variable frequency (1350-1400 kHz, see Figure 2). The analyte solution is pumped to the crystal through tygon tubing, followed by 1.0 mm (i.d.) polyethylene tubing, by a peristaltic pump (Ismatec). The delivery tube is positioned extremely close to, but not touching, the upper-center portion of the crystal face. The carrier gas is introduced through a side-arm in the drain tube to avoid flow obstruction by the condensed aerosol. Normal operating conditions include an incident power of 15W, 1.0 to 1.25 ℓ/min argon flow rate, and a solution delivery rate of 2.3 mℓ/min. However, unlike the nebulizers previously discussed, the ultrasonic nebulizer functions acceptably at argon flow rates as low as 0.3 ℓ/min or with helium as the carrier gas.

D. Data Acquisition Circuitry

1. Introduction

The MNS data acquisition circuitry consists of a fast trigger, gated integrate-and-hold electronics (or sample-and-hold), a computer interface, and a monochromator

interface. The heart of the system is housed in a modified rack mount (Varipak, Elco Corp.) as six printed circuit boards which plug into a backplane bus. The six mainframe boards are the delay scalar, the integrate scaler, the analog integrate, the clock/initialize/sample-and-hold, the primary computer interface, and the monochromator interface. The optical trigger, photomultiplier gate circuitry, and a portion of the monochromator electronics are external to the mainframe. Power is supplied by a commercial power supply (Power-One, Inc., HCBB-75W), which provides +5 and $\pm$15 volts.

Figure 9 is a functional outline of the data acquisition system. As the spark discharges, emitted background radiation from the secondary gap begins the timing sequence when it strikes the optical trigger. A pulse from the trigger circuitry enters the delay scaler and gates on a 20 MHz clock. The delay time required can be varied in 0.1 μs increments and is set either manually using rotary switches (0.1 to 99.9 μs), or via the minicomputer (0.1 to 409.6 μs). Upon the completion of the delay period, the photomultiplier gate returns all dynodes of the photomultiplier (PM) tube to their full operating tube voltages while either the sample-and-hold (S/H) or the gated integrate-and-hold (GI/H) begin to receive the photocurrent. If the S/H is selected on the front panel, the end-of-delay pulse initiates the sample function, whereas if the

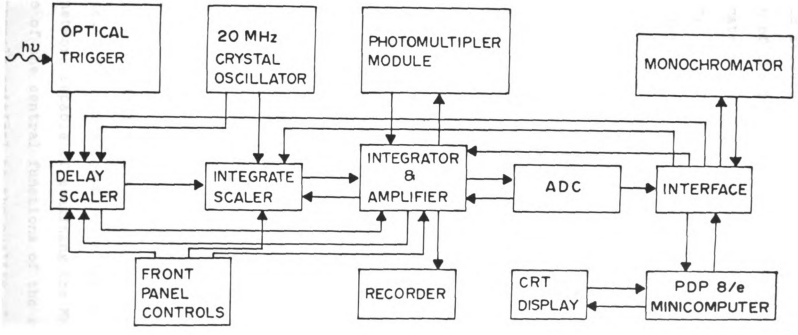

Figure 9. MNS data acquisition system.

GI/H is selected, integration begins under the supervision of the integrate scaler. User control of the integrate scaler is equivalent to that of the delay scaler. Amplification of the integrated signal can be manually adjusted from a gain of 1 to 100 in stages. Both the S/H and the GI/H pass their analog signals to the analog-to-digital converter (ADC). The GI/H signal is also available from a remote monitoring connector. The digital output of the ADC is accepted by the minicomputer through the interface. Spectral scans or fast multielement data collection is also possible under computer control via the monochromator interface.

To understand the capabilities and limitations of the data acquisition system more fully, a detailed examination of the circuitry is warranted. The remainder of this chapter is devoted to such an examination.

2. Timing Circuitry

To accurately characterize the discharge, observe early spark emission, and achieve optimum analytical results, a fast trigger and fast photocurrent measurement is necessary. The optical trigger, delay scaler, integrate scaler, PM gate, I/H and S/H, combine to form a fast data collection network capable of examining the MNS. Since timing is one of the central functions of the electronics and is extremely critical to the quality of the analytical

results obtained, the optical trigger, delay scaler, integrate scaler, clock, and PM gate are presented first. The entire system was constructed within the sequencer framework described by Crouch, et al. (74).

a. Optical Trigger

Studies of the MNS early in time require that the timing circuitry consistently detect the spark immediately after the onset of the emission. The original MNS relied on high-frequency noise to initiate timing. This was somewhat unreliable due to inconsistencies in the actual time of formation of the discharge. Glass (23) used a phototransistor (Ti164, Texas Instruments) to determine the time of formation optically in the manner shown in Figure 10a. Although the phototransistor is a step in the right direction, it is moderately slow (1.5 μs rise time) when compared to the sub-microsecond time scale in which the remainder of the MNS electronics operates.

Of the remaining optical triggers available, it was found that only the photodiode was sufficiently fast for possible application (1.0 ns rise time). These devices have been employed in laser research for some time. Unfortunately, they possess low spectral sensitivities and in stand-alone usage with the MNS, initial studies indicated that the photodiode could not supply the necessary current and voltage for direct interface to digital circuitry.

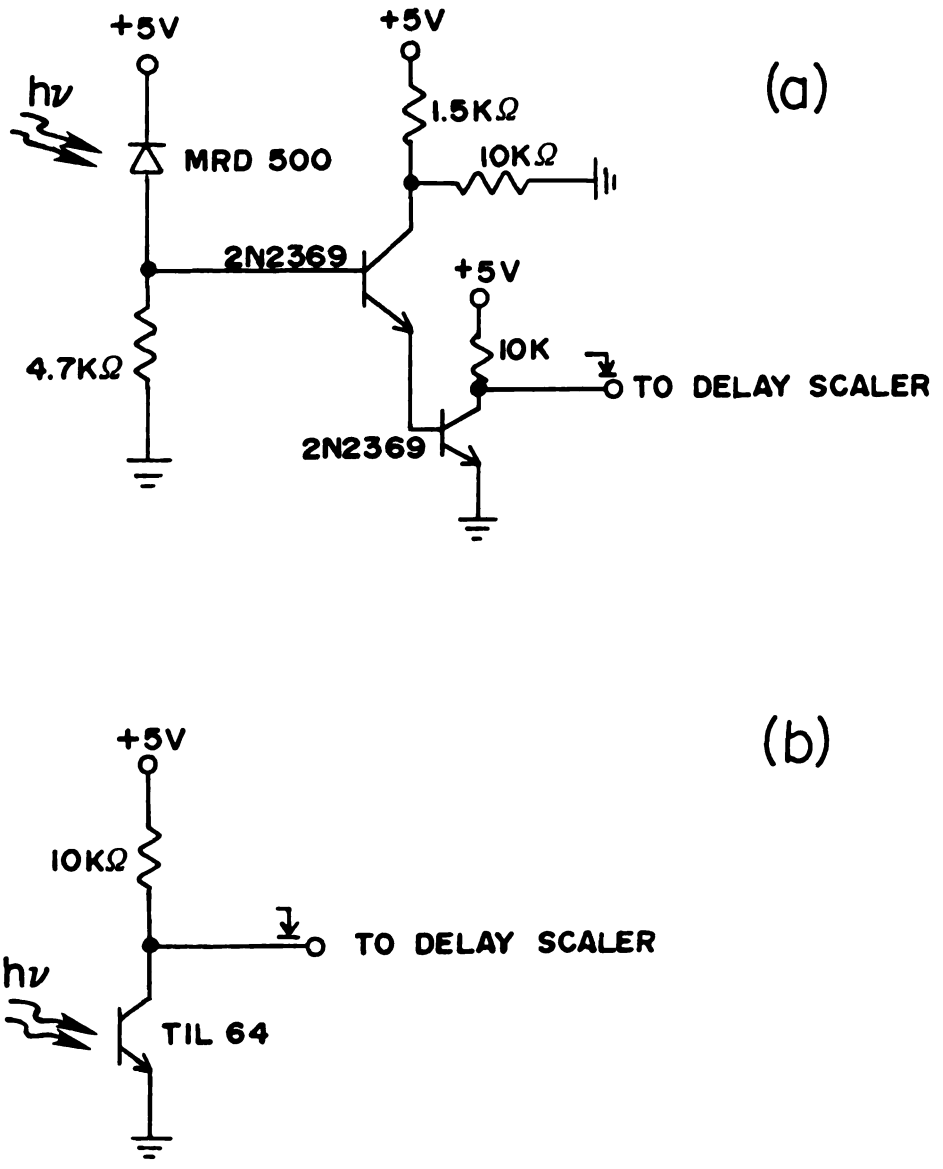

Figure 10. Optical trigger circuitry.

To increase the photodiode signal strengths to workable levels, fast video amplifiers are often combined with photodiodes. These combination units are commercially available, but are somewhat expensive and are easily ruined by high-frequency noise such as that created by the MNS. All attempts to construct a combination from discrete parts and use it as an optical trigger failed in spite of heavy shielding and other noise-reducing precautions.

The combination type optical trigger was abandoned in favor of the photodiode-Darlington circuit shown in Figure 10b. Emission from the secondary gap of the spark is transmitted to the photodiode via an optical light pipe. The 4700 Ω resistor to ground was chosen as a compromise between the RC time constant of the circuit and the voltage developed at the base of the first amplifying transistor. The use of greater resistance results in large rise times due to the 4pF capacitance associated with the photodiode, while smaller resistances result in voltages below the transistor threshold. In practice, the photodiode-Darlington circuit produces negative-going spikes with fall times of less than 75 ns duration and rise times of 200 ns. It has been found to perform well with either argon or helium in the analyte gap and for all gap distances examined. However, it fails when helium is used in the secondary gap due to the low background emitted by the discharge. In this case, the previously

presented phototransistor circuit must be employed.

b. Delay Scaler

The delay scaler (Figure 11) and the clock (Figure 14) combine to form the timing circuitry necessary to delay integration or sampling of the photocurrent following spark initiation. Figure 15 summarizes the timing functions of the MNS electronics. The magnitude of the delay time can either be set manually using front panel rotary switches or via the minicomputer under interactive user control. To ensure that the delay scaler is capable of handling the high-frequency clock and that the propagation delay through the timing chips is within reasonable limits on the 0.1 μs time scale, the timing circuitry has been constructed from Schottky TTL integrated circuits.

The timing sequence begins as the external trigger signal from the optical trigger signal sets an RS flip-flop (74S00, gates 3 and 4). This, in turn, gates on the external 20 MHz clock via JK flip-flop 1 (74S112-1). The output of this flip-flop supplies the cascaded counters (74S161, 1-3) with 10 MHz clock pulses. The magnitude of the delay selected by the user is contained in three 74161 binary counters. As the 74S161 counters are clocked, the outputs of both sets of binary counters (74S161 and 74161, 1-3) are continuously compared by three 74S85 magnitude comparators. Upon completion of the delay

Figure 11. The delay scaler circuit.

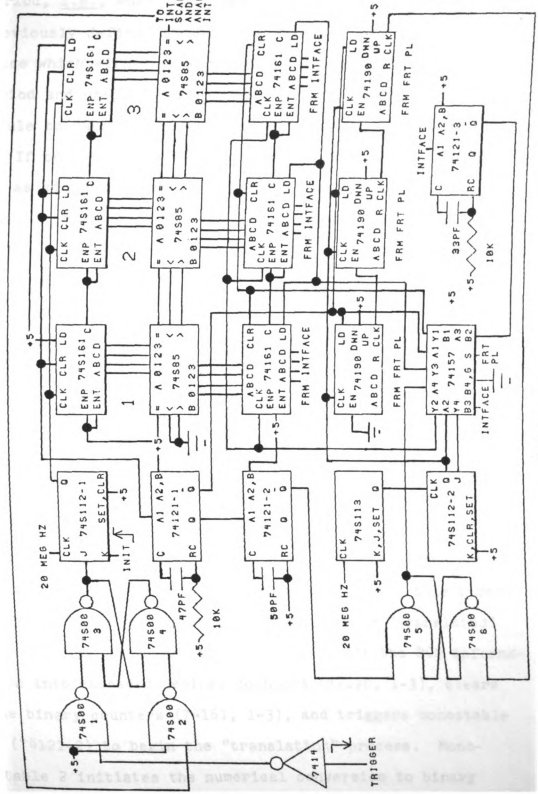
20 MEG HZ
INIT
47PF
10K
50PF
TRIGGER
TO INT SCALER ANALOG INT
FRM INTFACE
FRM FRT PL
INTFACE
33PF
10K

Figure 11.

period, i.e., when the number of clock pulses equals the previously defined number, the comparators provide a high pulse which either simultaneously starts the integrate period and photocurrent integration, or directs the S/H module to sample the photocurrent.

If the computer mode is selected, the 74161 counters act as simple latches. The binary number to be loaded into the counters is stored in the minicomputer Accumulator (AC) and is presented to the counter data inputs through the interface card. As the number appears at the inputs, a computer timing pulse draws the load lines low to complete the sequence. To assure correct loading, the clock inputs of the counters are held low by the $\overline{Q}$ output of a monostable (74121-3).

Under manual control, it is necessary to convert the decimal number set on the front panel rotary switches to binary. To accomplish this task, a three stage operation is necessary. First, the decimal information is converted to a BCD encoded number through a hard-wired network on the four-stage rotary switches. Next, this number is loaded into BCD counters, and finally is "translated" into binary. A monostable (74121-1) loads the BCD information into cascaded decimal counters (74190, 1-3), clears the binary counters (74161, 1-3), and triggers monostable 2 (74121-2) to begin the "translation" process. Monostable 2 initiates the numerical conversion to binary

approximately 0.4 μs following the previous end-of-delay by enabling JK flip-flop 2 (74S112-2). The 5 MHz clock pulses are directed to the clock inputs of both sets of counters simultaneously. As the decimal counters count down, the binary counters count up. When the cascaded decimal counters register zero, a ripple clock pulse from the most significant counter disables JK flip-flop 2, and the binary counters contain the binary equivalent of the decimal number requested.

c. Integrate Scaler

User control of the integrate scaler (Figure 12) is identical to that of the delay scaler. In operation, the integrate scaler is extremely similar to the delay scaler. Computer and manual control of the timing is accomplished in the same fashion. However, in the case of the integrate scaler, the end-of-delay pulse starts the integrate timer and the end-of-integrate pulse is bused to the analog integrate card alone. The RS flip-flop (74S00, gates 5 and 6), associated with manual control, is set by a pulse from the analog integrate circuitry following completion of the hold period.

Figure 12. The integrate scaler circuit.

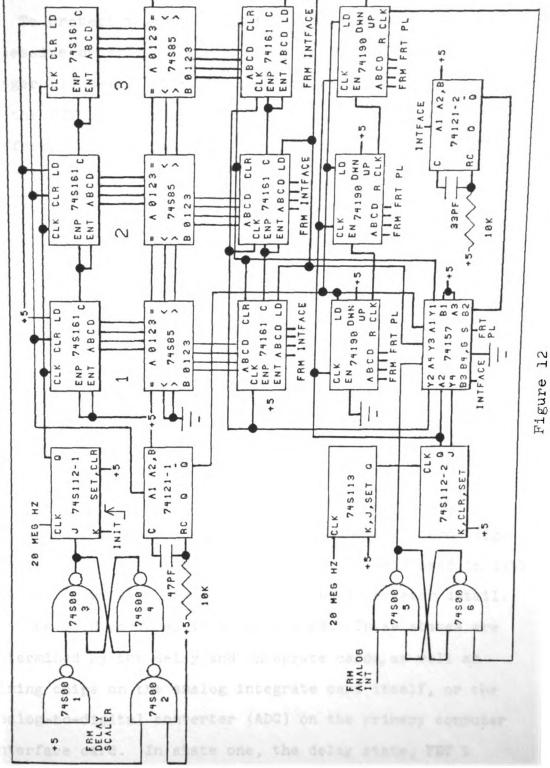
20 MEG HZ
74S112-1
74S00
74S121-1
47PF
10K
INIT
FRM DELAY SCALER
74S161 C
74S85
FRM INTFACE
74190 DWN UP
74157 A3
74S113
74S112-2
FRM ANALOG INT
TO ANALOG INT
INTFACE
FRT PL
33PF

Figure 12

d. Photomultiplier Gate Circuitry

To protect the photomultiplier (PM) tube from the excessive emission present early in the life of the spark, Zynger (1) designed a TTL compatible PM gating circuit. In the off state, this circuitry reduces the voltage difference between dynodes 2 and 3 of the dynode chain to 5 volts, thereby lowering the tube gain considerably. In the on state, dynodes 2 and 3 are returned to their normal 150 V difference, and the PM functions normally. In the present system, this gate is controlled by the end-of-delay and end-of-integrate pulses via an RS flip-flop on the analog integrate card (Figure 13).

3. Analog Electronics

The analog portion of the circuitry consists of the gated integrate-and-hold (GI/H) electronics on the analog integrate card (Figure 13) and the sample-and-hold (S/H) module on the clock/initialize/sample-and-hold card (Figure 14). Since the GI/H is almost exclusively used in data taking, it will be presented first and in greater detail.

The GI/H operates in three states. These states are determined by the delay and integrate cards, as well as timing chips on the analog integrate card itself, or the analog-to-digital converter (ADC) on the primary computer interface card. In state one, the delay state, FET 1

Figure 13. The analog integrate circuit.

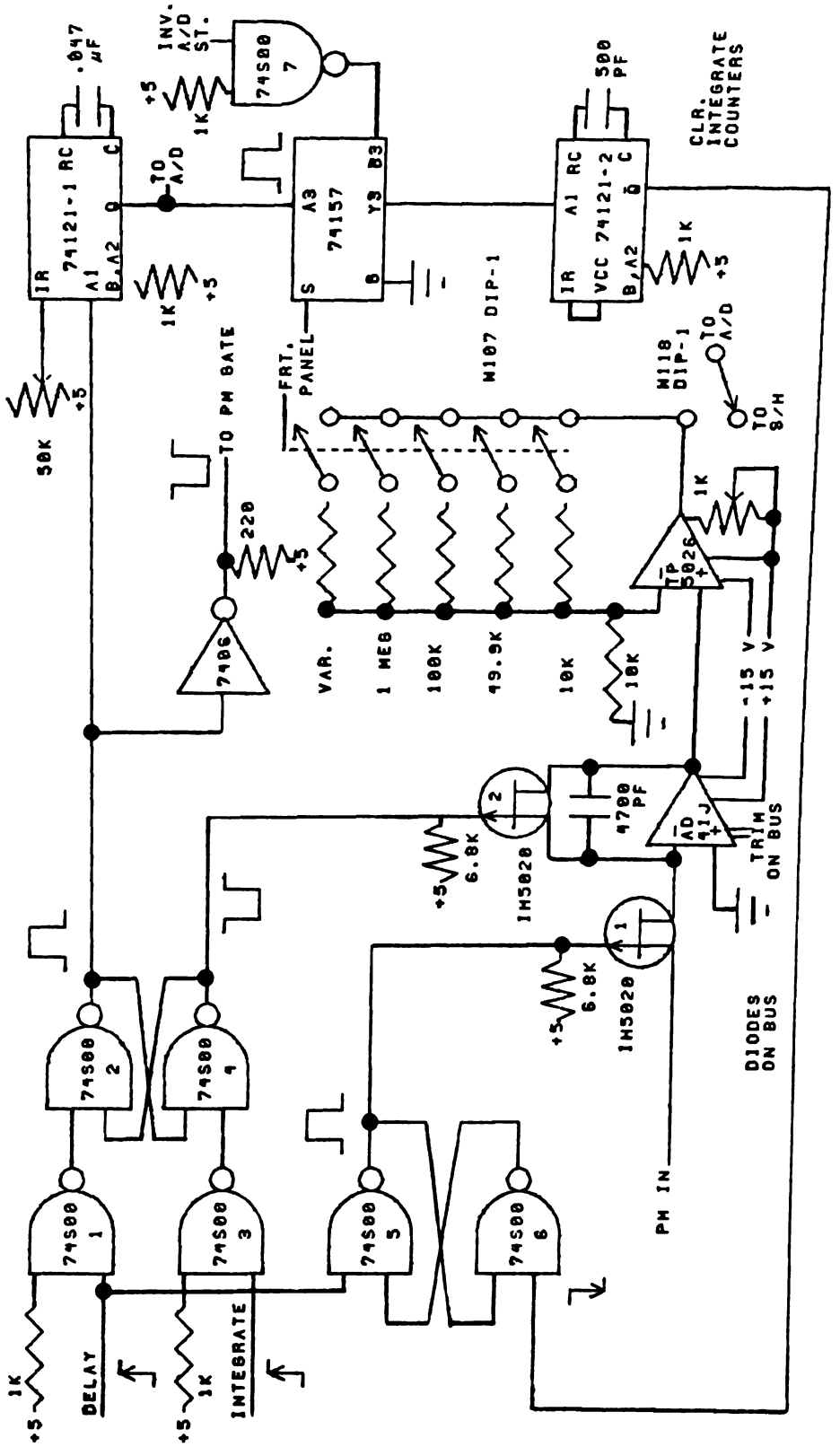
74S00 1
74S00 2
74S00 3
74S00 4
74S00 5
74S00 6
74S00 7
74121-1 RC
74121-2
74157
7406
IH5020
IH5020
5026
DELAY
INTEGRATE
FRT. PANEL
W107 DIP-1
W118 DIP-1
TO PM GATE
TO A/D
TO S/H
INV. A/D ST.
CLR. INTEGRATE COUNTERS
VAR.
1 MEG
100K
49.9K
10K
10K
50K
1K
220
6.8K
6.8K
4700 PF
500 PF
.047 µF
-15 V
+15 V
TRIM
DIODES ON BUS
PH IN

Figure 13

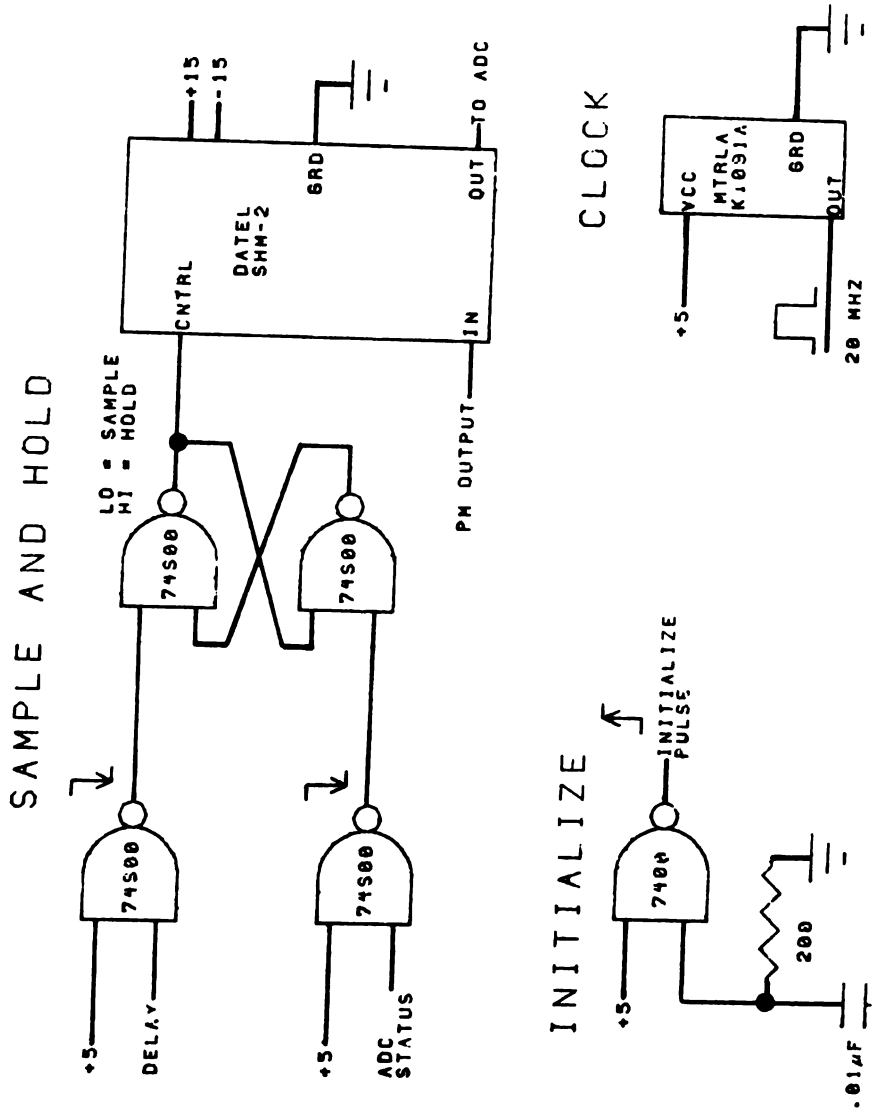

Figure 14. The clock/initialize/sample-and-hold circuitry.

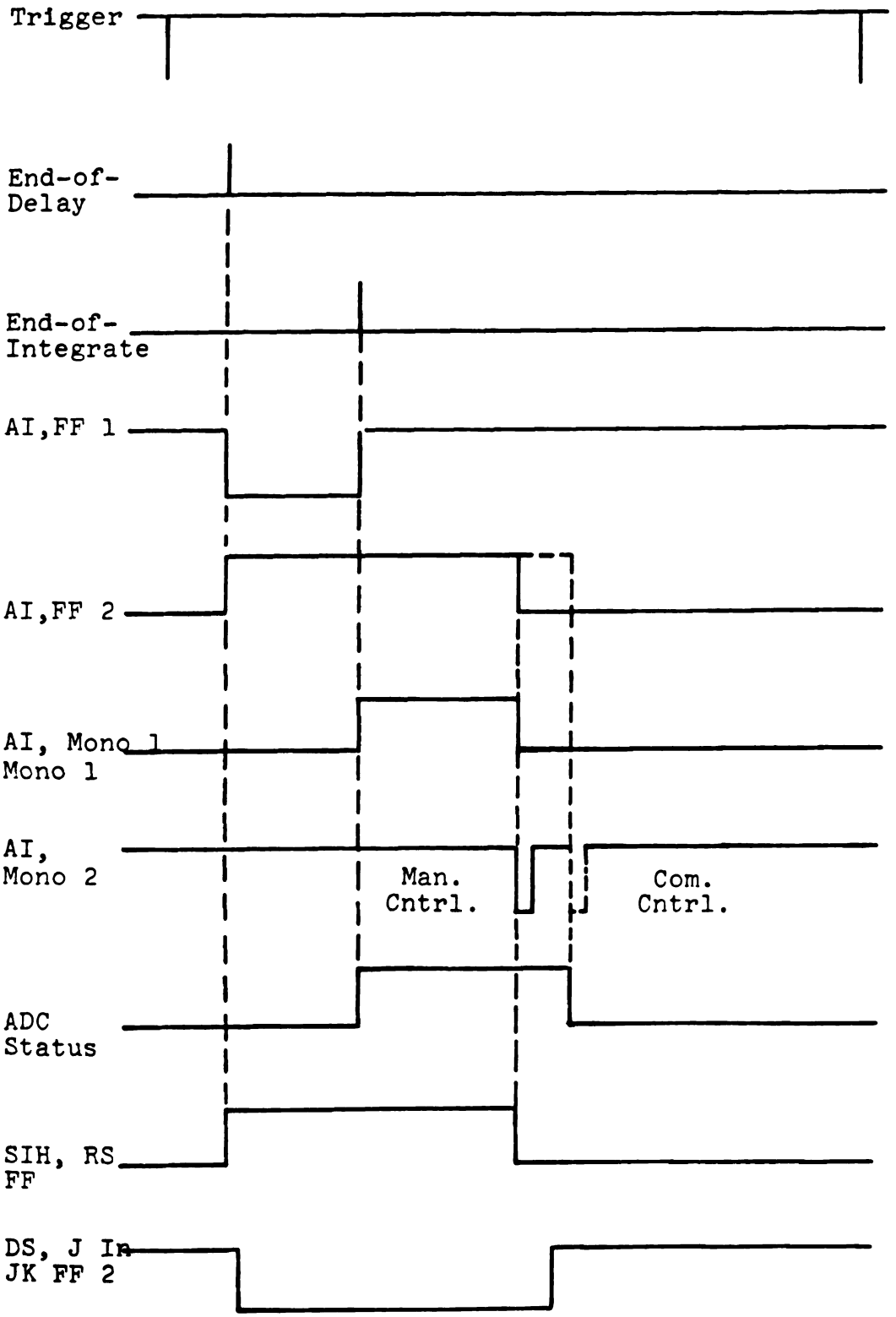

Figure 15. Data acquisition timing diagram.

(IH5020, Intersil) is open and FET 2 is closed. Thus, the integrator is or is in the process of being discharged and the PM output is "disconnected". In state two, the integrate state, the end-of-delay pulse sets the two controlling RS flip-flops (74S00, gates 2, 4, 5, 6). The $\overline{Q}$ output of RS flip-flop 1 (gates 2 and 4) opens FET 2, while the Q output of flip-flop 1 closes FET 1. Integration of the photocurrent is now possible. State three is the hold state. In this condition, the end-of-integrate pulse clears flip-flop 2 (sets $\overline{Q}$) and opens FET 1. The hold time of the integrated signal is determined by either monostable 1 (when the system is under manual control), or the ADC (when under computer control). If the manual mode is selected, the hold time is varied by adjusting a 50 kΩ potentiometer on the analog integrate card. To aid the user in the adjustment, the $\overline{Q}$ output of the hold monostable is available at the side of the mainframe. In the computer control mode, the ADC status line ends the hold state. In either case, the falling edge of the hold pulse triggers monostable 2 which closes FET 2 and returns the system to the delay state.

The 41J operational amplifier (Analog Devices), which performs integration of the photocurrent, was chosen for its low bias current (0.5 pA) and high input impedence ($10^{13}\Omega$). The 4700 pF integrate capacitor is of a polystyrene, low-leakage variety to permit long hold periods.

The 5026 operational amplifier (Teledyne-Philbrick) was chosen for the high open loop gain, high common mode rejection ratio and low offset voltage. The gain of the amplifier circuit is selected manually and ranges from a factor of 1 to 100. However, FET switching transients and non-linearity problems are observed at high gains. The output of the GI/H is available to the ADC and any other external signal monitoring devices the user may deem necessary. Generally, the output is connected to an oscilloscope. However, a recorder (Heath SR255-B) has also been employed. To smooth the output for recorder use, a second order passive filter (0.5 μF, 100-400 kΩ) is necessary.

The S/H module is a Datel SHM-2 selected for its speed (acquisition time < 100 ns, aperature time < 10 ns). The input to the unit is either the direct PM photocurrent, or a voltage proportional to the photocurrent provided by a Keithly 427 current amplifier unit. The end-of-delay pulse initiates the hold, and the ADC status line returns the module to the sample mode. At present, only computer control is possible. However, the circuitry is amenable to simple modifications which would expand the output capabilities to be equal to those available from the GI/H. The S/H system is generally not employed in normal spark usage due to imprecision observed in the data caused primarily by clock, computer and RF noise.

4. Minicomputer and Peripherals

Computer control of the electronics and data acquisition is provided by a Digital Equipment Corporation (DEC) PDP-8/e minicomputer. The core memory available is sufficient to support an OS/8 operating system and a complete FORTRAN IV software package. In addition to the mainframe, the system includes a DEC hard disk drive (RK05), and a Sykes dual flexible disk drive (model 7000) for mass storage, a Decwriter or Decwriter II (DEC) for hard copy production, and one of two possible interactive terminals with display (Applied Digital Data Systems consul 980, or Tektronix model 4006-1) for communication.

The PDP-8/e minicomputer provides an external bus for interfacing user-designed instrumentation to the system (75). The DEC KA8-E Positive I/O Bus interface board converts the internal omnibus of the PDP-8/e to that of an earlier DEC computer, the PDP-8/I which generates external synchronization pulses, and provides direct access to the Accumulator (AC) and to the Memory Data (MD) lines. Where user-designed instrumentation is interfaced to the computer, all programmed input/output (I/O) is accomplished through the KA8-E Positive I/O board.

5. Computer Interface

a. Introduction

Communication between the minicomputer and the MNS data acquisition electronics is performed via a rather lengthy communication network. Programmed I/O functions are available from the KA8-E board through an external Computer Interface Buffer (CIB, Heath Co.). The CIB is patched into a transmitter/receiver (T/R) unit which permits signal transfers over the 125 ft of distance between the minicomputer and the MNS electronics (47). The MNS interface is, in turn, directly patched into the receiver end of the T/R unit using standard 34 line ribbon cable and printed circuit paddles.

The programmed I/O sequence is initiated through execution of an I/O Transfer (IOT) instruction (75). During the execution, MD bits 3 to 11 are monitored by the Positive I/O Bus interface. Bits 3-8 carry the device select code indicating which peripheral is accepting or providing I/O. Interpretation of bits 9-11 by the KA8-E board results in the generation of any combination of three timing pulses (IOP). During an IOP pulse, the AC input and output lines are active for data transfer to and from the minicomputer. To complete the I/O process, it is often necessary to indicate to the computer that a peripheral is ready to transmit information to, or accept

information from the AC. One possible method involves the use of the skip (SKP) line provided by the KA8-E board. Implementation of this method is performed by designing the peripheral such that it sets a "flag" flip-flop when it is to be serviced. The computer repeatedly strobes the output of this flag via IOT instructions in a software DO loop. When the combination of the flag and IOT sequence is true, (i.e., the peripheral is ready to be serviced) the SKP line is asserted low and the computer skips out of the DO loop. The instruction following the SKP is generally another IOT instruction which transfers numerical information from the AC to the peripheral or vice versa. Data are passed from the MNS interface to the minicomputer in this fashion.

b. Primary Minicomputer Interface

The MNS computer interface performs four tasks. Delay and integrate times are passed from the AC to the appropriate cards. Data from the ADC are passed to the AC. The monochromator drive control is provided, and movement of the monochromator is monitored. The first two tasks are handled by the primary MNS interface and will be presented first. The latter two are handled by the monochromator interface through the primary interface and are discussed in the following section. The IOT instructions for all interface functions are presented

in Table 1.

The MNS primary interface is shown in Figure 16. Device select codes which appear on MD bits 3-8 are decoded by the 7442 device decoders and the 7402 NOR gates. Each incoming bit is clamped to ground through a 1N4148 diode. The IOP pulses and the INITIALIZE pulse are squared up on the interface paddle by an open collector NAND (7438, not shown). At the interface card, the signals are inverted and again sharpened using 7414 hex Schmitt triggers. The IOP pulses and the device select pulses are combined by AND gates (1-4) and NAND gates (1 and 2) to initiate the various interface functions.

The diode clamped AC out lines are directly connected to the latches (74161) on the delay and integrate scaler cards via the MNS backplane bus.

In addition to control of the delay and integrate time, the computer accepts data from the ADC (Burr-Brown, ADC80AG) through the interface. The process begins with a convert command from the analog integrate card (74121-1) at the end of the integrate state (this is also true when the S/H is used). The ADC is configured to produce a digital number in complimentary straight binary code for voltages between 0.0 V and +10.0 V. After completion of the conversion cycle, the status line of the ADC sets a flag (JK flip-flop, 7476). During the conversion period the minicomputer continuously performs a skip test and upon

Table 1. MNS IOT Instructions.

IOT Instruction	Description
	Primary Interface
6441	ADC Flag check (SKP test)
6442	Load Delay Scaler Counters
6444	Load Integrate Scaler Counters
6451	Clear ADC Flag
6452	Gate Data to AC
6454	Unused
	Monochromator Interface
6421	Clear Slew up Flag (Slew)
6422	Clear Slew Down Flag (Slew)
6424	Set Slew Flags (Halt)
6431	Scan Oscillator Code
6432	Set Scan Flag (Scan Up)
6434	Clear Scan Flag (Scan Down)
6461	Encoder Flag Check (SKP Test)
6462	Unused
6464	Clear Encoder Flag

Figure 16. The primary minicomputer interface circuit.

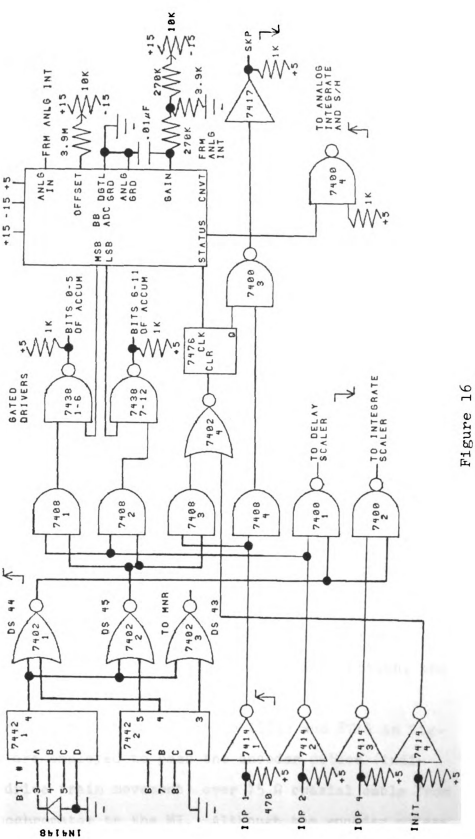
BIT #
7442
1 4
A
B
C
D
3
4
5
1N4148
7442
2 5
6
7
8
4
3
DS 44
7402
1
DS 45
7402
2
TO MNR
7402
3
DS 43
IOP 1
IOP 2
IOP 4
INIT
7414
1
2
3
4
470
+5
7408
1
2
3
4
7400
1
2
7402
4
7476
CLR
CLK
D
Q
GATED
DRIVERS
7438
1-6
7438
7-12
1K
+5
BITS 0-5
OF ACCUM
BITS 6-11
OF ACCUM
TO DELAY
SCALER
TO INTEGRATE
SCALER
+15 -15 +5
ANLG
IN
OFFSET
BB DGTL
ADC GRD
ANLG
GRD
GAIN
STATUS
CNVT
MSB
LSB
FRM ANLG INT
3.9K +15
10K
-15
.01μF
270K
3.9K
FRM
ANLG
INT
10K
7417
SKP
TO ANALOG
INTEGRATE
AND S/H

Figure 16

finding the ADC ready, drives the 12 data bits into the AC using 12 gated drivers (7438, 1-12). Finally, the ADC flag is cleared, and the data stored in memory for future use.

c. Monochromator Interface

To place the GCA McPherson monochromator (EU-700-77) and controller (EU-700-32) under programmable control, the interface shown in Figures 17 and 18 has been constructed. The monochromator interface (MI) receives all computer commands through the primary interface. In turn, the direction and movement commands are passed to the monochromator via a cable-paddle combination which plugs directly into the McPherson external bus.

In the scan mode, the system requires clock pulses and a direction. Clock pulses are provided by the computer at the maximum allowable rate of 200 Hz. The direction is selected by setting or clearing JK flip-flop 1 (7476). Slewing is initiated by providing a lo logic level to either the slew up or slew down line as is the task of flip-flops 2 and 3. To terminate the slew function, the slew flip-flops are simply reset.

A transmitter/receiver couple (8T13 and 8T14 in Figure 18) are employed to pass the encoder pulses (indicating drive train movement) over 75 Ω coaxial cable from the monochromator to the MI. Although the encoder pulses

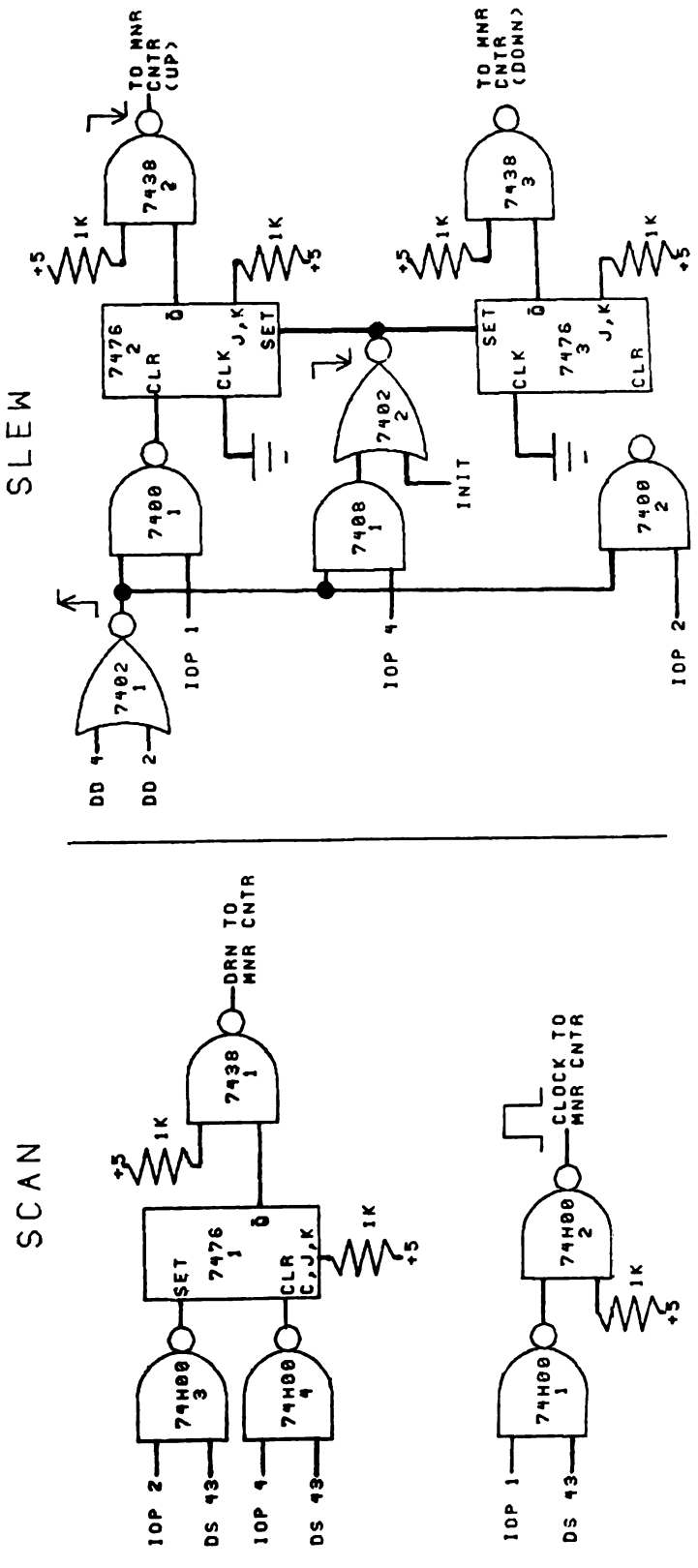

Figure 17. The monochromator interface circuit (scan and slew control).

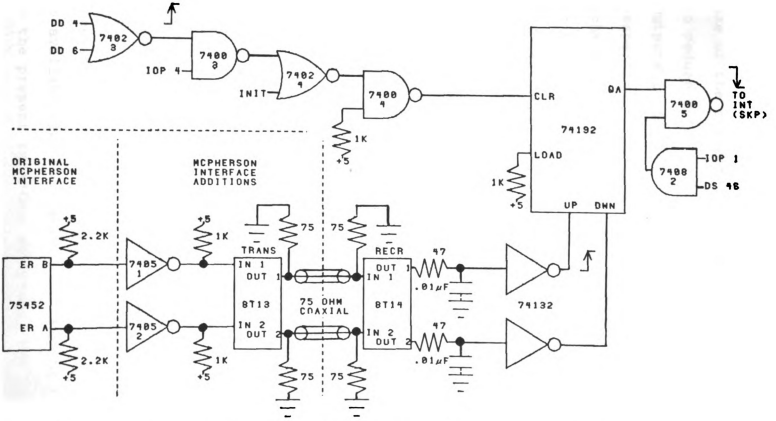

Figure 18. The monochromator interface circuit (encoder monitor).

are available through the external McPherson bus, the use of the separate, shielded communication lines appears to reduce noise problems which seem to plague the system. Outputs 1 and 2 of the receiver chip on the MI card are respectively the up and down movement pulses. The 74132 Schmitt triggers sharpen the pulses prior to passing them to the flag (74192). A positive skip test is indicative of one encoder pulse which signifies one step (0.1 Å movement). Each step is added to a software counter which monitors the progress of the movement.

6. Perspectives

Although the present electronics show definite improvements over earlier designs, there is still room for some major revisions. Rather than "tie-up" the minicomputer exclusively for MNS use, it should prove advantageous to interface the MNS electronic system to a microprocessor (MP). A resident MP would eliminate the need for the present complicated manual circuitry, and reduce noise problems associated with the PDP-8/e. High level calculations could be passed to the minicomputer. The technology necessary to multiplex several MP systems to the PDP-8/e is available in this laboratory. Due to its similarities to the present interface structure, the Intersil 6100 MP system should prove to be the most advantageous choice.

With total MP control of the system, the reduction in

the number of chips required to perform the timing function should permit one to incorporate all timing electronics into a one card network. This would reduce the complexity of the MNS backplane bus and substantially reduce circuitry noise.

Also included in timing considerations are the PM gate circuitry and the photodiode-Darlington trigger system. For early investigations in the life of the spark, it should now be possible to design a faster PM gate which could be enabled after small (<100 ns) delay times relative tc spark initiatien. Physical and electronic modifications to the photodiode-Darlington trigger system would increase the reliability and decrease the fall time of the unit.

Another major group of modificatiens applies to the GI/H system. The FET switches have continuously been a problem in achieving early spark investigations (due to the on time) and especially in high signal gain work (due to switching transient feed-through. Faster switching systems are now available to combat early observation problems. Furthermore, there has been some success in reducing transient feed-through by employing compensation circuitry which directs an equal spike of opposite voltage into the analog channel during switching periods. To further reduce analog noise problems, the ADC should be on the analog integrate card, rather than on the interface card. Finally, it would be moderately simple to replace

the present follower with gain by a programmable amplifier which would be under MP control.

Experience has shown that the present control of the monochromator is somewhat unreliable. To improve the performance, a more sophisticated control system should be developed, such as a modern version of that devised by Malmstadt and Cordos (45). The encoder counting circuitry conceptualized could take a form very similar to that used for the delay and integrate scalers.

IV. MINIATURE SPARK SOFTWARE

A. Introduction

Within the past few years, dedicated minicomputers have become a common sight in the analytical laboratory. In addition to decreasing data reduction times, the minicomputer has been increasingly applied to instrument supervision. Such automation has been the key in dealing with ever-growing laboratory work loads.

As a result of the recent tremendous upsurge in the number of resident minicomputers, and in response to user demands, vendors have developed sophisticated software packages to accompany their hardware systems. Such operating systems bring programming and minicomputer-user communication to a level that permits a high degree of versatility and yet is easily understood. The Digital Equipment Corporation (DEC) supplies the OS/8 operating system to users of the PDP-8/e minicomputer. The system supports up to 32K words of core memory and as many as 15 peripherals (80). It permits direct communication through a console terminal and places a wide variety of useful programs at the user's disposal. The library of programs available provide the programmer with the ability to create, debug, edit and execute programs in a number of languages including PAL8, SABR, RALF,

FORTRAN II, FORTRAN IV, and BASIC.

The choice of a programming language depends on a number of factors such as core memory availability, mass storage availability, the operating system, the complexity of the task to be completed, the initial programming time, and the ease of program additions or deletions. In general, calculations and input/output (I/O) are more easily accomplished in a higher level language, i.e., FORTRAN II, FORTRAN IV, or BASIC. On the other hand, for communication between the minicomputer and user built instrumentation, the use of lower level languages is mandatory. In the cases where calculations and complex I/O are involved in the completion of the task in addition to data collection and instrument supervision, it is advantageous to create a program which is a meld of a higher and lower level language. Since the MNS software is an example of such a case, it was necessary to examine FORTRAN II, FORTRAN IV and BASIC, and compatible lower level languages for possible use.

Although BASIC has much future potential, particularly in the world of microcomputers, the programmer was unfamiliar with both the instruction set, and the process involved in the incorporation of a lower level language into a BASIC program. Therefore, FORTRAN II and IV were selected for system programming. Of the two, FORTRAN II is the simplest language to use due to the fact that an

assembly language (SABR) can be interspersed directly into FORTRAN II programming. For this reason, the original MNS software was written in FORTRAN II. On the other hand, in spite of the fact that FORTRAN IV does not permit the direct insertion of lower level codes, there are some advantages to FORTRAN IV which makes its use attractive. The advantageous features include the following: the availability of logical variables, logical IF statements, and Hollerith formats; improved calculation times, improved program execution times, a more powerful library, and full ANSI compatibility (which offers the possibility of incorporating outside FORTRAN IV software) (81). Thus, it was decided to convert the existing MNS software to FORTRAN IV and create all remaining programs in this language.

B. MNS Software Structure

The software prepared for the MNS system is divisible into two separate units based on whether or not the available multielement capabilities are to be exercised. GSPARK.F4, which is presented in Appendix B, was developed for use when manual monochromator control is sufficient, and the largest portion of the present spark data was collected under the supervision of this program. For complete spectral scans, and fast multielement analyses, the main program, GSMLEL.F4 (see Appendix B), was

created to collect MNS data and coordinate a series of subroutines developed primarily by S. Koeplin (72).

1. GSPARK.F4 and Associated Subroutines

All user interaction, final I/O, and calculations are handled by the main program, GSPARK.F4. A flow chart outlining the program is presented in Figure 19. Communication between the minicomputer and the MNS electronics is accomplished by GSPARK calls to subroutines SET.RA and ADC.RA (Figure 20 and Appendix B) which are written in RALF, the assembly language for FORTRAN IV. In SET.RA, the portion of the program titled "eight-mode code" instructs the minicomputer to pass the magnitude of the delay and integrate times selected by the user to latches on the proper scaler card. Floating point numbers from 0.0 to 4096.0 are acceptable to SET.RA. The corresponding section in ADC.RA transfers digital data from the analog-to-digital converter (ADC) to the accumulator (AC) of the minicomputer. The user may average any number of ADC conversions from 1 to 4096 to form one data point and may request up to 1000 data points for each trial. A data point ranges in magnitude from 0.0000 to 1.0000 for ADC input voltages from 0.0 to +10.0 volts, respectively. The number of significant figures in the data is limited by the accuracy of the 12-bit ADC. After the completion of the data collection process, GSPARK

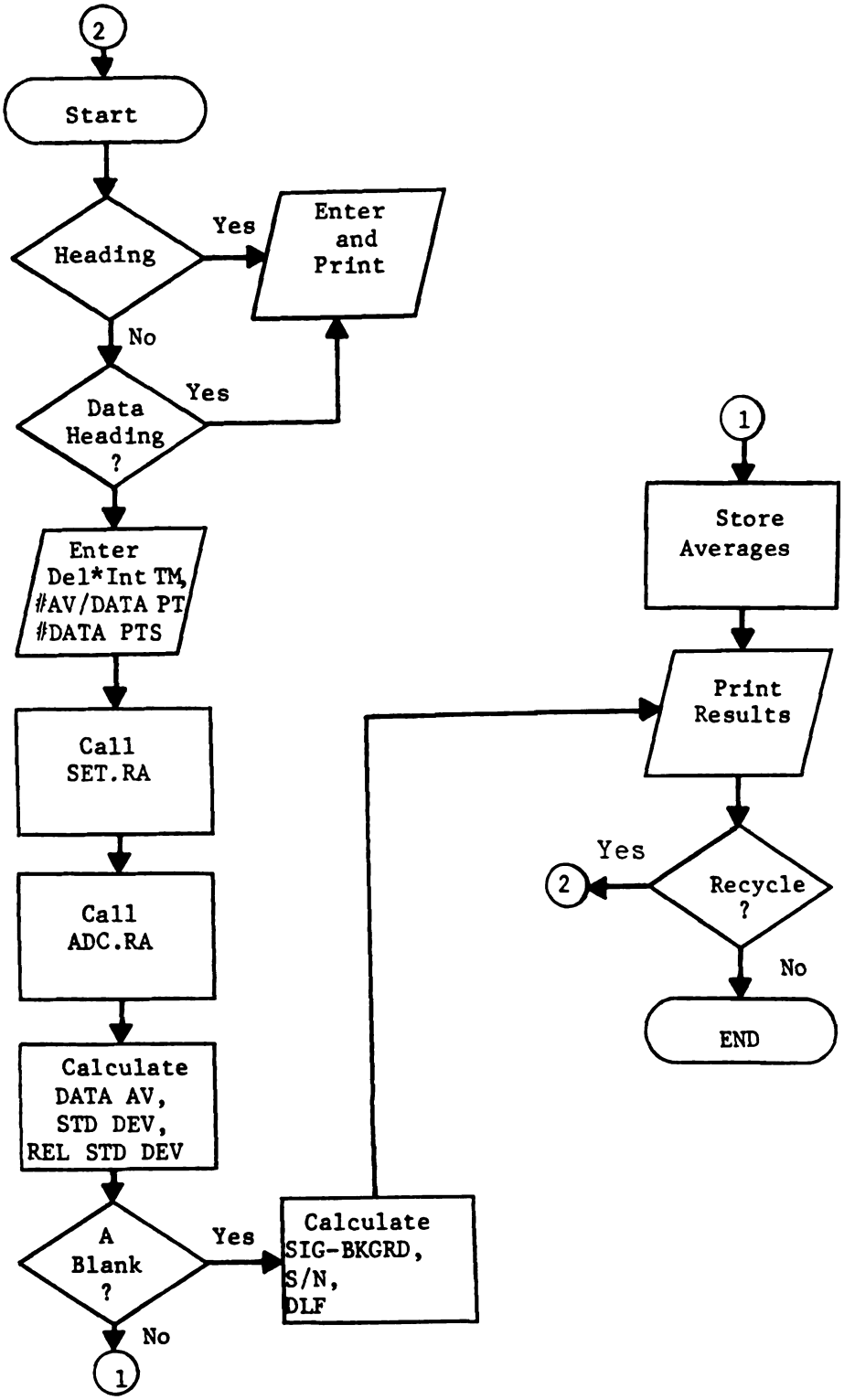

Figure 19. Flow diagram of GSPARK.F4.

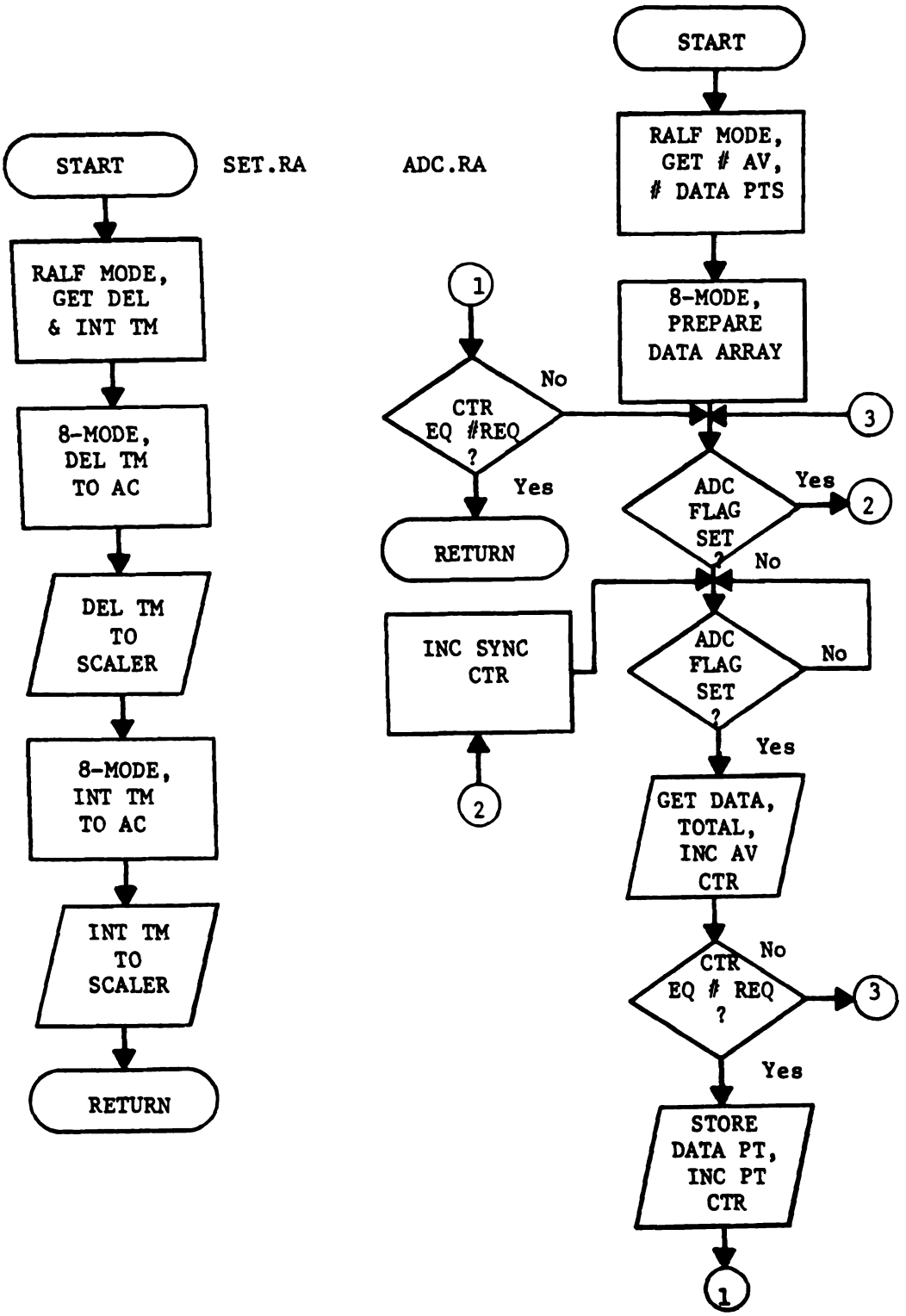

Figure 20. Flow diagrams of subroutines SET.RA and ADC.RA.

calculates the average, the standard deviation, and the relative standard deviation of the data set. If the user has indicated that the data collected are from a blank, the computer assumes that the data from the previous trial were from a sample. The computer then performs a subtraction of the two averages to yield the signal minus background value. In addition, the signal-to-noise (S/N) ratio is calculated,as well as a detection limit factor (DLF). The DLF is a ratio of the observed S/N value to a S/N value of 2 (defined as the detection limit). It provides information on the amount of dilution that would be necessary to reduce the present analyte concentration to the detection limit. The final results of all calculations are provided on the console and as a hard copy. The value obtained for each data point is also available to the user on the console only, as is a total from the synchronization counter (see Figure 20, ADC.RA). The counter is incremented each time the minicomputer enters the data collection loop in ADC.RA to find the ADC flag previously set. The counter value is useful in monitoring MNS discharge frequency stability and software-discharge frequency interaction. After all output has been completed, the program is ready to recycle at the user's discretion.

2. GSMLEL.F4 and Associated Subroutines

The general, overall structure of the MNS multi-element software is outlined in Figure 21. This program and the associated subroutines form the software portion of the GCA McPherson monochromator supervision system. The main program, GSMLEL.F4, provides all user interaction, final I/O, and calculations in a fashion similar to GSPARK. GSMLEL operates in a scan or a slew mode. If the scan mode is selected by the user, an entire spectral region is temporally examined in preset wavelength increments. The program requests the region length (in Å), the increment length (in Å), the delay time (in μs), the integrate time (in μs), and the number of data points to be collected at each wavelength examined. Subroutine GSCAN.F4 supervises the scan, timing process and data collection through sequential calls to SET.RA, SCNTO.RA and ADC.RA, respectively. The data collected are stored in files which are preserved for future inspection or plotting. Chapter V, Section E2 provides an example of plotted results. A scan over 4000Å using three different time windows requires approximately four hours of scanning time.

If the slew mode is selected, the monochromator is slewed between analyte lines for fast multielement work. The main program requests the symbols of any combination of 10 possible elements (B, Cu, P, Ca(I), Ca(II),

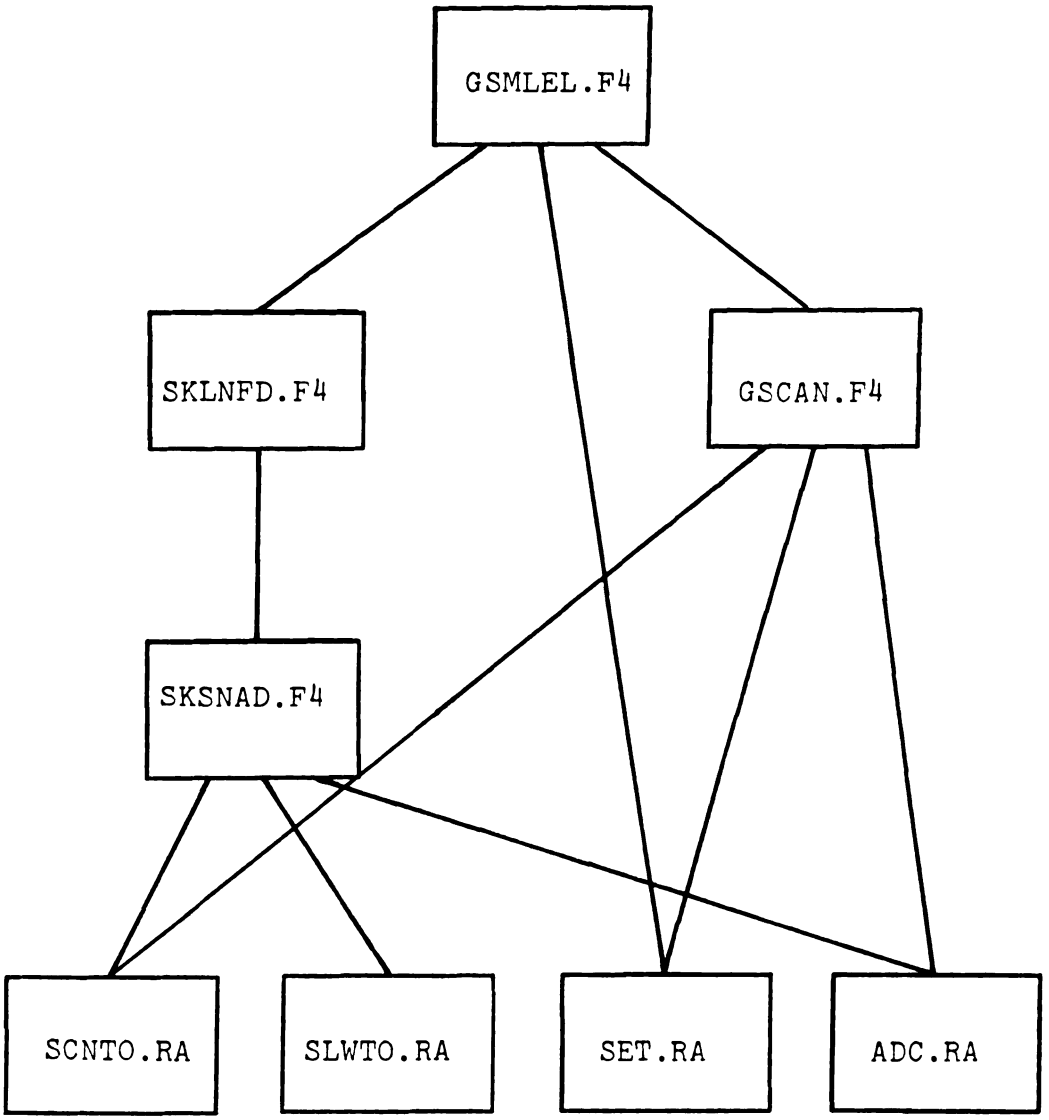

Figure 21. Software structure of the multi-element programs.

C, Al, Mo, Si), the delay and integrate times, and the present monochromator wavelength setting. GSMLEL sets the delay and integrate time via SET.RA, then passes the remaining information to SKLNFD.F4. This subroutine calculates the number of monochromator steps and the direction necessary to reach the first element selected. It calls subroutine SLWTO.RA to begin the slew operation. Due to the fact that the drive train does not stop immediately upon termination of the slew, the termination sequence is implemented 3.0 Å prior to reaching the analyte line. Uncertainty in the wavelength value due to noise in the electronic monitoring system, and the large movement rate make it necessary to determine the analyte wavelength maximum by scanning over a small spectral interval while collecting data averages of 1000 sparks per step (0.1 Å). SKSNAD.F4 performs the search through calls to subroutines SCNTO.RA and ADC.RA. Following the scan, SKSNAD supervises the return to the maximum, and stores both the average of 10,000 sparks and the wavelength value in a common array. Control is then returned to SKLNFD to repeat the sequence for the next element requested. Following the completion of data collection for the final element, SKLNFD yields control to GSMLEL. The user is subsequently prompted to replace the sample with the blank and, after signifying completion of this task, the data collection process is repeated. However, for the blank

trials, SKSNAD uses the previously stored wavelength maxima. Final calculations and I/O are performed by GSMLEL. The multielement studies which employ this software are discussed in Chapter V, Section F.

C. Perspectives

It might prove interesting to examine the possibilities of writing the MNS programs in BASIC, especially if microcomputer control is to be used. However, if the present programs are retained, it is acknowledged that several alterations would simplify and increase the efficiency of the software. In terms of software additions, the most obvious improvement lies in the expansion of the multielement software to include the time of maximum S/N for each element, as well as a larger elemental repertoire. Improved electronics (see Chapter III, Section D6) would eliminate the need for individually determining emission maxima during each multielement trial, and thus, reduce the time of analysis. Finally, if standard curves are recorded prior to sample analysis, direct analyte concentrations could be reported to the user.

V. MINIATURE SPARK CHARACTERIZATION

A. Introduction

The primary purpose of any analytical study involving the design and construction of instrumentation is to evaluate its use in sample analysis, and to understand its basic nature to a degree which permits future improvements. In the case of the MNS, this entails an examination of important electrical properties, plasma diagnostics, and analytical findings. The following sections are devoted to such an examination.

B. Determination of Electrical Properties

1. Capacitance Determination

The capacitance of the coaxial cable and the coaxial housing capacitor were physically measured through a capacitance substitution procedure. The housing and cable were placed in an RC circuit which consisted of a function generator, operated at 100 Hz, a 1.0 MΩ resistor, and an oscilloscope. The final value was obtained by matching the housing and/or cable discharge curve to that of a known capacitor. The determination yielded housing and cable capacitances of 300 pF and 50 pF, respectively.

The capacitance can also be calculated from physical

measurements of the length and thickness of the polyethylene dielectric, and the radius of the inner aluminum bar (82,1). The capacitance of the cable can be calculated from manufacturers' specifications. The values obtained in this manner are 290 pF and 45 pF for the housing and cable, respectively. Considering the fact that the RC method in itself is accurate to ca. 10% (due to capacitor tolerances and oscilloscope decay time measurements), the capacitances determined using the two methods are in good agreement.

The 350 pF total capacitance is a factor of 1.75 times larger than that employed in the original MNS. Since the total energy consumed in a spark circuit is $1/2\ CV_C^2$ (where C equals the capacitance, and V_C is the total voltage on the capacitor), it was felt that the increase in capacitance would partially compensate for the decrease in V_C expected for the DC power supply presently employed (as compared to the overvolting pulsed supply).

2. Breakdown Voltage Studies

The breakdown voltage, in conjunction with the spark capacitor, determines the total energy available to the discharge. The magnitude of the voltage depends on the instantaneous gap conditions at the time of breakdown. Important factors include the gap environment (i.e., gas

employed, presence of impurities, and application of external radiation), and the electrode sizes, shapes, composition, and temperature. Due to the fact that there is a time lag between attainment of the breakdown potential, and formation of the discharge, the "true" breakdown voltage of any gap is realized only when the capacitor is charged slowly (78,79). In the case of the original MNS, the pulsed supply employed overvolted the gap considerably. The DC supply currently used overvolts much less.

The breakdown voltage observed in the present system varies with the secondary and analytical gap gas flow rates, the gap length, and the DC supply voltage setting. At low gas flow rates, the diffusion of air into the gap region causes large breakdown voltages and erratic firing. Excessive gas flow rates appear to increase the breakdown voltage over that found for typical operating conditions, probably by efficiently removing ions remaining in the gap region from the previous spark. Gap length effects have not been studied in detail, but limited observations indicate that the relationship between the breakdown voltage and the gap length is not a direct one. Experiments conducted by researchers using needle-point electrodes in an air atmosphere indicate that a complex relationship is not uncommon (78).

The discharge frequency is also an important factor

in determining the breakdown voltage. Figure 22 shows the relationship between the observed breakdown voltage and the discharge frequency. The exponential-like decay of the curve at high frequencies supports the earlier premise that ions may remain in the gap region long after the end of spark life. As the DC supply voltage is increased, the spark frequency increases, and the charging capacitor "sees" a lower resistance through an atmosphere which has an increased concentration of ions.

Finally, it should also be pointed out that after sharpening the electrodes, or beginning daily research, the breakdown voltage will vary for several minutes, until the electrodes have been conditioned.

3. Current Measurements

The electrical property which most directly determines the plasma characteristics is the current. Therefore, it is important to gain some knowledge of the current magnitude and, how physical changes influence the current.

The method chosen to evaluate the current involved the use of a probe, designed by Glass (23), which directs the current through a small piece of nichrome wire. The spark current in this wire creates a voltage-time profile which was monitored through an impedence-matched attenuator by a Tektronix 564 storage scope equipped

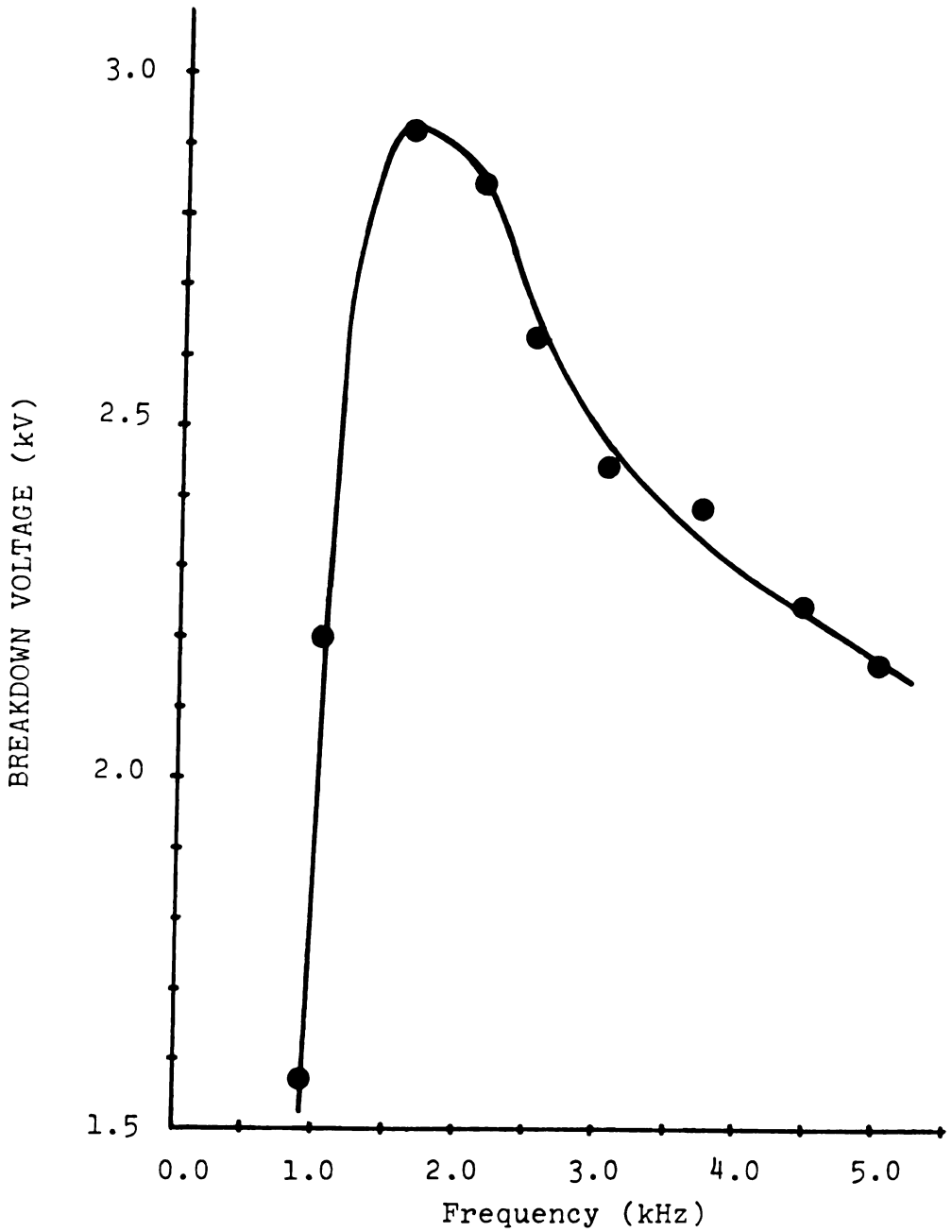

Figure 22. Discharge frequency effects on the spark breakdown voltage.

with a fast sampling module and a camera. Voltage-time profiles were recorded on film, enlarged, and digitized. An example of such a curve is presented in Figure 23.

The current-time profiles were generated by S. Koeplin (72) using a Runge-Kutta (83,84) solution to the first order differential equation which relates the voltage-time profile to the current-time profile. This relationship is expressed by the following equation:

$$V(t) = L(dI(t)/dt) + I(t)R + I(t)t/C, \qquad (2)$$

where I is the spark current and L, R, and C are the nichrome wire inductance, resistance, and capacitance, respectively. The capacitance was estimated to be in the pico-Farad range (85). The resistance was accurately obtained by measuring the voltage drop across the wire from a standard current. The value obtained was 0.0792 Ω. The inductance is more difficult to determine and is important because it affects the results rather dramatically. Indications are that the value lies somewhere between 1 nH and 10 nH (86,87). A value in the center of these extremes was chosen due to the fact that the current profiles obtained were consistent with the circuit calculations presented in Appendix A. Figure 24 shows a typical current-time profile. Although the profiles obtained are probably close to the "true"

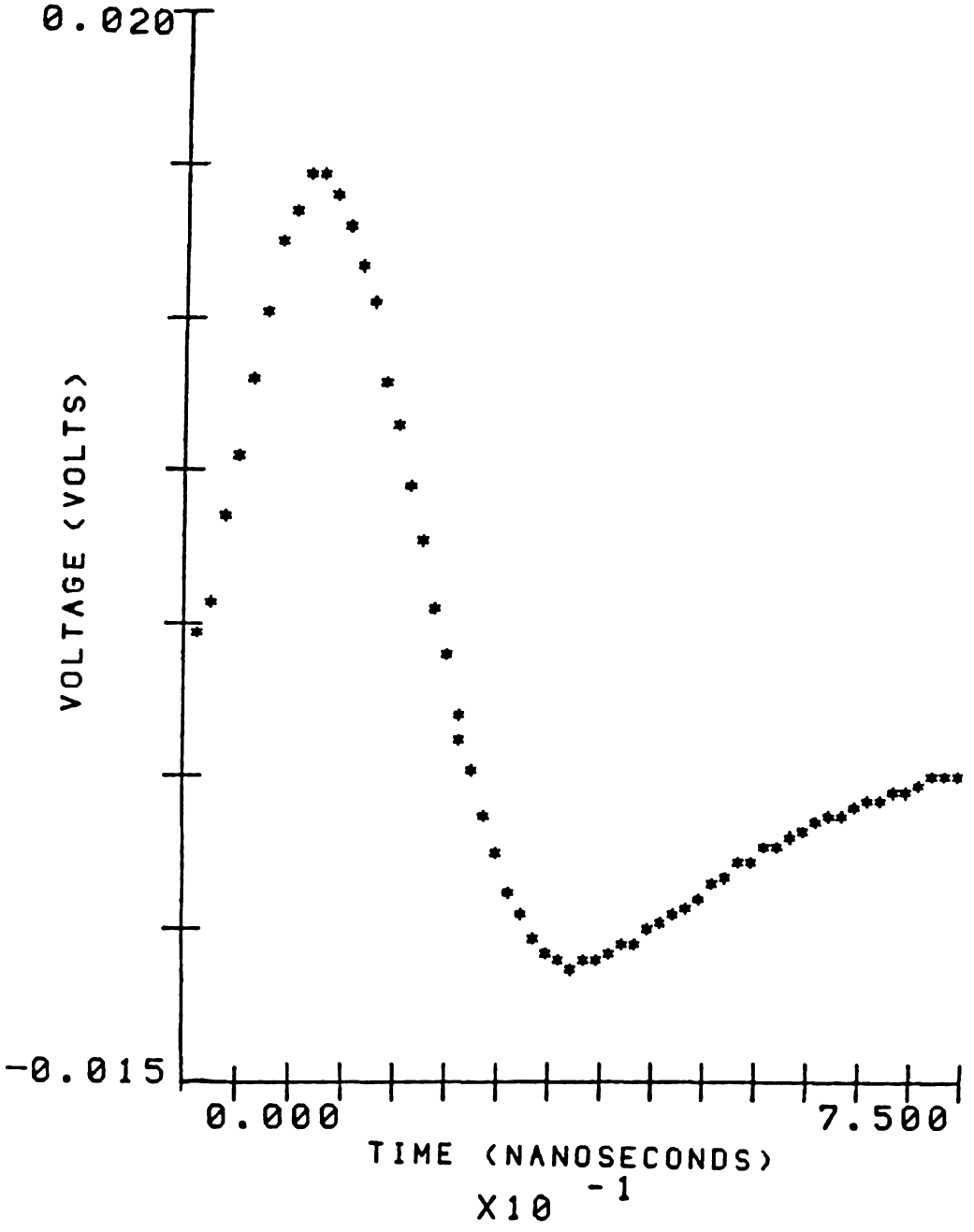

Figure 23. A typical voltage-time profile.

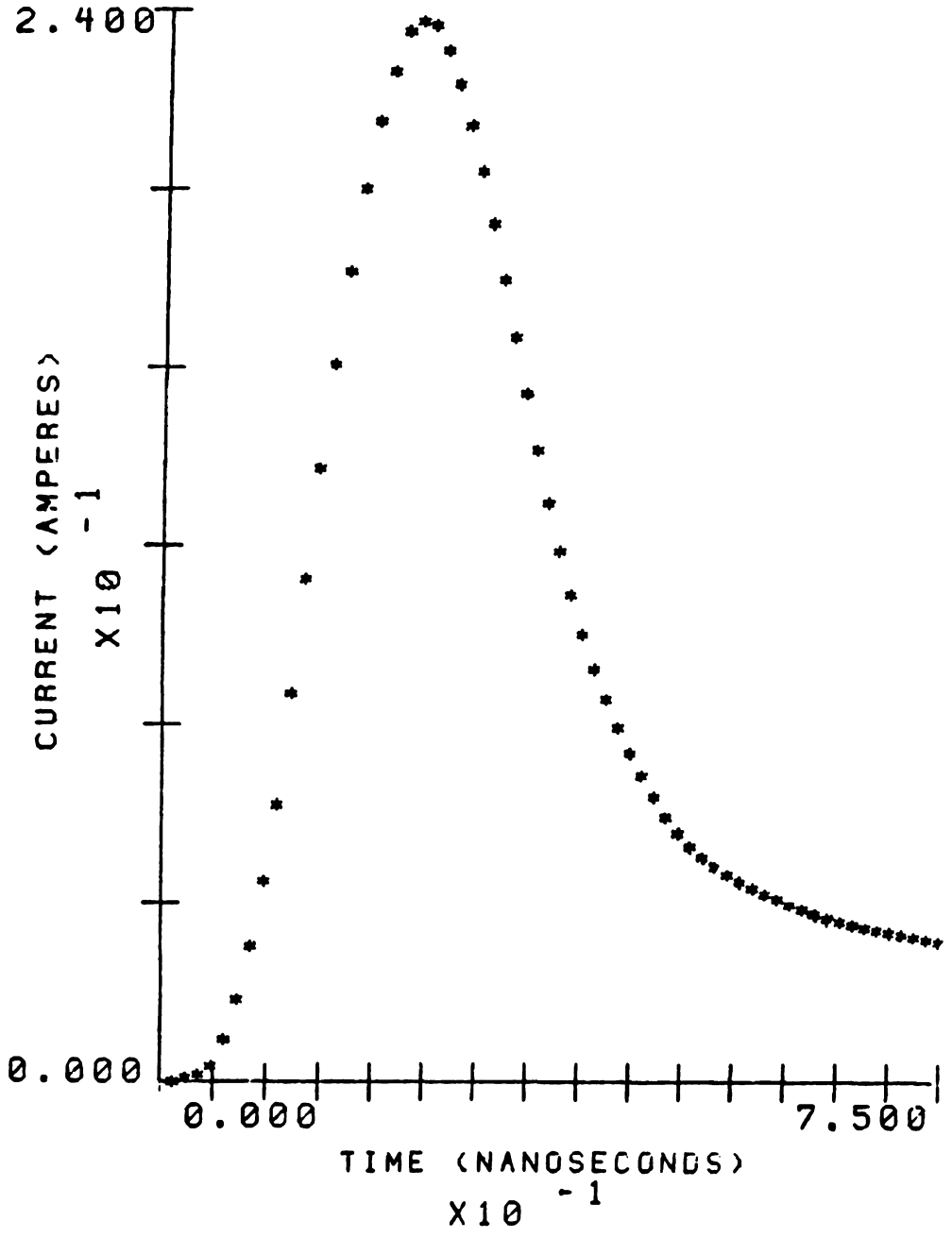

Figure 24. A typical current-time profile.

profiles, it is best to use the results presented for relative comparisons only. Table 2 summarizes the results of the studies. The same dependence on the frequency (DC supply voltage) found in the breakdown voltage studies are suggested by the results of the helium trails. Furthermore, it is evident that helium produces lower currents than argon under similar conditions. The data also demonstrate gap length effects and gap atmosphere effects. It appears that water vapor increases the current, as has been found to be the case with sparks in air (78). It also appears that Glass (23) was correct in his studies involving current observations in high analyte concentration solutions. He stated that the water vapor acted as a buffer which prevented large current changes with analyte introduction. Finally, although current profiles were not determined for the original MNS, a similar one-gap system using the pulsed supply yielded voltage-time profiles which appeared to be oscillatory and which had an initial peak ca. three times that found for the largest peak presented in Table 2.

C. Temperature Determinations

The plasma temperature(s) bear a more direct relationship to the observable physical properties of the spark than the electrical parameters previously discussed.

Table 2. Current Measurement Results.

Gap* Length- Sec., Anal. (mm)	Atmosphere	Maximum Current (amps)	Time of Maximum Current (ns)	DC Supply Voltage kV
3.4,2.0	He	17.8	26.5	4.0
3.4,2.0	He	23.7	22.9	3.0
3.0,2.0	Ar	40.1	30.1	4.0
3.0,3.0	Ar	52.5	26.5	4.0
4.0,2.0	Ar	57.0	32.5	4.0
3.0,2.0	Ar	46.9	24.1	4.3
3.0,2.0	Ar, H_2O vapor	55.0	26.5	4.3
3.0,2.0	Ar, H_2O vapor 500 ppm Ca	56.5	26.5	4.3

*No bridging resistor was employed in any trials reported.

In fact, the temperature is the most vital parameter governing the characteristics of a plasma (76). Four possible temperatures may be used to describe a monatomic gas plasma (i.e., the electron, gas, excitation, and the ionization temperatures). In the sections which follow, the excitation and ionization temperatures are examined for the present MNS.

1. Excitation Temperature

The excitation temperature describes the population of various energy levels in the gaseous system. For a Maxwell-Boltzmann distribution of atoms at some temperature, T, the intensity, I, of a spectral line produced by transitions from energy level E_2 to level E_1 is given by:

$$I = \frac{Cg_2A_{2\to1}}{\lambda} \exp\ (-E_2/kT), \qquad (3)$$

where C is a constant, g_2 is the statistical weight of state 2, $A_{2\to1}$ is the transition probability (Einstein Coefficient), λ is the wavelength of emission, and k is the Boltzmann constant (1,76,78). For determination of the excitation temperature, Equation 3 can be expressed in a more convenient form.

$$\log\ (\frac{I\lambda}{g_2A_{2\to1}}) = \log\ C - \frac{E_2}{2.303kT} \qquad (4)$$

A plot of the left hand side of this equation versus E_2 should produce a straight line with a slope that is proportional to the excitation temperature. This method is applicable with the constraints that self-absorption is negligible, accurate transition probabilities are available, and the spectrometer exhibits a uniform spectral response over the wavelength region used (88). The first requirement is true for argon plasmas below 6500Å, and the latter two are true if the correct series of argon lines are chosen.

The slopes of the lines fitted to the data were calculated by a least squares routine. Transition probabilities for the spectral lines employed were reported by Adcock and Plumtree (89). Table 3 lists the results of the determinations, the results found for the original MNS, and the spectral lines employed. Temperatures were determined for several gap lengths with and without the bridging resistor, and over various time intervals. It is apparent from the values obtained, that the bridging resistor does at least partially remove the analytical gap from the circuit during the charging period. A comparison of the data with those obtained by Zynger (1) and Lantz (24) supports the previous findings of a lower discharge energy for the present system. Furthermore, the temperature appears to decrease more quickly than was observed by Zynger and Lantz. It is therefore expected

Table 3. Discharge Excitation Temperatures.

Gap Length-Sec., Anal. (mm)	Time Period (μs)	Temperature (°K)	Orig. Spark Results[b] (°K)
3.0,3.0	0.5-2.0	4800±400	----
	1.0-3.0	4400±400	----
	2.0-5.0	4000±400	4300
	5.0-10.0	3600±400	4700
	10.0-15.0	3000±400	4550
	15.0-20.0	--------	3800
3.5,3.0[a]	0.5-2.0	4500±400	
	2.0-5.0	3700±400	
	5.0-10.0	3000±400	
4.5,3.0[a]	0.5-2.0	4600±400	
	2.0-5.0	3800±400	
	5.0-10.0	3300±400	

[a]Bridging resistor employed.

[b]Single gap, pulsed supply.

that the time window of maximum signal-to-noise for each element will occur earlier in time and for a shorter period of time than was found by previous workers. Zynger (1) pointed out that the MNS resembles the microwave plasma in argon reported by Taylor et al. (90), as far as the excitation temperature is concerned.

2. Ionization Temperature and Electron Density

The ionization temperature describes ionization equilibria and is mathematically expressed by the Saha equation (76). The following equation, derived from the Saha relationship, relates the intensity ratio of an ion-atom line pair of one element to the ionization temperature. The equation states that:

$$\log (I^+/I) = - \log P_e + \log \frac{g^+ A^+_{2\to1} \lambda}{g A_{2\to1} \lambda^+}$$

$$\frac{5040}{T} (V_{ij} + V_q^+ - V_q) + 5/2 \log T - 6.18, \qquad (5)$$

where "+" designates the ions, V_{ij} is the apparent ionization potential, which contains the partition functions, V_q is the energy level from which emission occurs, and P_e is the electron pressure (76,91). The electron pressure is defined as:

$$P_e = \frac{N_e T}{7.34 \times 10^{21}}, \qquad (6)$$

where N_e is the electron density (76). In turn, the electron density can be obtained from the half width of the 4861Å H_β line which is subject to a linear Stark effect (92). The relationship is:

$$N_e = C(N_e,T)\Delta\lambda^{3/2} \quad . \qquad (7)$$

The coefficient, C, is slightly dependent on the electron density and the electron temperature, and therefore, the final value employed is an average over electron densities previously reported for the MNS and over an electron temperature range of 10,000 to 30,000 °K. The half widths, $\Delta\lambda$, were obtained by scanning slowly over the H_β line and monitoring the emission intensity on a strip chart recorder. N_e values, determined under various conditions, are presented in Table 4.

With the electron density and the intensities of the Ca ion (3933Å) and Ca neutral (4227Å) lines, the ionization temperatures were determined through an iterative technique. The results of calculations are presented in Table 4, together with other pertinent information. As is the case with the original MNS, the ionization temperatures are larger than the excitation temperatures determined under the same conditions. However, the temperature differences observed in the present system are much smaller than those found previously, which suggests a

Table 4. Discharge Ionization Temperatures and Electron Densities.

Gap Length-Sec., Anal (mm)	Time Period (μsec)	Ne (e/cm^3)	Ioniz. Temp. (°K)	Orig. Spark[b] Ne (e/cm^3)	Orig. Spark[b] Temp. (°K)
3.0,3.0	0.5-2.0	1.4×10^{16}	5500±600	5.6×10^{16}	----
	1.0-3.0	9.4×10^{15}	5400±600	----	----
	2.0-5.0	6.7×10^{15}	5200±600	2.4×10^{16}	----
3.5,3.0[a]	0.5-2.0	1.3×10^{16}	5100±600	----	----
	1.0-3.0	8.5×10^{15}	--------	----	----
4.5,3.0[a]	0.5-2.0	1.4×10^{16}	5200±600	----	----
	1.0-3.0	9.1×10^{15}	--------	----	----
	2.0-5.0	5.7×10^{15}	--------	----	----
	2-15				6600
	15-30				5150
	5-10			6.1×10^{16}	----

[a]Bridging resistor employed.

[b]Single gap, pulsed supply.

plasma that is somewhat closer to a state of equilibrium during the time intervals chosen. The large difference between present and past findings is a further indication that the present discharge is less energetic.

D. Introduction Systems

Analytical findings using the three nebulizers previously discussed are sufficiently unique to the present flow systems and discharge to warrant a detailed explanation. Each nebulizer will be briefly discussed followed by a general comparison of the three. In addition to the axial aerosol injection system described in Chapter III, side introduction, as was employed in the original MNS system, was also used. Normal operating conditions for the nebulizers with both flow configurations are presented in Table 5.

1. Ultrasonic Nebulizer

As was expected, of the three nebulizers studied, the ultrasonic nebulizer produced the best results. The detection limits found while using each nebulizer are presented later in this chapter. For axial gas flow, signal-to-noise (S/N) ratio studies at various argon flow rates indicated that a maximum occurred in the curve at *ca.* 1.25 ℓ/min, as is shown in Figure 25.

Table 5. Typical Operating Conditions for all Nebulizers Studied Using Axial and Side Flow Configurations.

Nebulizer	Flow Configuration	Flow Rate or Tank Pressure
Ultrasonic[a]	Side	2.0 ℓ/min
"	Axial	1.25 ℓ/min
Crossed-Flow	Side	35 psi[b]
"	Axial	30 psi
Modified V and M	Side	50 psi
"	Axial	25 psi

[a]Incident power equals 15 W, cooling H_2O equals 2 gal/hr.

[b]Auxiliary gas flow of 1.0 ℓ/min used.

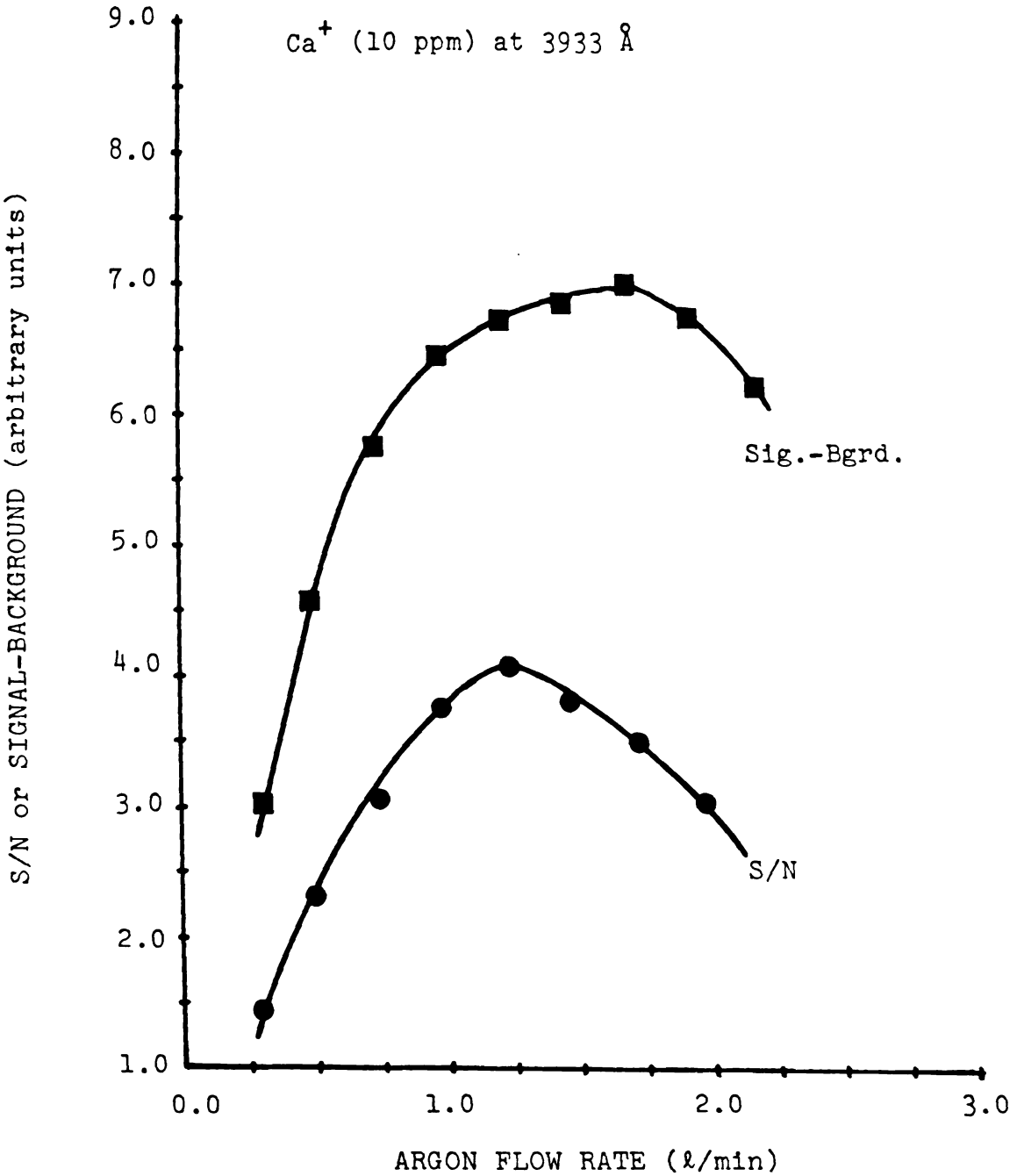

Figure 25. Argon flow rate effects on the observed S/N ratio and the signal-background value (using the ultrasonic nebulizer).

On the other hand, a plot of the signal minus background value (data scaled for plotting convenience), as a function of the flow rate does not reach a maximum until ca. 1.75 ℓ/min argon. These facts, combined with detection limit studies (which yielded poorer results than was found for the original MNS system), suggested that a less restricted flow configuration might prove beneficial. The most convenient and well-researched design was the side introduction system employed by Glass (23), Lantz (24), and Zynger (1). It was therefore decided to compare the results of side introduction to those obtained using axial flow.

Helium was also employed as a carrier gas in the ultrasonic system. Figure 26 shows that the maximum S/N value for helium occurs at 2.3 ℓ/min. The increased optimum flow rate for helium over argon is not surprising considering the difference in density between argon and helium.

2. Modified Veillon and Margoshes, and Crossed-Flow Nebulizers

As Figure 27 clearly shows, both the Veillon and Margoshes, and the crossed-flow nebulizers also exhibit a S/N dependence on the carrier gas flow rate (α pressure). For the Veillon and Margoshes nebulizer, the maximum at 25 psi represents a pressure of about one-half that

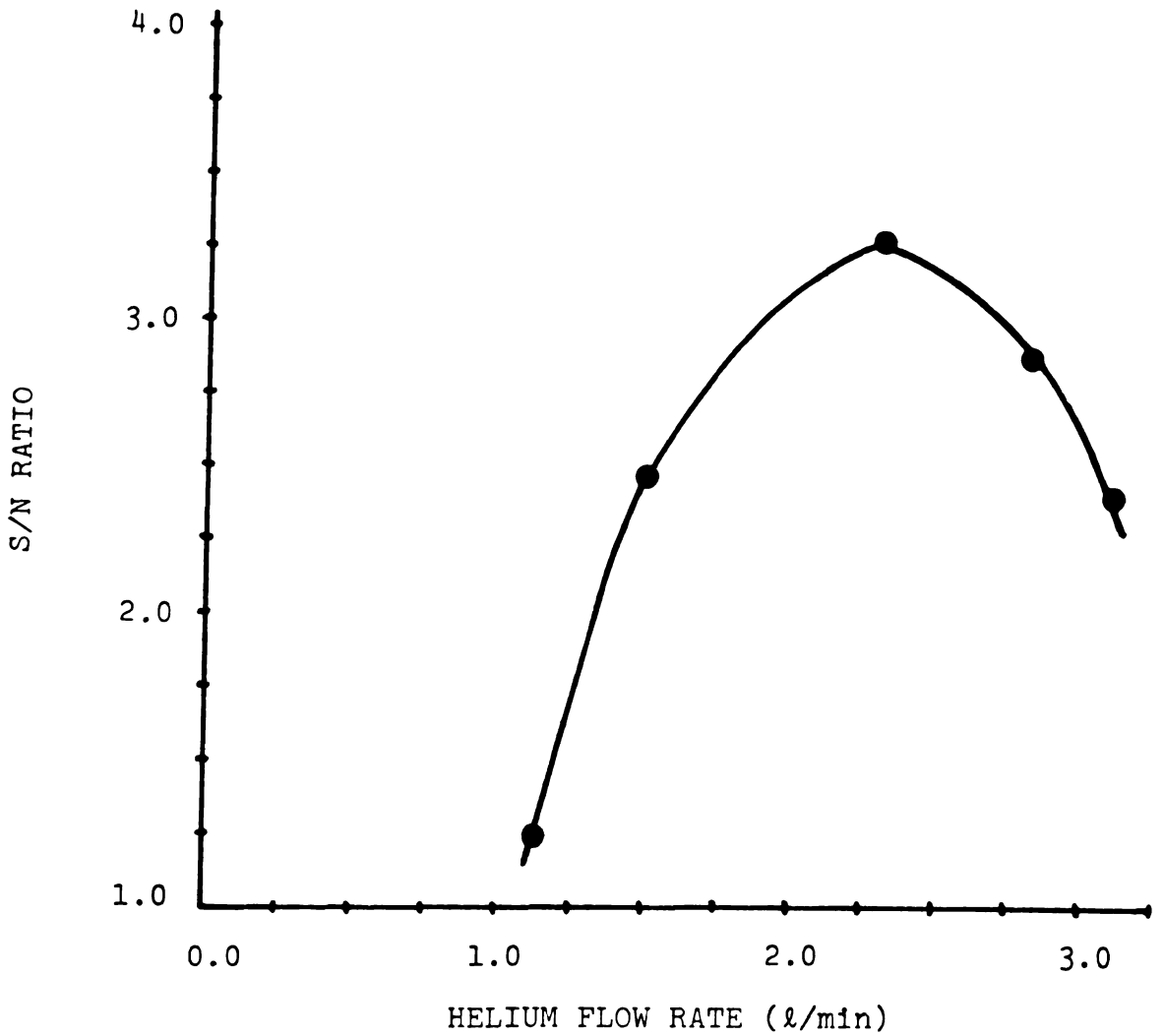

Figure 26. Helium flow rate effects on the observed S/N ratio (using the ultrasonic nebulizer).

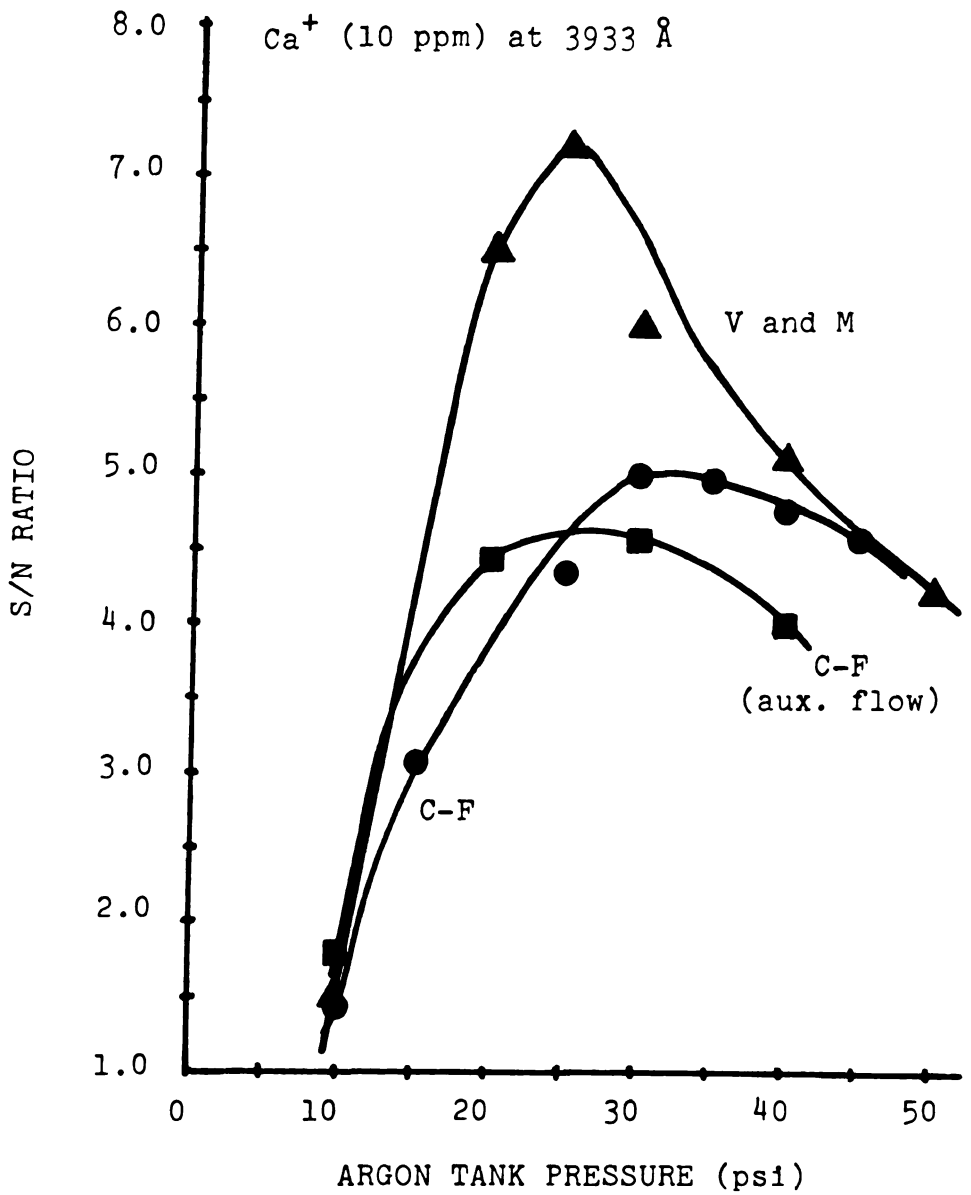

Figure 27. Argon tank pressure effects on the observed S/N ratio (using the pneumatic nebulizers).

used for side introduction (past and present). Although the average droplet size is only slightly affected by this reduction, the amount of aerosol produced per unit time is definitely smaller. For the crossed-flow nebulizer, the maximum occurs at 30 psi. At low pressures, an auxiliary gas flow (Figure 7b) improves the S/N ratio. However, at high pressure, the added flow destabilizes the discharges and reduces the S/N ratio.

3. Nebulizer and Flow System Comparisons

It is readily apparent from the detection limit data presented later in this chapter that the ultrasonic nebulizer produces superior results in both flow configurations. However, the ultimate decision on which nebulizer is to be used must take into account the substantial increase in complexity of the construction and control of the ultrasonic nebulizer as compared to the two pneumatic nebulizers. In spite of the increased discharge stability observed for the axial flow configuration, side introduction yields better overall results. The ratio of axial to side introduction detection limits is approximately 4.5:1. This difference is partially attributed to the less restricted flow design of the side introduction system. A redesign of the present axial flow system, eliminating the sheath gas system (since it is only desirable at low gas flow rates), and

increasing the entrance and cone orifices, may improve axial results. However, there may always be an inherent advantage to side introduction where particulate matter is concerned.

In the case of the two pneumatic nebulizers, which have efficiencies at least partially dependent on the tank pressure, the differences observed between the two flow systems are more dramatic. For the modified Veillon and Margoshes nebulizer, the axial to side ratio averages 7.4:1. This ratio physically demonstrates the previously discussed decrease in aerosol production per unit time at the lower pressures required for axial flow. Initially, it may seem surprising that the crossed-flow nebulizer (axial to side ratio is 5.0:1) does not fare much better than the modified Veillon and Margoshes nebulizer, especially at the lower tank pressures (axial flow) where it should be more efficient. The reason probably lies in the present design. A smaller aerosol chamber, an improved capillary adjustment system, a smaller diameter solution capillary, and a better aerosol chamber to heated chamber interface should improve the relative results.

E. Emission Studies

1. Background Emission Studies

The background radiation emitted by the spark, like the temperature, provides some direct insight into the nature of discharge. Furthermore, the time profile of any optical noise in the background radiation emitted primarily determines the ultimate detection limits observed. Figure 28 is a time-resolved view of the emission of the present MNS using tank argon over a spectral range extending from 2000Å to 5000Å. From the diagram it is relatively easy to observe the increase and decrease of emission from carbon (2478Å - impurity in tank argon), hydroxyl radicals (band head at 3064Å - from water impurity), the second positive band system of nitrogen (band heads at 3977Å, 3371Å, 3576Å, 3805Å, 4059Å - impurity in tank), oxygen (3370Å, 3517Å, 3734Å - impurity in tank), and the group of argon lines used in the excitation temperature determinations (4150Å - 4300Å) (93,94). In comparison to the original MNS, the findings here again indicate a less energetic plasma. Very little continuum radiation is observed in the present discharge, while Zynger (1,3) observed a fairly strong continuum which reached a maximum intensity in the 0.5-2 μs time period. Furthermore, hydroxyl band emission in the present system is observed to be present during the

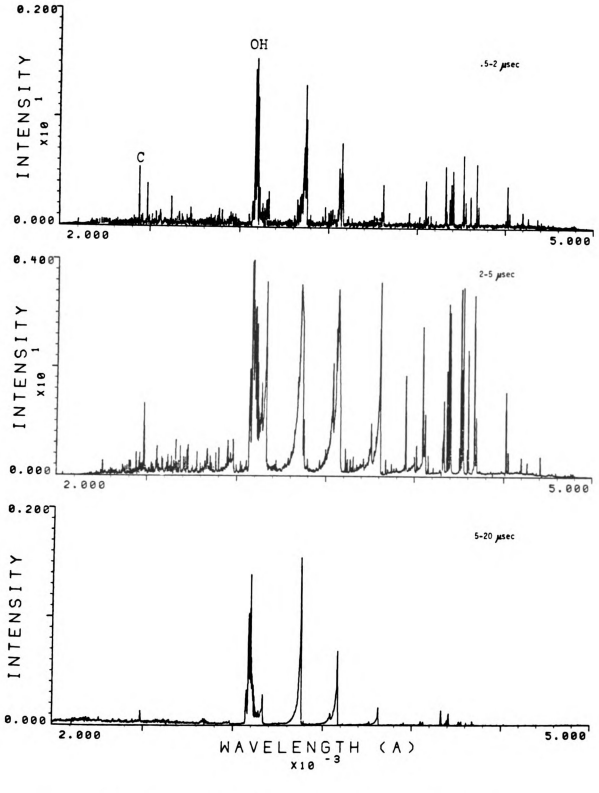

Figure 28. Time-resolved spectra of the MNS background emission.

0.5-2.0 μs time interval with maximum emission occurring between 2.0 and 5.0 μs, whereas in the original spark, the time periods were found to be 5-10 μs and 30-100 μs, respectively. It appears that for the present system, maximum elemental emission should occur in the 2.0-5.0 μs time period.

2. Analyte Signal-to-Noise Studies

The maximum signal-to-noise observed during any analytical determination is dependent on a number of variables, several of which are unique to the MNS system. The effect of the delay period on the S/N ratio has been previously explained. Figure 29 is an example of typical curves. The figure also demonstrates one possible effect of an added matrix. The curve shown is that of the calcium ion S/N ratio versus time with a five-fold excess of aluminum added. Aluminum is a known calcium emission depressant, and is thought to physically reduce the free calcium concentration in plasmas (95). As would be predicted, the calcium ion curve in the presence of aluminum is shifted to earlier times where the discharge is more energetic.

As is expected, any gap changes which effect the breakdown voltage produce a shift in the value and temporal position of the maximum S/N ratio. For example, calcium ion S/N ratios were simultaneously monitored

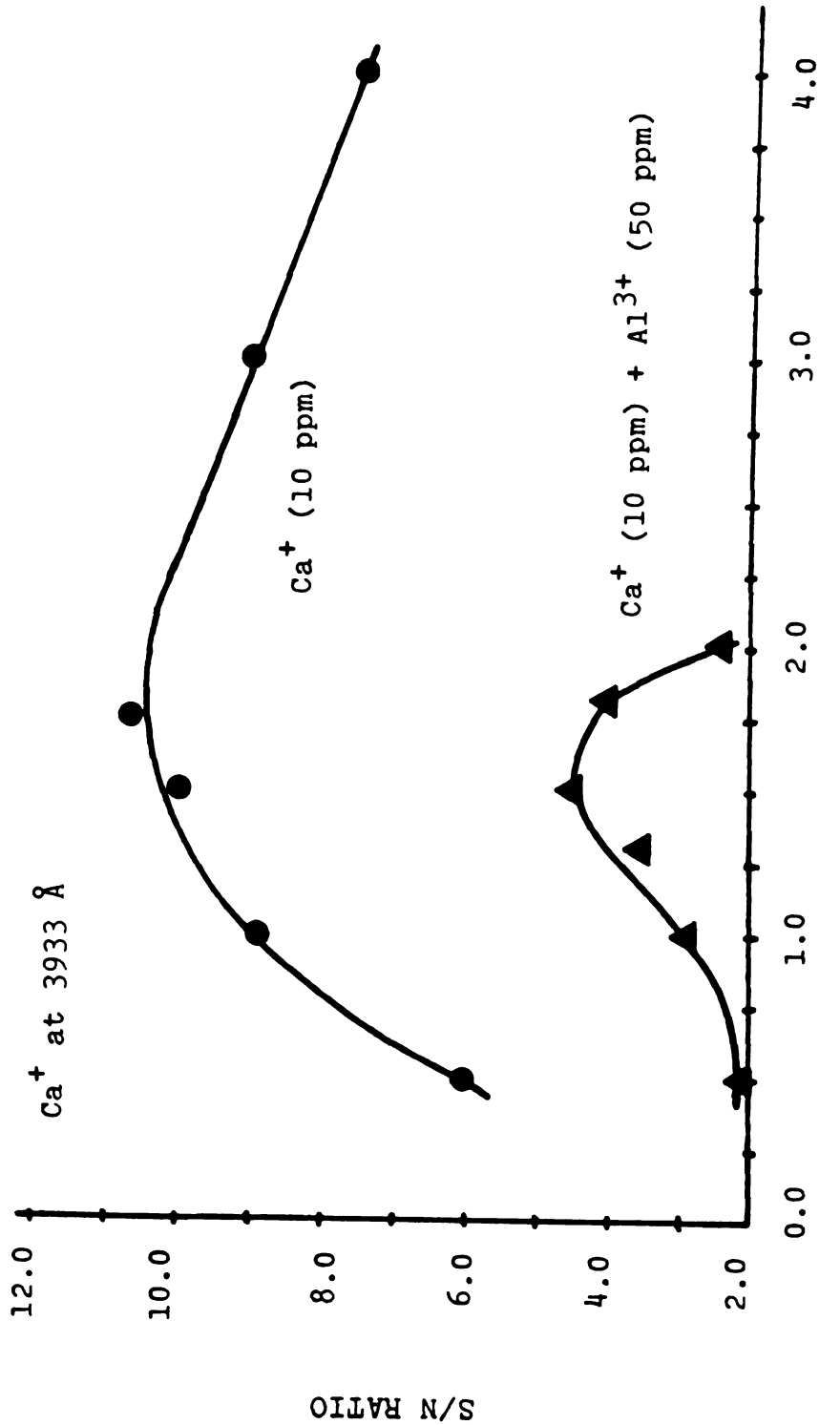

Figure 29. Temporal dependence of the S/N ratio for calcium (1on).

during the breakdown voltage studies of Figure 22. The S/N curve parallels the breakdown voltage curve over the entire range of frequencies examined. Furthermore, the S/N maximum is shifted to slightly later times as the breakdown voltage is increased and to earlier times as it is decreased. These findings seem to apply to all other previously discussed gap length and flow rate changes as well. Another effect due at least partially to a change in breakdown voltage is the shift of S/N versus time maxima with changes in the carrier gas. Figure 30 demonstrates the difference observed for atomic calcium in argon and helium. The less energetic helium plasma shifts the S/N maximum to 1.7 μs from the 3.2 μs value found in argon.

One final factor which was also important in the original MNS system is the gap observation position. This is especially important at high carrier gas flow rates. Zynger (1,3) found that with side introduction, the emitting species may be blown away from the inter-electrode axis. With axial introduction, the same phenomenon is observed. However, in this case, the maximum S/N is found to occur near the cathode (lower electrode).

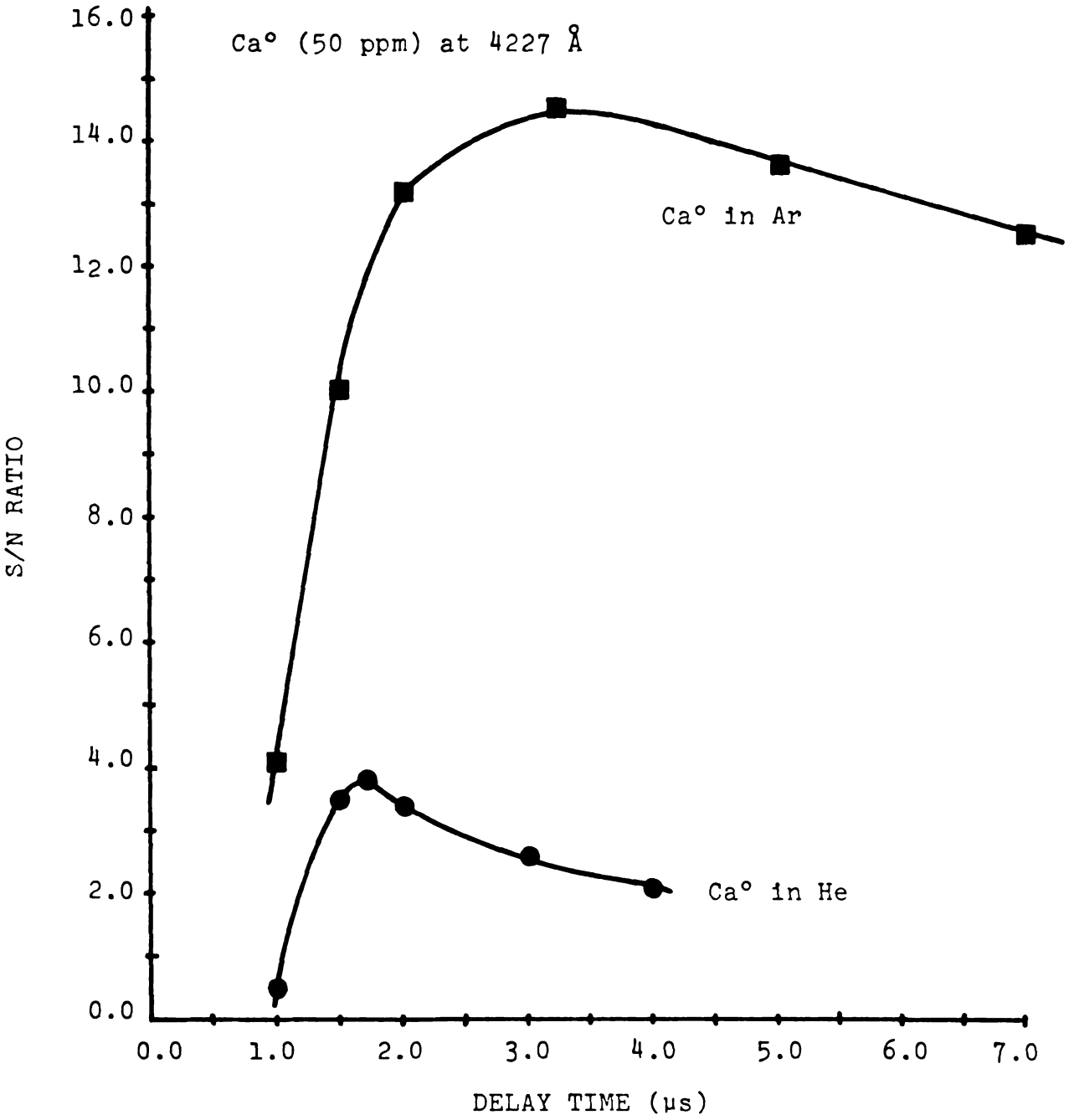

Figure 30. Temporal dependence of the S/N ratio for atomic calcium on the gap atmosphere.

3. Analytical Findings

The stability and detection limit information for the present MNS system and for the original MNS is presented in Tables 6 and 7. Table 8 is a comparison of the present detection limits to those obtained using other spectroscopic methods (96).

At low gas flow rates (0.6 ℓ/min), using axial introduction, the precision has been improved by a factor of 2.6 over that found for the original MNS. Under normal operating conditions (1.25 ℓ/min), the factor is ca. 2. When side introduction is employed with the present system the precision is similar to that obtained by Zynger (1,3). However, the long term stability of the present system is slightly worse than that obtained for the original MNS.

The detection limits presented are defined as those analyte concentrations which yield a S/N value of two. The noise value used in the determinations was that of the blank alone since small signal (total signal-background) values result in signal variances which are small compared to those observed for the blank.

Figure 31 is a plot of calcium ion emission in arbitrary units versus concentration. The calibration curve is linear from the detection limit to ca. 40 ppm Ca. The slope of the curve is 1.04 ± .05.

Table 6. MNS Detection Limits.

Nebulizer	Flow Confg. A=Axial S=Side	Element	Line (Å)	Time Max. S/N (μs)	Present DL (ppm)	Orig. Spark DL (ppm)	Comparison Ratio
Ultra.	S	Ca(II)	3933	2.0-3.0	0.01	0.008[b]	0.8[a]
		Ca(I)	4227	3.2-4.2	0.08	0.1	1.2
		Si	2516	1.8-2.8	0.07	0.08	1.1
		B	2497	2.0-3.0	0.1	0.07[b]	0.7
		Al	3961	2.5-3.5	0.15	0.32[b]	2.1
		P	2535	2.3-3.3	0.2	0.5[b]	2.5
		Cu	3247	3.0-4.0	0.02	0.07	3.5
Ultra.	A	Ca(II)	3933	2.0-3.0	0.04	----	4.0[c]
		Cu	3247	3.0-4.0	0.08	----	4.0
CF	S	Ca(II)	----	-------	0.09	----	9.0[c]
		Cu	----	-------	0.20	----	10.0
CF	A	Ca(II)	----	-------	0.45	----	45.0[c]
		Cu	----	-------	1.0	----	50.0
V and M	S	Ca(II)	----	-------	0.06	----	6.0[c]
		Cu	----	-------	0.15	----	7.5
V and M	A	Ca(II)	----	-------	0.5	----	50.0[c]
		Cu	----	-------	1.0	----	50.0

[a]Ratio of original MNS DL to present ultrasonic DL (side intro.). [b]Time-resolved DL.
[c]Ratio of DL presented to ultrasonic DL (side intro.).

Table 7. MNS Stability Information.

MNS	Flow Config.	Precision	Conditions
Present	Axial	1.5%	4200Å Ar line, 0.6 ℓ/min flow
"	"	1.9%	3933Å Ca^+, 1 ppm, 1.25 ℓ/min flow, ultrasonic nebulizer
"	Side	3.8%	3933Å Ca^+, 1 ppm, 2.0 ℓ/min flow, ultrasonic nebulizer
Orig.	Side	3.9%	3247Å Cu, 2 ppm, 3.8 ℓ/min flow, V and M nebulizer

Table 8. A Comparison of the Present MNS Detection Limits to Those of Other Spectroscopic Techniques.

Element	MNS (ppm)	Induct. Coupled Plasma (ppm)	AAS	Flame AFS (ppm)	AES
Ca	0.01	2.0×10^{-5}	0.001	1.0×10^{-6}	0.0001
Si	0.07	0.01	0.1	---	5
B	0.1	0.005	6	---	30
Al	0.15	0.002	0.03	0.005	0.005
P	0.2	0.04	----	-----	3
Cu	0.02	0.001	0.002	0.001	0.01

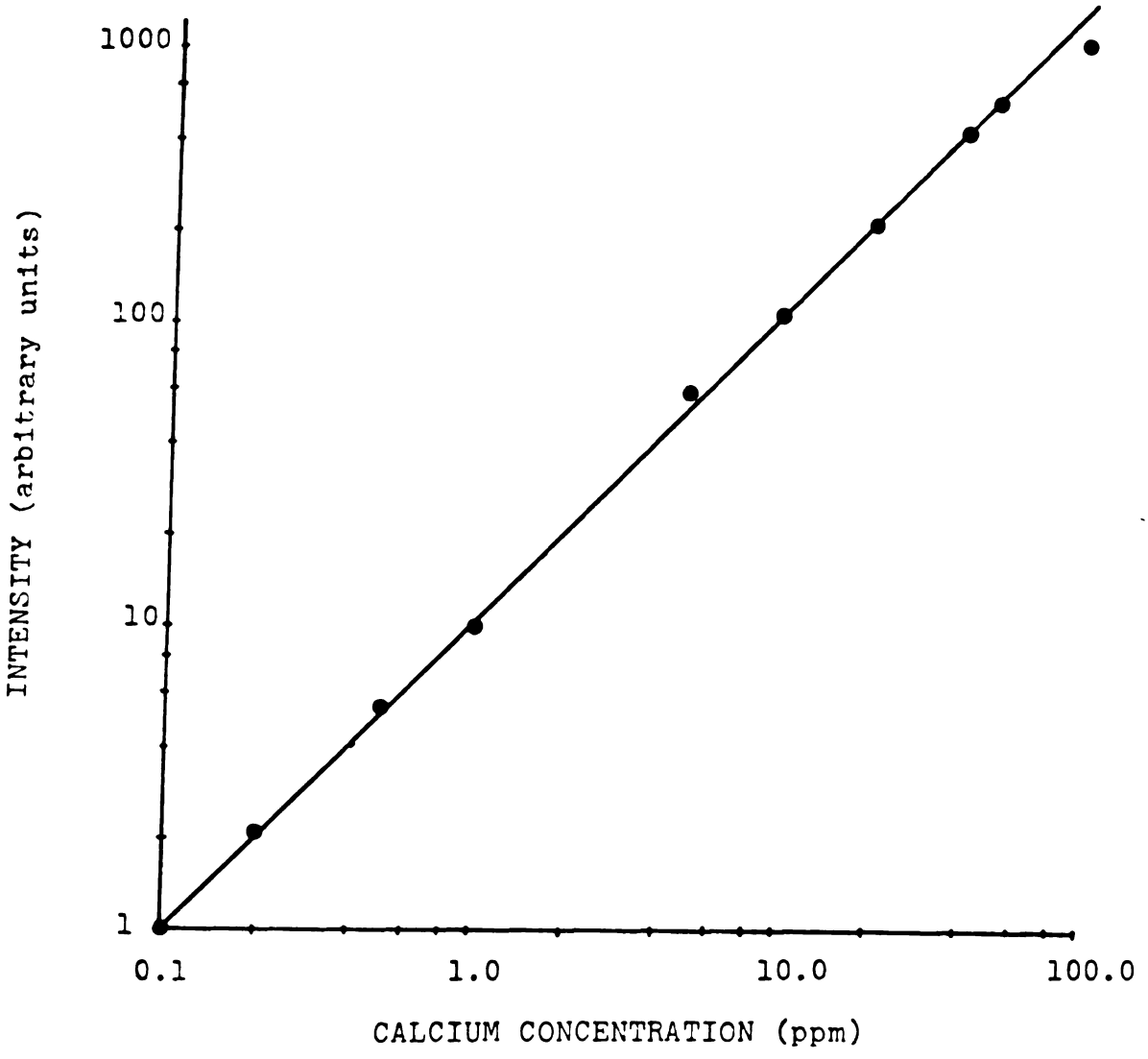

Figure 31. (Calibration curve for calcium (ion at 393 Å; log-log plot).

F. Multielement Studies

Table 9 summarizes the results of fast multielement determinations performed by the hardware (Chapter III, Section 5C) and the software (Chapter IV, Section B2) previously described. Solutions containing various concentrations of Si, Cu and Ca were prepared by combining stock solutions of each element. The monochromator was set at 2450Å for each trial. The solutions were analyzed by slewing to within 3.0Å of each of the three analyte lines (in the order shown in Table 9), scanning over the line, and finally, taking intensity data at the line maximum. Blanks were run at the wavelength maxima previously determined. The detection limits reported were obtained from those concentrations of analytes which consistently gave S/N ratios equal to two. The increase in the detection limits observed are probably the result of the electronic monitoring system which often times slightly misses the analyte wavelength maximum. One complete determination requires 10 min excluding solution preparation time. However, since most of the time is associated with manual tasks, a larger number of elements can be determined without a substantial increase in the total analysis time.

Table 9. A Summary of Multielement Results.

Element	Line (Å)	Multielement DL (ppm)	MNS* DL (ppm)	Ratio of Multielement DL to MNS* DL
Si	2516	0.2	0.07	2.9
Cu	3247	0.05	0.02	2.5
Ca(II)	3933	0.02	0.01	2.0

*See Table 6.

G. Real Sample Analysis

Table 10 summarizes the results of the semiquantitative analysis of a non-toxic flame retardant sample requested by a member of the Michigan State University Chemical Engineering Department. The sample solution was prepared by heating a 0.500 g of the sample powder to boiling, and filtering the resulting mixture. Approximately one-third of the sample was insoluable in hot water. The solution was diluted by a factor of ten and analyzed for Na, Ca, Al, B, Si, P, and C using the ultrasonic nebulizer, and side introduction. Although it was predicted that B and Al would be present and none was found, it is known that PO_4^{-3} and CO_3^{-2} are also common anions in non-toxic flame retardants (97).

Table 10. Flame Retardant Analysis Results.

Element Found	Analysis Line (Å)	Conc. (ppm)	% of Dissolved Sample
P	2535	10 ± 2	10
C	2478	7 ± 1	7
Na	5896	50 ± 5	50

VI. COMMENTARY

A. General Perspectives

Although the present MNS system has been shown to be a viable spectrochemical instrument, there is still much room for improvement. Suggestions for software and electronic modifications have been previously presented. First in priority are modifications to the gas flow system of the MNS housing. To provide the capability of employing secondary gap lengths over 5.0 mm, a larger gap chamber should be designed which promotes spatial stability via an axial stream of gas provided at low flow rates. Erratic firing resulting from air leakage into the gap region at low flow rates can be reduced by flushing the inside of the brass housing (which supports the secondary gap chamber) with the gas used in the study. Further studies should be performed to determine whether the axial flow system of the analytical gap can be improved to the point that it can compete favorably with side introduction in the area of detection limits. A less restricted axial flow system should improve results. Since it appears that the sheath gas flow is unimportant except at low axial flow rates ($\leq$ 0.5 ℓ/min), it might be advantageous to redesign the present analytical gap flow system such that it provides a simple, direct flow from

the heated chamber to the cone (which directs the gas along the inter-electrode axis). It might also prove to be beneficial to increase the size of the cone orifice somewhat from the present 2.6 mm diameter. However, any modifications should be tempered by the following relationship:

$$L \alpha v/R, \qquad (8)$$

where L is the amount of analyte lost through an orifice or constriction, R is the radius of curvature through which the particle must travel to avoid impact with the barrier, and v is the particle velocity (98). If the modifications implemented do not result in attainment of the detection limits sought, and the user is willing to sacrifice spatial stability, a permanent side introduction system should be designed. It might prove interesting to perform electron microscope studies of the amount of analyte reaching the gap per unit time for various flow configurations.

Recently, as a logical extension of its use as a gas chromatographic detector, the MNS has been investigated as a liquid chromatographic (LC) detector (24). Further investigations are presently being conducted in this laboratory. The major efforts include reduction of the system dead volume, construction of an interface between

the LC and the MNS nebulizer, and lessening of the effect of high concentrations of organic solvents on the discharge. Water has been successfully used as a solvent in MNS-LC experiments (24). However, organic solvents tend to extinguish the spark.

There are several important experiments to be performed on the MNS which would further define the overall capabilities of the system. It might prove interesting to investigate the effects of using air or nitrogen as secondary gap atmospheres. Furthermore, although the original MNS pulsed supply does not appear to break down two gaps well, no attempts were made with the bridging resistor in the circuit. Such an experiment should be conducted in argon and helium, and, if successful, emission studies should be performed using this system. Finally, simplex optimization of many of the user-controlled parameters discussed in Chapter V might prove beneficial.

B. Present MNS Capabilities

As was found to be the case with the original MNS, the present source has been found to be an excellent spectrochemical tool. It is felt that several significant improvements have been made in the overall structure of the MNS since it was first constructed. The present system permits a ten-fold or larger increase in the rate of data acquisition via the high voltage and digital/analog

electronics constructed. This same digital/analog system, when combined with the MNS software, and the fast optical trigger, also provides increased timing accuracy, simple, fast user-instrument interaction and rapid multielement capabilities. Furthermore, the user has more direct control over the characteristics of the plasma through variations of such parameters as gap lengths, gas flow rates, DC supply voltage, and, if necessary, two different atmospheres in the analytical and secondary gap regions.

The axial flow system, described in this work, performs as expected by improving the spark precision by a factor of as much as 2.6 (to a value of ca. 1.5%, RSD). However, in spite of the decrease in spatial stability associated with side introduction of the sample, detection limits for the latter method were found to be superior to those found with axial flow.

As has been shown in this work, the present MNS exhibits somewhat different characteristics than its predecessor. It is felt that the present spark system, like the original, requires more than one graduate career to fully develop its analytical potential. It is hoped that this work provides a sound basis from which to perform future research toward this end.

APPENDIX A

Calculation of the Average Resistance and Inductance During Typical Operation of the MNS

This Appendix is devoted to the calculation of the MNS average resistance and inductance. For information concerning the high-voltage circuit discussed, see Figure 4 and pages 33-36 of this Dissertation.

To simplify the calculations involved, it is necessary to assume that the separate inductances and resistances in the MNS circuit are directly additive ($L=L_L+L_C+L_A$, $R=R_C+R_A$). The total resistance for a typical gap combination (secondary = 3.0 mm, analytical = 3.0 mm) can now be obtained from the following equation:

$$R = \frac{k\ell}{Q} , \qquad (9)$$

where R is the total resistance, k is the Toepler constant which is dependent on the atmosphere in the gap region, ℓ is the gap length, and Q is the total charge passed through the gap (77). For argon, k is approximately 4.0×10^{-4} Ω/cm (77). The total charge, Q, can be calculated from the product of the spark period (0.4 ms) and the average current (2.8 mA) supplied by the DC power supply. From these data, R is found to be ca. 210 Ω.

The capacitance of the system is almost exclusively provided by the cable and coaxial capacitor. The value of the capacitance has been found to be 350 pF using the discharge time method presented in Chapter V (Section B1., Capacitance Measurement).

The inductance is obtained through the use of Equation 10, which relates the current magnitude at any time, t, to the circuit R, L, and C values as follows:

$$I = k(\sin\omega t)(e^{-at}), \qquad (10)$$

where k is a proportionality constant,

$$\omega = (1/LC - R^2/4L^2)^{1/2}, \qquad (11)$$

and

$$a = R/2L \quad (82,83). \qquad (12)$$

For an overdamped discharge, ω^2 is less than zero and Equation 10 becomes:

$$I = k'(e^{\beta t} - e^{-\beta t})e^{-at}\ , \qquad (13)$$

where the sin(iωt) was replaced by an equivalent expression, k' is a new proportionality constant, and

$$\beta^2 = -\omega^2 \quad (83). \qquad (14)$$

Given the values of R and C previously determined, L can be found if two current values, I_1 and I_2, at times t_1

and t_2 are ratioed to eliminate k'. Although current values are not directly accessible from the MNS data collected, the ratio of the currents at two times is available from the voltage-time profiles (Chapter V, Section B3), if the curve is examined late in spark life (ca. 70-80 ns). It is assumed that the inductance and capacitance of the nichrome wire do not substantially affect the voltage observed during this period, and thus, the voltage is proportional to the current. This assumption is true only within the semiquantitative framework applied to this problem. Using the ratioed voltage values, it was possible to solve for L by iteration using a FORTRAN II program executed on a minicomputer. The value of the inductance was found to be 0.3 μH.

APPENDIX B

MNS Software

```
C       PROGRAM NAME: GSPARK.F4
C       DATE OF MOST RECENT VERSION: 9/2/78
C       PROGRAMMER: G. T. SENG
C       AT: MICHIGAN STATE UNIVERSITY
C       EXTERNAL ROUTINES CALLED: SET.RA, ADC.RA
C       PROGRAM FUNCTION: TO COLLECT TIME-RESOLVED EMISSION DATA
C                         FROM THE MNS AND PERFORM STATISTICAL
C                         CALCULATIONS ON THE DATA OBTAINED.
C
C       USER ENTERS BY PROMPT:
C       1. HEADING (IF DESIRED)
C       2. DATA HEADING (IF DESIRED)
C       3. DELAY TIME (F FORMAT) IN MICROSECONDS
C       4. INTEGRATE TIME (F FORMAT) IN MICROSECONDS
C       5. NUMBER OF PTS. AVERAGED PER DATA PT
C       6. NUMBER OF DATA PTS.
C       7. A BLANK? Y OR N
C
C       PROGRAM OUTPUTS:
C       A. BLANK= N : VALUES OF DATA PTS., STANDARD DEVIATION,
C                     RELATIVE STANDARD DEVIATION
C       B. BLANK= Y : VALUES OF DATA PTS., STANDARD DEVIATION,
C                     RELATIVE STANDARD DEVIATION, S/N RATIO,
C                     DETECTION LIMIT FACTOR, SIGNAL - BACKGRD.
C
C       REFERENCE: G.T. SENG PH.D. THESIS, MICHIGAN STATE UNIV.,
C                  DEPT. OF CHEM., E. LANSING, MICH.,1978.
C
C       **BEGIN PROGRAM**
C
C
        DIMENSION ARRAY(1000), HEADR(11)
C       BEGIN HEADING SECTION
5       WRITE(0,10)
10      FORMAT(' ENTER HEADING')
        READ(4,15)( HEADR(M),M=1,11)
15      FORMAT(11A6)
        WRITE(3,20)(HEADR(N),N=1,11)
20      FORMAT(' ',11A6)
        WRITE(3,40)
        WRITE(3,45)
40      FORMAT(1H0,25X,'DEL    INT NUMAV NUMDP')
45      FORMAT(1H ,15X,'AVERAGE',10X,'STANDARD  DEV',8X,'REL STD DEV %')
50      WRITE(0,55)
C       BEGIN DATA HEADING SECTION
55      FORMAT(' DATA HEADER? - YES=Y;NO=N')
        READ(4,60)DATH
60      FORMAT(A6)
        IF(DATH.EQ.'N')GO TO 75
        WRITE(0,56)
56      FORMAT(' ENTER HEADING')
        READ(4,65)(HEADR(I),I=1,11)
        WRITE(3,70)(HEADR(J),J=1,11)
65      FORMAT(11A6)
70      FORMAT(' ',11A6)
75      WRITE(0,80)
C       ENTER DELAY ,INTEGRATE TIMES- DATA PTS. AV.,#DATA PTS>
80      FORMAT(' DELAY TIME(F)=',$)
        READ(4,85) DELAYT
        DELAYT=DELAYT*10.
85      FORMAT(G13.6)
        WRITE(0,87)
87      FORMAT(' INTEGRATE TIME(F)=',$)
        READ(4,85) FINIT
        FINIT=FINIT*10.
        WRITE (0,90)
90      FORMAT(' POINTS PER DATA POINT(I)=' ,$)
        READ(4,95) NUMAV
95      FORMAT(I4)
        WRITE(0,88)
88      FORMAT(' NUMBER OF DATA POINTS(I)=',$)
```

```
      READ(4,95) NUMDP
      MISS=0
C     CALL RALF ROUTINES TO SET ELECTRONICS CTRS, AND
      CALL SET (DELAYT,FINIT)
      CALL ADC(ARRAY,NUMAV,NUMDP,MISS)
      SQSUM=0.0
      DATOT=0.0
      RSDEV=0.0
      STDEV=0.0
C     ROUND DATA AND CALCULATE AVERAGE
      DO 100 L=1,NUMDP
      IN=INT(ARRAY(L)*10000/FLOAT(NUMAV))
      ARRAY(L)=FLOAT(IN/10000.)
      DATOT=DATOT + ARRAY(L)
100   CONTINUE
      DATAV=DATOT/FLOAT(NUMDP)
C     CALCULATE STATISTICS
      DO 105 K=1,NUMDP
      DEV=0.0
      DEV=ARRAY(K)-DATAV
      SQSUM=SQSUM + DEV**2
      STDEV=SQRT(SQSUM/(FLOAT(NUMDP)-1.0))
      RSDEV=100*STDEV/DATAV
      WRITE(0,125)
      READ(4,130)BLANK
      IF(BLANK.EQ.'Y')GO TO 110
      SDATAV=DATAV
      SSTDEV=STDEV
110   WRITE(0,135)(ARRAY(I),I=1,NUMDP)
      WRITE(0,140)DATAV
      WRITE(0,145)STDEV
      WRITE(0,150)RSDEV
      WRITE(3,155)DELAYT,FINIT,NUMAV,NUMDP
      WRITE(3,170)DATAV,STDEV,RSDEV
      IF(MISS.GT.0)GO TO 115
      WRITE(0,160)
      GO TO 120
115   WRITE(0,165)MISS,NUMAV
120   IF(BLANK.NE.'Y')GO TO 175
      SIGNAL=SDATAV-DATAV
      STONR=SIGNAL/SQRT((SSTDEV**2)+(2*(STDEV**2)))
      DLFAC=SIGNAL/(2.828*STDEV)
      WRITE(3,205)SIGNAL
      WRITE(3,206)STONR
      WRITE(3,207)DLFAC
      WRITE(0,205)SIGNAL
      WRITE(0,206)STONR
      WRITE(0,207)DLFAC
175   WRITE(0,180)
180   FORMAT(' DO YOU WANT MORE RUNS MASTER? - YES=Y;NO=N')
      READ(4,185)YKNAVE
185   FORMAT(A6)
      IF(YKNAVE.EQ.'N')GO TO 215
      WRITE(0,195)
195   FORMAT(' NEW HEADER? - YES=Y;NO=N')
      READ(4,200)DIFHD
200   FORMAT(A6)
210   IF(DIFHD.EQ.'Y')GO TO 5
      GO TO 50
215   CONTINUE
125   FORMAT(' A BLANK? -YES=Y;NO=N')
130   FORMAT(A6)
135   FORMAT(1H ,5F13.4)
140   FORMAT(' THE AVERAGE=' ,F13.4,5X)
145   FORMAT(' THE STANDARD DEVIATION= ',F13.4,5X)
150   FORMAT(' THE RELATIVE STANDARD DEVIATION= ',F13.4,' %')
155   FORMAT(1H0,25X,F5.0,1X,F5.0,1X,I4,1X,I4)
160   FORMAT(' SYNC CTR = 0, NO FLAGS SET EARLY')
165   FORMAT(' SYNC CTR = ',I4,' FOR',I4,' SPARKS')
170   FORMAT(1H ,8X,F13.4,5X,F13.4,5X,F13.4)
```

```
205       FORMAT(' ',//,10X,'SIGNAL-BKGRD=',F7.4)
206       FORMAT(' ',//,10X,'SIGNAL/NOISE',F7.2)
207       FORMAT(' ',//,10X,'DETEC LMT FACTOR=',F7.2,///)
          END
```

```
PROGRAM NAME:  GSMLEL.F4
DATE OF MOST RECENT VERSION:  9/6/78
PROGRAMMER:  G.T. SENG, ALL NON GS.... SUBROUTINES
                    PREPARED BY S. KOEPLIN
AT:  MICHIGAN STATE UNIVERSITY
EXTERNAL ROUTINES CALLED:  SKLNFD.F4, GSCAN.F4, SET.RA
PROGRAM FUNCTION:  TO DIRECT SLEW AND SCAN SUBROUTINES
                   FOR MNS FAST MULTIELEMENT WORK AND
                   SPECTRAL SCANS.

USER ENTERS BY PROMPT:
  (1) HEADING
  (2) SCAN? - Y OR N
  (3) SCAN = Y - ENTER INIT WL(A), FNL WL(A), INCR
      LENGTH(A), DEL TMS (UP TO 5 MICROSEC), INT
      TMS (MICROSEC), NUM DATA PTS, NUM DATA PTS AV
  (4) SCAN = N (SLEW), ENTER EL, DEL TM, INT TM,
      INIT WL - ROUTINE WILL PROMPT
**START BLANK** - WHEN COMPLETE TYPE "D".
FIRST 5 VARIABLES, G13.6 FORMAT - FINAL 2, I5 FORMAT
PROGRAM OUTPUTS:
  (1) SCAN:  DATA FILE ON DISK
  (2) SLEW:  DATA AVERAGES FOR ALL ELEMENTS, STATISTI-
      CAL CALCULATIONS FOR ALL ELEMENTS AND BLANKS, S/N.
REFERENCE:  G.T. SENG, PH.D. THESIS, M.S.U., 1978,
                    CHAPTER IV.
**BEGIN PROGRAM**

      COMMON ELEMT (10)
      COMMON DATA (10,4)
 10   WRITE (0,20)
 20   FORMAT (' SCAN OR SLEW - SC = SCAN, SL = SLEW ')
      READ (4,30) CHOICE
 30   FORMAT (2A6)
      IF (CHOICE .EQ. 'SL') GO TO 90
      WRITE (0,40)
 40   FORMAT (' ENTER - IN WL(A), FLWL(A), WL INC(A),
             DEL TM (MS), INT TM (MS), DAT PTS/AV,
             NUM DAT AV ')
      READ (4,50) TIWL, FWL, WLI, DTM, TITM, NDPTS,
                  NDAV

 50   FORMAT (5G13.6, 2I5)
      CALL GSCAN (TIWL, FWL, WLI, DTM, TITM, NDPTS,
                  NDAV)
 60   WRITE (0,70)
 70   FORMAT (' REPEAT? - Y OR N ')
      READ (4,80) REPEAT
 80   FORMAT (A6)
      IF (REPEAT .EQ. 'Y') GO TO 10
      GO TO 190
 90   WRITE (0,100)
100   FORMAT (' ENTER - NUMBER OF ELEMENTS AND ELEMENT
```

```
              SYMBOL(S) ')
       READ (4,110) K
110    FORMAT (I2)
       READ (4,115)(ELEMT(L), L = 1,K)
115    FORMAT (10A6)
       WRITE (0,120)
120    FORMAT (' ENTER - DEL TM (MS), INT TM (MS),
              INIT WL ')
       READ (4,130)
130    FORMAT (3G13.6) DT, IT, WL
       CALL SKLNFD (TDT, TOI, IWL)
       WRITE (0,140)
140    FORMAT (' BEGIN BLANK - WHEN COMPLETE ENTER D ')
       READ (4,180) DONE
180    FORMAT (A6)
       IF (DONE .EQ. 'D') CALL SKLNFD (TDT, TOI, IWL)
       WRITE (3,150)
150    FORMAT (' ', 10X, 'SIGNAL', 10X, 'BLANK', 10X,
              'STD. DEV.', 10X, 'AVERAGE')
       DO 170 J = 1,K
       DATA(J4) = DATA(J,1) - DATA(J,2)
       WRITE (3,160) (DATA(J,M), M = 1,4)
160    FORMAT (' ', 10X, F10.6, 9X, F10.6, 8X, F10.6,
              11X, F10.6)
170    CONTINUE
       GO TO 60
190    CONTINUE
       END
```

```
      SUBPROGRAM NAME:  GSCAN.F4
      CALLED BY:  GSMLEL.F4
      DATE OF MOST RECENT VERSION:  9/6/78
      PROGRAMMER:  G.T. SENG, ALL NON-GS SUBROUTINES
                           PREPARED BY S. KOEPLIN
      AT:  MICHIGAN STATE UNIVERSITY
      EXTERNAL ROUTINES CALLED:  SET.RA, ADC.RA, SCNTO.RA
      PROG. FUNC.:  CONTROLS SPECTRAL SCAN SUBROUTINES FOR
                    MNS OVER VARIOUS TIME PERIODS.
      USER ENTERS AFTER CALLING FRTS:
        (FILE.DA /5, TO STORE WAVELENGTHS


        (1) FILE.DA /5, TO STORE WAVELENGTHS
        (2) FILE.DA /6. TO STORE DATA AVERAGES
      PROGRAM OUTPUTS:  DATA FILES ON DISK
      **BEGIN PROGRAM**

      SUBROUTINE GSCAN (TIV, FV, WI, DT, TOI, IDP, IDA)
      DIMENSION ARRAY(1000)
      IDIR = 0
      WL = 0.0
      NSTEP = INT((FV - TIV)/0.1)
      IF (NSTEP .LT. 0) IDIR = 1
      NSTP = IABS(NSTEP)
      IN = INT(WI)
      I = NSTP/IN
      CALL SET (DT, TOI)
      DO 20 K = 1,I
      CALL ADC (ARRAY, IDA, IDP)
      DO 10 L = 1,IDP
      IDAPT = INT(ARRAY(L)*10000/FLOAT(IDA))
      ARRAY(L) = FLOAT(IDAPT/10000.)
      DATOT = DATOT + ARRAY(L)
10    CONTINUE
      DATAV = DATOT/FLOAT(IDP)
      WL = TIV + WI
      WRITE (5,30) WL
30    FORMAT (G13.6)
      WRITE (6,40) DATAV
40    FORMAT (G13.6)
      CALL SCNTO (IDIR, IN)
20    CONTINUE
      RETURN
      END
```

```
SUBPROGRAM NAME:  ADC.RA
CALLED BY:  GSPARK.F4
DATE OF MOST RECENT VERSION:  7/8/77
PROGRAMMERS:  G.T. SENG, S.M. KOEPLIN, E.H. PALS
AT:  MICHIGAN STATE UNIVERSITY
NO EXTERNAL ROUTINES CALLED
PROGRAM FUNCTION:  TO ACCEPT TOTAL NUMBER DATA PTS.
                   FROM GSPARK AND STORE DATA PTS.
                   GENERATED BY THE ELECTRONICS IN A
                   CORE MEMORY ARRAY.
THE "8-MODE" CODE SECTION IS PRESENTED-
THE RALF SECTION MUST ACCEPT THE NUMBER OF DATA
POINTS AVERAGED, AND THE NUMBER OF AVERAGES AND PASS
THE INFORMATION TO THE "8-MODE" SECTION
(NPTAV,NUMDP8). THEN, RETURN "8-MODE" DATA TO THE
GSPARK ARRAY VIA VARIABLE AR.
**BEGIN PROGRAM**

          SKPAD 6441   /SKIP ON ADC FLAG
          DRIVE 6452   /DRIVE DATA TO AC
          CLRFG 6451   /CLEAR ADC FLAG
          FIELD1 #ADC
          0            /SAVE RETURN
          IOF          /DONT INTERRUPT THIS CODE
          CLA          /CLEAR AC
          TAD AR       /PICK UP DATA FIELD
          AND N7       /MASK
          CLL RTL      /MOVE TO
          RAL          /PROPER BITS
          TAD N6201    /SKELETON CDF INSTRUCTIONS
          DCA . +1     /SET TO EXECUTE
          0            /AS IN LINE CODE
          TAD . -1     /SAVE FOR FUTURE REFERENCE
          DCA CCDF     /ELSEWHERE
          TAD NPTAV1   /SAVE THE NUMAV COUNTER
          DCA NPTAV
          ISZ AR +1
          SKP
          JMS SUB
          ISZ AR +1
          SKP
          JMS SUB
          ISZ AR +1
          SKP
          JMS SUB
          JMP CHECK
STR,      CLA CLL
          SKPAD        /MISSED A POINT ?
          JMP . +3     /NO, CONTINUE
          ISZ MISSED   /YES, INC. POINTER
          CLRFG        /DISCARD MISSED POINT
```

```
CHECK,  SKPAD          /CONVERSION YET ?
        JMP . -1       /NO, WAIT
        DRIVE          /YES, GET IT
        CLRFG          /CLEAR FLAG
        RAL            /SET FOR INPUT
        CML            /COMPLEMENT MOST SIGNIFICANT BIT
        RAR            /RESTORE TO PROPER POSITION
        CMA            /COMPLEMENT AC
        TAD PRAD       /ADD PREVIOUS RESULT
        DCA PRAD       /SAVE IT
        SZL            /OVERFLOW ?
        ISZ MSWRD      /YES, INC. MOST SIGN.WORD
        JMP . +2       /NO, CONTINUE UNABATED
        HLT            / ADDEND OVERFLOW ?
        ISZ NPTAV      /DONE YET ?
        JMP STR        /NO, GET ANOTHER POINT
        CLA CLL        /PREPARE TO STORE A POINT
        TAD N13        /NECESSARY FOR NORMALIZATION
        DCA% AR+1      /PUT 13 INTO EXPONENT
        ISZ AR+1       /MOVE POINTER TO NEXT LOCATION
        SKP
        JMS SUB        /CHANGE THE DATA FIELD
        TAD MSWRD      /PICK UP MOST SIGN WORD
        DCA% AR+1      /DEPOSIT WORD 2 FORT. VARIABLE
        ISZ AR+1       /INCREMENT POINTER
        SKP
        JMS SUB
        TAD PRAD
        DCA% AR+1
        ISZ AR+1
        SKP
        JMS SUB
        CLA CLL
        DCA PRAD       /CLEAR STORAGE
        DCA MSWRD
        TAD NPTAV1     /RESET COUNTER
        DCA NPTAV
        ISZ NUMDP8     /TAKEN NUMBER OF REQUESTED DATA PTS. ?
        JMP STR        /NO, GET SOME MORE
        ION            /TURN INTERRUPT BACK ON BEFORE EXITING
        CDF CIF Ø      /PREPARE TO RETURN
        JMP% #ADC      /GO BACK TO RALF MODE
SUB,    Ø              /SAVE THE RETURN
        CLA CLL
        TAD N1Ø
        TAD CCDF       /INCREMENT THE DATA FIELD
        DCA . +1
CCDF,   Ø              /SET TO EXECUTE AS IN LINE CODE
        CLA CLL
```

```
                JMP% SUB

/DEFINE THE NECESSARY CONSTANTS
AR,         0000
            0000
N7,         0007
N1Ø,        0010
N62Ø1,      6201
N13,        0013
AV8,        0000
            0000
NPTAV1,     0000
NPTAV,      0000
DP8,        0000
            0000
NUMDP8,     0000
XMISS,      0027
            0000
MISSED,     0000
PRAD,       0000
MSWRD,      0000
```

```
SUBPROGRAM NAME:  SET.RA
CALLED BY:  GSPARK.F4
DATE OF MOST RECENT VERSION:  7/8/77
PROGRAMMERS:  G.T. SENG, S.M. KOEPLIN, E.H. PALS
AT:  MICHIGAN STATE UNIVERSITY
NO EXTERNAL ROUTINES CALLED
PROGRAM FUNCTION:  TO ACCEPT DELAY AND INTEGRATE
                   TIMES FROM PROGRAM GSPARK.F4
                   AND PASS TO THE TIMING
                   CIRCUITRY IN PROPER FORM.
THE "8-MODE" CODE SECTION IS PRESENTED-
THE RALF SECTION MUST ACCEPT THE DELAY
AND INTEGRATE TIMES FROM GSPARK.F4, AND
PASS THE VARIABLES TO THE "8-MODE" CODE SECTION
(DEL8 AND INT8) IN THE PROPER FORM.
**BEGIN PROGRAM**

          OUT1 6442       /LATCH OUT DELAY TIME
          OUT2 6444       /LATCH OUT INTEGRATE TIME
          FIELD1 #SET8    /LOAD THIS SECTION IN FIELD1
          Ø               /SAVE RETURN ADDRESS
          IOF             /TURN OFF INTERRUPT
          CLA CLL
          TAD DEL8 2      /GET 1 WORD DELAY TIME
          CMA             /INVERT FOR PROPER TIME VALUE
          OUT1            /LATCH OUT VALUE
          CLA CLL
          TAD INT8 2      /GET 1 WORD INTEGRATE TIME
          CMA             /INVERT FOR PROPER TIME VALUE
          OUT2            /LATCH OUT VALUE
          CLA CLL
          ION             /RESTART INTERRUPT SYSTEM
          CDF CIF Ø       /PREPARE FOR RETURN
          JMP% #SET8      /RETURN TO RALF MODE
DEL8,     0000            /STORAGE-DELAY TIME
          0000
          0000
INT8,     0000            /STORAGE AREA FOR TIME
          0000
          0000
```

REFERENCES

REFERENCES

1. Zynger, J., Ph.D. Thesis, Michigan State University, East Lansing, MI (1973).

2. Zynger, J. and S. R. Crouch, Appl. Spec. 26, 631 (1972).

3. Zynger, J. and S. R. Crouch, Appl. Spec., 29, 244 (1975).

4. Veillon, C. and M. Margoshes, Spectrochim. Acta 23B, 553 (1968).

5. Beams, J. W., A. R. Kuhlthau, A. C. Tapsley, J. H. McQueen, L. B. Snoddy and W. D. Whitehead, Jr., J. Opt. Soc. Am., 37, 868 (1947).

6. McMahon, D. H., A. R. Franklin and H. R. Carleton, Rev. Sci. Instr. 37, 1142 (1966).

7. Jolibois, D. and R. Bossuet, Comp. Rend., 204, 1189 (1937).

8. Twyman, F., W. Zehden, and E. S. Dreblow, Ind. Eng. Chem. Anal. Ed., 12, 238 (1940).

9. Schribner, B. F., and M. Margoshes in "Treatise on Analytical Chemistry", I. M. Kolthoff and P. J. Elving, Eds., Vol. VI, Wiley, New York, NY, 1965, Part L.

10. Feldman, C., Anal. Chem., 21, 1041 (1949).

11. Uzumasa, Y., and H. Okuno, J. Chem. Soc., Japan 54, 631 (1933).

12. Malmstadt, H. V., and R. G. Sholz, Anal. Chem., 27, 881 (1955).

13. Hell, A., W. F. Ulrich, N. Shifrin, and J. Ramirez-Munoz, Appl. Optics, 7, 1317 (1968).

14. A. A. Venghiattis, Appl. Optics, 7, 1313 (1968).

15. Shuster, A. and G. Hemsaleck, Trans. Roy. Soc., 193, 189 (1900).

16. Beams, J. W., J. Opt. Soc. Am., 13, 597 (1926).

17. Bardócz, A., Appl. Spec., 21, 100 (1967).

18. Crosswhite, H. M., D. W. Steinhaus, and G. H. Dieke, J. Op. Soc. Am., 41, 299 (1951).

19. Steinhaus, D. W., H. M. Crosswhite and G. H. Dieke, J. Opt. Soc. Am., 43, 257 (1953).

20. Walters, J. P., Anal. Chem., 39, 771 (1967).

21. van der Piepen, H. and W. W. Shroeder, Spectrochim. Acta, 26B, 471 (1971).

22. Glass, E. and S. R. Crouch, Pittsburgh Conf. on Analytical Chemistry and Applied Spectroscopy 1975, paper #110.

23. Glass, E., Michigan State University, East Lansing, MI, personal communications, 1973-1976.

24. Lantz, R. K., Ph.D. Thesis, Michigan State University, East Lansing, MI (1977).

25. Lantz, R. K., and S. R. Crouch, Pittsburgh Conf. on Analytical Chemistry and Applied Spectroscopy, 1976, paper #286.

26. van der Piepen, H. and W. W. Schroeder, J. Phys. D: Appl. Phys., 5, 2190 (1972).

27. Thackeray, D. P. C., Nature, Lond., 180, 913 (1957).

28. Walters, J. P. and S. A. Goldstein, ASTM Special Technical Publication #540, American Society for Testing and Materials, Phil., PA, 1973.

29. Mika, J. and T. Török, "Analytical Emission Spectroscopy", Crane and Russak, New York, 1974.

30. Bardócz, A., Spectrochim. Acta, 7, 307 (1955).

31. Levy, S., J. Op. Soc. Am., 35, 221 (1945).

32. Coleman, D. M. and J. P. Watters, Spectrochim. Acta, 31B, 547 (1976).

33. Malmstadt, H. V., Enke, C. G., Crouch, S. R., and Horlick, G., "Optimization of Electronic Measurements", W. A. Benjamin, Inc., Menlo Park, CA (1974).

34. Winefordner, J. D., J. J. Fitzgerald, and N. Omenetto, Appl. Spec., 29, 369 (1975).

35. Busch, K. and G. H. Morrison, Anal. Chem., 45, 712A (1973).

36. Santini, R. E., M. J. Milano, and H. L. Pardue, Anal. Chem., 45, 915A (1973).

37. Golightly, D. W., R. N. Kniseley, and V. A. Fassel, Spectrochem. Acta, 25B, 451 (1970).

38. Felkel, H. L., Jr., H. L. Pardue, Anal. Chem., 50, 602 (1978).

39. Horlick, G., Appl. Spec., 30, 113 (1976).

40. Codding, E., Michigan State University, personal communication, 1975.

41. Winefordner, J. D., R. P. Cooney and G. D. Boutilier, Anal. Chem., 49, 1048 (1977).

42. Chester, T. L., H. Haraguchi, D. O. Knapp, and J. D. Winefordner, Appl. Spec., 30, 410 (1976).

43. Dawson, J. B., D. J. Ellis, and R. Milner, Spectrochim. Acta, 23B, 695 (1968).

44. Cordos, E. and H. V. Malmstadt, Amer. Lab., 4, 35 (1972).

45. Cordos, E. and H. V. Malmstadt, Anal. Chem., 45, 425 (1973).

46. Olson, D. W., W. J. Haas, Jr. and V. A. Fassel, Anal. Chem., 49, 632 (1977).

47. Baxter, D. N., Ph.D. Thesis, Michigan State University, East Lansing, MI (1977).

48. Syty, A., Crit. Rev. Anal. Chem., 4, 155 (1974).

49. Schmidt, F. J. and J. L. Royer, Anal. Lett., 6, 17 (1973).

50. Holak, W., Anal. Chem., 41, 1712 (1969).

51. Chu, R. C., G. P. Barron, and A. W. Baumgarner, Anal. Chem., 44, 1476 (1972).

52. Gilbert, P. T., Jr., Anal. Chem., 34, 1025 (1962).

53. Willis, J. B., Anal. Chem., 47, 1752 (1975).

54. Jones, J. L., R. L. Dahlquist, and R. E. Hoyt, Appl. Spec., 25, 628 (1971).

55. Winge, R. K., V. A. Fassel and R. N. Kniseley, Appl. Spec., 25, 636 (1971).

56. Davies, R., R. Venn and J. B. Willis, J. Sci. Instr., 42, 816 (1965).

57. Valente, S. E. and Schrenk, W. G., Appl. Spec., 24, 197 (1970).

58. Kniseley, R. N., H. Amenson, C. C. Butter, and V. A. Fassel, Appl. Spec., 28, 285 (1974).

59. Donohue, D. L., and J. A. Carter, Anal. Chem., 50, 686 (1978).

60. West, C. D., and D. N. Hume, Anal. Chem., 36, 413 (1964).

61. Kirsten, W. J., and G. O. B. Bertilsson, Anal. Chem., 38, 648 (1966).

62. Hoare, H. C., and R. A. Mostyn, Anal. Chem., 39, 1153 (1967).

63. Denton, M. B., Ph.D. Thesis, University of Illinois, Urbana-Champaign, Il., 1972.

64. Denton, M. B., and H. V. Malmstadt, Anal. Chem., 44, 241 (1972).

65. Korte, N. E., J. L. Moyers and M. B. Denton, Anal. Chem., 45, 530 (1973).

66. Stupar, J. and J. B. Dawson, Appl. Opt., 7, 1351 (1968).

67. Copeland, T. R., K. W. Olson, and R. K. Skoegerboe, Anal. Chem., 44, 1471 (1972).

68. Issaq, H. J., and L. P. Morgenthaler, Anal. Chem., 47, 1661 (1975).

69. Issaq, H. J., and L. P. Morgenthaler, Anal. Chem., 47, 1668 (1975).

70. Uchida, H. and H. Matsui, Spec. Lett., 11, 1 (1978).

71. Glass, E., and S. R. Crouch, Pittsburgh Conf. on Analytical Chemistry and Applied Spectroscopy 1976, paper #73.

72. Koeplin, S., Ph.D. Thesis, Michigan State University, East Lansing, MI (1978).

73. Walters, J., FACSS Meeting, Detroit, MI, personal communication (1978).

74. Crouch, S. R., D. N. Baxter, E. H. Pals and E. R. Johnson, Anal. Chem., 50, 291A (1978).

75. Digital Equipment Corporation, "Small Computer Handbook", Maynard, MA, 1972.

76. Grove, E. L., Ed., "Analytical Emission Spectroscopy", Vol. II, Marcel Dekker, Inc., New York, NY (1972).

77. Frungel, F. B. A., "High Speed Pulse Technology", Vol. II, Academic Press, New York, NY, 1965.

78. Meek, J. M., and J. D. Craggs, "Electrical Breakdown of Gases", Oxford University Press, New York, NY, 1953.

79. Cobine, J. D., "Gaseous Conductors", McGraw-Hill, Inc., New York, NY, 1941.

80. Digital Equipment Corporation, "OS/8 Handbook", Maynard, MA, 1974.

81. Pals, G., Ph.D. Thesis, Michigan State University, East Lansing, MI, 1978.

82. Halliday, D., and R. Resnick, "Physics", John Wiley and Sons, New York, NY, 1967.

83. DiStasio, M., Michigan State University, East Lansing, MI, personal communication, 1978.

84. Ralston, A. and H. Wilf, Eds., "Mathematical Methods for Digital Computers", John Wiley & Sons, New York, NY, 1967.

85. Rabb, M., Michigan State University, East Lansing, MI, personal communication, 1978.

86. Lyman, T., Ed. "Metals Handbook", The American Society for Metals, Cleveland, OH, 1948.

87. Skilling, H. H., "Transient Electric Currents", McGraw-Hill, Inc., New York, NY, 1937.

88. Reif, I., V. A. Fassel, and R. N. Kniseley, Spectrochim. Acta, 28B, 105 (1973).

89. Adcock, B. D., and W. E. G. Plumtree, J. Quant. Spectry. Rad. Trans., 4, 29 (1964).

90. Taylor, H. E., J. H. Gibson, and R. K. Skoegerboe Anal. Chem., 42, 1569 (1970).

91. Boumans, P. W. J. M., "Theory of Spectrochemical Excitation", Plenum Press, New York, NY, 1966.

92. Griem, H. R., "Plasma Spectroscopy", McGraw-Hill, Inc., New York, NY, 1964.

93. Pearse, R. W. B., and A. G. Gaydon, "The Identification of Molecular Spectra", John Wiley & Sons, New York, NY, 1963.

94. Gaydon, A. G., "Dissociation Energies and Spectra of Diatomic Molecules," Chapman and Hall, London, 1963.

95. Kawaguchi, H., M. Hasegawa, and A. Mizuike, Spectrochim. Acta, 23B, 265 (1968).

96. Fassel, V. A., and R. N. Kniseley, Anal. Chem., 46, 1110A (1974).

97. Hawley, M., Michigan State University, East Lansing, MI, personal communication, 1978.

98. Skoegerboe, R. K. and K. W. Olson, Appl. Spec., 32, 181 (1978).

99. Slavin, M., "Emission Spectrochemical Analysis", Wiley-Interscience, New York, NY, 1971.

100. Bunshak, R. F., Ed., "Modern Analytical Techniques for Metals and Alloys", John Wiley and Sons, New York, NY, 1970.

101. Weast, R. C., Ed., "Handbook of Chemistry and Physics", 51st ed., Chemical Rubber Co., Cleveland, OH, 1971.

102. Winefordner, J. D., Ed., "Spectrochemical Methods of Analysis", Wiley-Interscience, New York, NY, 1971.

103. Willard, H., L. Merritt, and J. Dean, "Instrumental Methods of Analysis," 5th ed., D. Van Nostrand Co., New York, NY, 1974.

MICHIGAN STATE UNIVERSITY LIBRARIES
3 1293 03146 0128